SLOW WAVE CHARACTERISTICS OF METAMATERIAL LOADED HELICAL GUIDE

By

DUSHYANT KUMAR SHARMA

(ENGG06201204001)

Institute for Plasma Research, Gandhinagar

A thesis submitted to the

Board of Studies in Engineering Sciences

In partial fulfilment of requirements

for the Degree of

DOCTOR OF PHILOSOPHY

of

HOMI BHABHA NATIONAL INSTITUTE

July, 2016

Homi Bhabha National Institute

Recommendations of the Viva Voce Committee

As members of the Viva Voce Committee, we certify that we have read the dissertation prepared by Dushyant Kumar Sharma entitled “Slow Wave Characteristics of Metamaterial Loaded Helical Guide” and recommend that it may be accepted as fulfilling the dissertation requirement for the award of Degree of Doctor of Philosophy.

Chairman - Dr. Shashank Chaturvedi **Date:**

Guide/Convener - Dr. Surya K. Pathak **Date:**

Co-Guide - Dr. Hem C. Joshi **Date:**

Examiner - Dr. V. Subramanian **Date:**

Member 1 - Prof. R. Jha **Date:**

Member 2 - Prof. S. Mukherjee **Date:**

Final approval and acceptance of this dissertation is contingent upon the candidate’s submission of the final copies of the thesis to HBNI.

I hereby certify that I have read this dissertation prepared under my direction and recommend that it may be accepted as fulfilling the thesis requirement.

Date:

Place: **Co-guide** **Guide**

STATEMENT BY AUTHOR

Dushyant Kumar Sharma

DECLARATION

I, hereby declare that the investigation presented in the thesis has been carried out by me. The work is original and has not been submitted earlier as a whole or in part for a degree / diploma at this or any other Institution / University.

Dushyant Kumar Sharma

List of publications arising from the Thesis

Journal

1. *Propagation characteristics of extremely anisotropic metamaterial loaded helical guide*, Dushyant K. Sharma and Surya K. Pathak, Optics Express (Accepted).

2. *Slowing and stopping of wave in dispersive metamaterial loaded helical guide*, Dushyant K. Sharma and Surya K. Pathak, Optics Express 24, 2687-2700 (2016)

3. *ENG-cladded metamaterial-loaded helical waveguide for optoelectronics applications*, Dushyant K. Sharma and Surya K. Pathak, Journal of Electromagnetic Waves and Applications 29, 2501-2511 (2015)

4. *Ultra Slow EM Wave Propagation Characteristics of Left-Handed Material Loaded Helical Guide*, Dushyant K. Sharma and Surya K. Pathak, Progress In Electromagnetics Research M 35, 11-19 (2014)

5. *Experimental analysis of novel FF-shaped metamaterial*, Dushyant K. Sharma and Surya K. Pathak, (*submitted to* IEEE Microwave and Components Letters)

6. *Cross polarization converter formed by four F-shaped chiral metamaterial*, Dushyant K. Sharma and Surya K. Pathak, (*to be submitted to* IEEE Microwave and Components Letters)

Conferences

1. *Dispersion Characteristics of Metamaterial Loaded Helical Guide*, Dushyant K. Sharma and Surya K. Pathak, IEEE International Conference on Microwave and Photonics, ISM, Dhanbad, 2013

2. *Enhanced Slow Wave through Dispersive Metamaterial Loaded Helical Guide: Analytical Study and Design*, Dushyant K. Sharma and Surya K. Pathak, OSA International Conference on Fibre Optics and Photonics, IIT, Kharagpura, 2014

3. *Enhanced Group Velocity Characteristics of a ENG Cladded Metamaterial Loaded Helical Guide*, Dushyant K. Sharma and Surya K. Pathak, Progress In Electromagnetics Research Symposium, Prague, European Union, 2015.

4. *Broadband Cross Polarization Converter Formed by Twisted F-Shaped Chiral Metamaterial*, Dushyant K. Sharma and Surya K. Pathak, Progress In Electromagnetics Research Symposium, Prague, European Union, 2015

Dushyant Kumar Sharma

DEDICATIONS

To the sweet anticipation of my *father*, *loving wife* and *cute little daughter*
and
To the memory of my *mother*

ACKNOWLEDGEMENTS

At the very outset, I convey my hearty gratitude to my thesis supervisor Dr. Surya K. Pathak. His diligent, friendly and spirited support and guidance through this long journey has been the source of inspiration for me. His enthusiasm, impeccable patience and understanding and availability for discussion at practically any time and anywhere made the journey that much easier. I am also thankful to him for providing incredible independence in charting the work, which went a long way in arriving at this shape.

I am obliged to Dr. S. Chaturvedi, Dr. H. Joshi, Prof. S. Mukherjee and Prof. R. Jha for consenting to be my Doctoral Committee members. Their unstinting support and listening to their advice through the years have been a pleasant experience. It was a privilege to have them on the committee.

I also want to thank my group members, Janmejay Buch, Varsha Siju, Abhishek Sinha, Umesh Nagora and Dharmendra Kumar for their support, encouragement and reviewing my writing. Special thanks go to my fellows, Rana Yadav, Veda Prakash, Sandeep Rimza, Santa Tiwari, Harish Charan for there warm company, stimulating discussions, and for all the fun we have had in the last four years.

A special gratitude and love goes to my family for their unfailing support. I would like to thank My father Ajay K. Sharma and my wife Deepika Sharma for continuous source of impeccable support and motivation. I thank my lovely daughter, Kaushiki, for his sweet smile and understanding. Finally, I want to express my deepest love and gratitude to my sister Manisha Sharma, my uncle Narendra sharma, my aunty Devial Sharma for their goodwill and support all through my life.

Contents

SYNOPSIS

Slow Wave is an emerging area of research which promises many potential applications in the field of Optical Communication Networks (OCN), Microwave Photonics (MWP) and Communication Network. In order to realize OCN architecture, the Optical Data Packet Switching (ODPS) is highly desirable. For ODPS, it is necessary to synchronize incoming data packets and regulate data traffic at network nodes or to implement congestion and contention resolution in the core routers. Nowadays, electrical router performs these operations through large banks of Static Random Access Memory (SRAM). In OCN architecture this activity will be performed by optical buffers. As compared to electric buffer the main advantage of optical buffer is its low cost. In ODPS, the cost per bit transmission of data is less as compared to its electric counterpart which makes it advantageous. Therefore, optical buffer should have low heat production, low power consumption and small footprints. Hence extensive research is going on to realize equivalent optical data packet switching (ODPS).

As described, optical buffers and memories are the key components to realize ODPS. The mechanism of slow wave is vital for development of such devices. The application of optical memories, optical buffers and delay lines ranges from optical storage, optical data processing, optical delay line, filters, phase shifter to microwave photonics (MWP) devices. MWP is an emerging area of research where photonics is involved in order to process microwave signals. The slow wave structures in MWP enable synchronizing the time delay or phase-shift of microwave signal which modulates the optical carrier. Slow wave devices also cater to other potential applications such as clock re-synchronization, pulse compression, enhancing light-matter interaction and enhancing nonlinear effects in the material etc.

It is a well-known fact that the wave velocity or group velocity is dependent on the dispersion characteristics of the medium. For slow wave or reduced group velocity, a medium should have sharp spectral characteristics which cause large dispersion. There are two possible ways to introduce dispersion in a device either by introducing a material or from structural aspect. Therefore, various proposed slow wave schemes are broadly classified in two categories (1) material induced dispersion and (2) structure induced dispersion. The conventional methods such as electromagnetic induced transparency, quantum-dot semiconductor optical amplification, coherent population oscillation and stimulated Brillouin scattering come in the category of material induced dispersion. Usually these methods are less preferred at room temperatures due to their strong temperature dependence and other inherent limitations. For instance, quantum-dot semiconductor optical amplifiers produce very small delays. Electromagnetic induced transparency requires ultracold atomic gases whereas, stimulated Brillouin scattering and coherent population oscillations have very narrow bandwidths. Usually, at room temperatures, structure induced dispersion methods are preferred because these methods are independent of temperature and at the same time are easier to implement. Photonic crystals (PC′s) and surface plasmon polaritons (SPP′s) based methods fall in the category of structure induced dispersion. However PC′s based methods have inherent issues of high multimode generation and strong impedance mismatch for slow light regime. This makes difficult to launch light energy in a single mode. SPP′s are also very sensitive to surface roughness and its excitation is also difficult.

Recently, different research groups have proposed and studied slow wave devices based on metamaterials. Metamaterials are novel and artificially engineered materials. They simultaneously possess negative values of permittivity and permeability over a certain frequency band. From these studies it has been observed that the presence of metamaterial medium can slow down the Electromagnetic (EM) wave.

In microwave engineering, Helical waveguide, which exhibits inherent characteristics of slow wave due to skewed boundary conditions, is widely used as a slow wave device over wide bandwidth in Travelling Wave Tubes, Backward Wave Oscillators and Helical antennas. Most of the slow wave structures studies in literature are based on planar as well as cylindrical geometries where complex mode behaviour has been studied in the context of various applications. To the best of our knowledge no one has investigated helical guide characteristics loaded with metamaterial with prospective applications in the field of optoelectronics and microwave photonics.

The motivation of the present investigation comes from different facts and objectives as discussed above and the inherent slow wave characteristics of a helical guide, known as Helical Slow Wave Structure. This inspired us to achieve ultra slow waves and even stop the waves in the helical guide by superimposing or combining its slow wave characteristics with metamaterial properties.

This research work includes analysis and design of novel helical slow wave devices embedded with metamaterial medium for optoelectronics as well as microwave photonics applications. For each proposed structure, analytical characterization as well as their possible engineering feasibility design is presented and discussed.

List of Figures

List of Tables

Chapter 1

Introduction

1.1 Metamaterial: A New Class of Material

In 1967, a Russian physicist V. G. Veselago [1] predicted the possibility of an extraordinary material having simultaneous negative values of permittivity and permeability. He referred this bizarre material as left-handed material and revealed the unusual phenomenon of electromagnetic wave propagation related to this bizarre material, such as the reversal of Snell's law, reversed Doppler effect, and reversed Cerenkov radiation. However, this striking prediction remained silent for four decades due to the absence of such materials in nature until Professor David R. Smith and his group at the University of California, San Diego (UCSD) 30 years later experimentally demonstrated such material. For designing metamaterial they used Professor Pendry's works of negative permeability and permittivity. They designed metamaterial using an array of thin wires and split ring resonators [2] shown in Fig. 1.1.

Left-handedness simultaneously requires negative values of permittivity and permeability. The UCSD group obtained such material parameters effectively through the periodic arrangement of split ring resonators (SRRs) plus metallic rods also shown in Fig. 1.1. In such a composite material, SRR is responsible for negative permeability while the metallic rod for negative permittivity. The spectra of resonance where material behaves like metamaterial can be changed by varying the physical size of the cell (containing split ring resonators and thin wires). This experimental verification brings the idea of Veselago into reality and opened the door to a wide area of research where researchers are trying to explore the use of metamaterials for different engineering applications such as in antennas, absorbers, superlenses, cloaking devices, seismic protection, light and sound filtering etc from microwave [3], terahertz to optical spectrum [4].

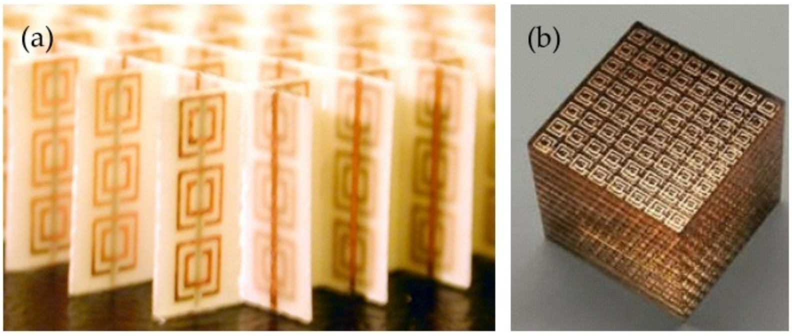

Figure 1.1: (a) Arrays of split ring resonators and thin wires and (b) its extension in three dimension. (*Source*: http:\\physics.ucsd.edu/lhmedia http:\\rsphy2.anu.edu.au nonlinear research lhm)

1.1.1 Terminologies of metamaterials

The term metamaterial usually refers to an artificially designed Electromagnetic (EM) structure which has unusual EM properties that are not found in nature. The word "*Meta*" is a Greek prefix meaning "*beyond*", so metamaterials can be described as a kind of materials having extraordinary EM response. A wide range of materials fall under the umbrella of metamaterials. Among them Left-Handed Materials (LHM's) or Double Negative (DNG) materials refer to a medium having simultaneously negative value of permittivity and permeability. Other terminologies which are commonly used for metamaterials are Negative Refractive Index (NRI) media, Backward Wave (BW) media, Negative Phase Velocity (NPV) media, Veselago's media, etc. All these terminologies belong to the abnormal behaviour of metamaterials. In this thesis, the term "metamaterial" refers to an artificial material having simultaneously negative real components of permittivity and permeability.

1.1.2 Electromagnetic analysis of LHM's and its properties

In 1967, Veselago had introduced the term Left-Handed Material (LHM) and predicted the existence of such a material where the electric field (E), the magnetic field (H) and the wave vector (k) obey left-handed rule whereas ordinary dielectric materials obey right handed rule. The LHM's in a broad sense are also described as Negative Index Materials (NIM's). Simultaneous negative material parameters such as permittivity (ϵ) and permeability (μ) produce extraordinary EM wave phenomena such as Inverse Snell's law, Backward wave radiation and Inverse Doppler effect. In order to investigate this extraordinary EM wave behaviour we first understand how the EM waves behave when a medium has $\epsilon < 0$ and $\mu < 0$.

The source-free Maxwell equations in time domain and their constitutive relations in a homogeneous and isotropic medium are:

$$\bigtriangledown \times E(t) = -\frac{\partial B(t)}{\partial t}, \tag{1.1}$$

$$\bigtriangledown \times H(t) = \frac{\partial D(t)}{\partial t}, \tag{1.2}$$

$$\bigtriangledown \cdot D(t) = 0, \tag{1.3}$$

$$\bigtriangledown \cdot B(t) = 0, \tag{1.4}$$

where

$$B = \mu H, \tag{1.5}$$

$$D = \epsilon E, \tag{1.6}$$

For plane wave propagation, all field components are proportional to $e^{i(kz-\omega t)}$ and the Eqs. (1.1) and (1.2) is mathematically written as:

$$k \times E = \omega\mu H, \tag{1.7}$$

$$k \times H = -\omega\epsilon E, \tag{1.8}$$

In Eq. (1.7) and (1.8), if $\epsilon < 0$ and $\mu < 0$, then a left-handed triplet vector of E, H and k are formed as shown in Fig. 1.2. Thus this material is termed as left-handed material.

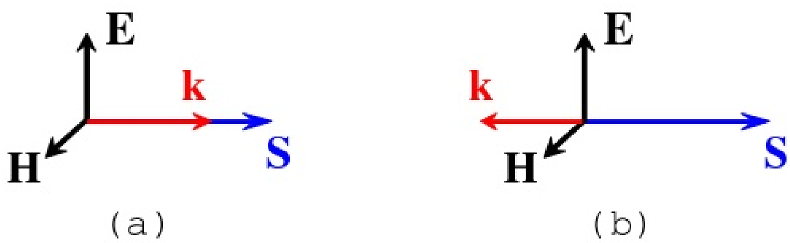

Figure 1.2: (a) Right-Handed Material (RHM), forms right-handed vector system with E, H and k, and the energy density flow S and wave vector k are in the same direction. (b) Left-Handed Material (LHM), forms left-handed vector system with E, H and k, and the energy density flow S and wave vector k are in the opposite direction.

The direction of energy flow is decided by the Poynting vector (S),

$$S = E \times H \tag{1.9}$$

and is independent of the signs of ϵ and μ. Poynting vector (S) always makes a right-handed coordinate system with E and H. In left-handed materials, the direction of the wave vector, k, is opposite to the energy density flow, S. This anti-parallel propagation of wave and energy flow supports propagation of Backward Wave (BW). In a normal or Right-Handed Material (RHM) the wave vector, k, and energy flow, S, are parallel and supports the propagation of Forward Wave (FW). The orientation of E, H, k and S in RHM and LHM are shown in Fig. 1.2.

In isotropic medium, the dispersion relation is given by,

$$k^2 = \omega^2 \sqrt{\epsilon\mu} \tag{1.10}$$

where $\epsilon, \mu \in \Re$, whether the EM wave decays or propagates is decided by the sign of ϵ and μ. For example when $\epsilon.\mu > 0$, $k = \omega \sqrt{\epsilon\mu}$, wave propagates, on the contrary wave exponentially decays when $\epsilon.\mu < 0$, $k = i\omega \sqrt{\epsilon\mu}$. Figure 1.3 illustrates the plane of ϵ and μ which has been classified into four quadrants. Each quadrant shows the possibility of different type of materials depending on the sign of ϵ and μ. The first quadrant accommodates most of the dielectric substances having positive ϵ and μ. Material with one constitutive negative parameter is easily available in nature. For instance, free electron gas in metals or ionized gas in plasma mediums have negative signs of permittivity all the way up to plasma frequency and exist in the second quadrant. Conversely antiferromagnetic and ferromagnetic materials have negative signs of permeability close to the ferromagnetic resonance and exist in the fourth quadrant. The third quadrant accommodates left-handed materials where permittivity and permeability both are negative although, these materials do not exist in nature.

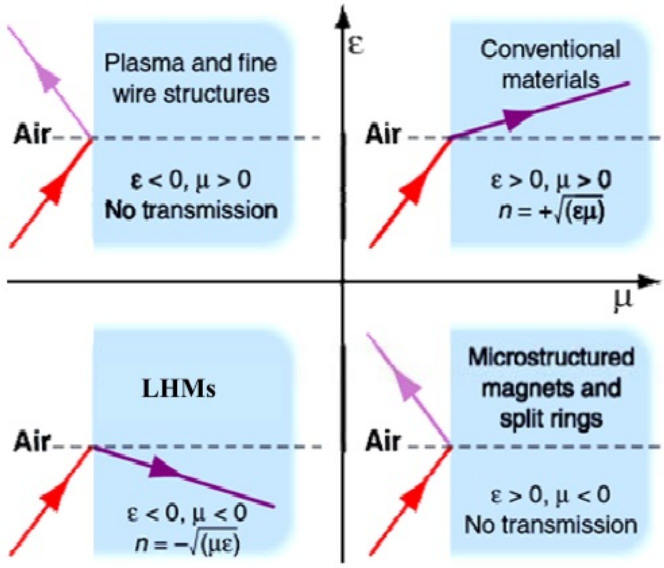

Figure 1.3: A diagram showing the possible classification of electromagnetic materials based on the signs of permittivity and permeability. The directions of wave vector in each medium is represented by arrows. In I and III quadrant the wave propagates whereas it decays in II and IV quadrant. (*Source*: M. C. K. Wiltshire, "Bending light the wrong way,"Science, vol. 292, Issue 5514, pp.60-61, 6 April 2001)

1.1.2.1 Dispersive and lossy nature of LHM's

In order to, simultaneously realize the negative value of ϵ and μ, the material should have frequency dispersion. This can be observed from the formula of the energy density of non-dispersive media [5]:

$$W = \epsilon E^2 + \mu H^2 \tag{1.11}$$

The energy density, W, becomes negative if $\epsilon < 0$ and $\mu < 0$. This is a non-physical result. A medium is dispersive when $\epsilon = \epsilon(\omega)$ and $\mu = \mu(\omega)$ are frequency dependent. For such a medium total energy density is written as [6]:

$$W = \frac{\partial(\epsilon\omega)}{\partial\omega} E^2 + \frac{\partial(\mu\omega)}{\partial\omega} H^2 \tag{1.12}$$

Since the energy density should always be positive,

$$\frac{\partial(\epsilon\omega)}{\partial\omega} = \epsilon + \omega\frac{\partial(\epsilon)}{\partial\omega} > 0 \tag{1.13}$$

$$\frac{\partial(\mu\omega)}{\partial\omega} = \mu + \omega\frac{\partial(\mu)}{\partial\omega} > 0 \tag{1.14}$$

This clearly describes that if any medium possesses, simultaneous, negative values of ϵ and μ, the medium is frequency dispersive and it should satisfy Eq. (1.13) and (1.14). Hence, a LHM must be dispersive medium.

However, a medium having frequency dispersion will always lossy. As per the principle of causality, the real (ϵ') and imaginary (ϵ'') part of permittivity is associated by Kramers-Kronig relations [6, 7]:

$$\frac{\epsilon'(\omega)}{\epsilon_0} = 1 + \frac{2}{\Pi}P\int_0^\infty \frac{\omega\epsilon''(\omega')/\epsilon_0}{\omega'^2 - \omega^2}d\omega' \tag{1.15}$$

$$\frac{\epsilon''(\omega)}{\epsilon_0} = -\frac{2\omega}{\Pi}P\int_0^\infty \frac{\epsilon'(\omega')/(\epsilon_0 - 1)}{\omega'^2 - \omega^2}d\omega' \tag{1.16}$$

where P is the principal value of integration. The real and imaginary values of permeability follow similar relations. Equation (1.15) and (1.16) show that real and imaginary part are Hilbert transforms pair of each other. Thus the imaginary parts of permeability and permittivity always exist together with the real parts in a dispersive media. Therefore LHM must be dissipative.

1.1.2.2 Negative refraction

The refraction and reflection of EM waves between two plane interfaces of different dielectric media are natural phenomena. The Fresnel formulas and Snell's Law determine the relationship between the reflection coefficients, the transmission coefficients and the refractive angle. Other interesting effects such as Brewster angle effect and total internal reflection also happen between the interface of two dielectrics.

Now, let's examine refraction phenomena at the interface of left-handed medium and right-handed medium. The refraction and reflection of a s-polarized wave at RHM and LHM interface are illustrated in Fig. 1.4. The relation between the incident angle, θ, and refractive angle, ϕ is obtained by Snell's Law:

$$\frac{sin(\theta)}{sin(\phi)} = \frac{n_2}{n_1} \tag{1.17}$$

The amount by which the beam is deflected in left-handed medium is determined by the refractive index $n_2 = \sqrt{\epsilon_2 \mu_2}$ where ϵ_2 are μ_2 are the permittivity and permeability of the LHM respectively and corresponding quantities of RHM are ϵ_1 and μ_1. It is very crucial to choose the signs of square root of ϵ_2 and μ_2 in left-handed medium. This ambiguity in the sign is resolved by proper analysis. For example in place of writing $\epsilon_2 = -1$ and $\mu_2 = -1$ we write $\epsilon = e^{i\pi}$ and $\mu = e^{i\pi}$, then:

$$n_2 = \sqrt{\epsilon_2 \mu_2} = e^{i\pi/2} e^{i\pi/2} = e^{i\pi} = -1 \tag{1.18}$$

and

$$\frac{sin(\theta)}{sin(\phi)} = -\frac{1}{\sqrt{\epsilon_1 \mu_1}} \tag{1.19}$$

If the sign of index is positive then the incident beam is deflected to another side of the normal. In left-handed material where the sign of index is negative, from Eq. (1.19) the beam is deflected on the same side of normal or it is refracted in the negative direction as shown in Fig. 1.4. In Fig. 1.4, one may observe that the propagation wave vector k'', of refracted wave progresses towards the interface of LHM and RHM. This indicates that the refracted wave propagates along the backward direction despite the energy travels away from the interface. Due to that the energy velocity, v_e, and phase velocity, v_p both are anti-parallel to each other.

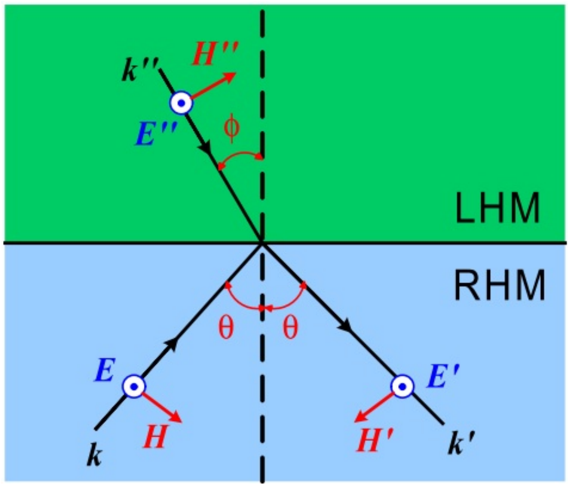

Figure 1.4: The refraction and reflection of an s-polarized EM wave at the interface between a left-handed medium and a right-handed medium. The incident EM wave propagation vector, k, the reflective wave propagation vector, k', and the refractive wave propagation vector, k'', are shown. (*Source*: J. Zhou, Study of left-handed materials, Ph.D. Thesis, Iowa State University Ames, Iowa, 2008.)

1.1.3 Realization of LHM's

Although left-handed materials have been theoretically proposed and studied since a few decades its experimental realization came up recently with the design of Split Ring Resonator (SRR). Sir J. B. Pendry [8] proposed this design which can attain negative permeability, μ, near to its resonance frequency, ω_m. Similarly an array of continuous wires can give negative value of permittivity, ϵ, up to the plasma frequency, ω_p. A composite design of SRR's with continuous wires produces negative value of permittivity and permeability or negative refractive index and the material as a whole then behaves as a left-handed material.

1.1.3.1 Medium of negative permittivity and permeability

In left-handed materials, negative permittivity and permeability can be achieved separately. As explained in section 1.1.2, negative ϵ materials exist in nature. All metals behave as plasma medium and have a negative permittivity, ϵ, up to the plasma frequency. However, solid metals are not utilized in left-handed materials due to their large values of negative permittivity, ϵ, at the working frequencies. So, it is required to scale down the permittivity, ϵ, value of metal to around an order of -1, to make it usable at the desired frequency range. Normally metal permittivity can be described through Drude model [7]:

$$\epsilon(\omega) = 1 - \frac{\omega_p^2}{\omega(\omega + i\omega_c)} \tag{1.20}$$

where ω_p is the plasma frequency and ω_c is the damping frequency given by:

$$\omega_p^2 = \frac{ne^2}{\epsilon_0 m_{eff}} \tag{1.21}$$

where m_{eff} is the effective mass of free electrons and n is the electron density.

In metals, plasma frequency is exceptionally high, for example, silver has $\omega_p = 2\pi \times 2184\ \ THz$ and $\omega_c = 2\pi \times 4.35\ THz$. Due to this, the real value of permittivity is extraordinarily large, Re(ϵ)$< -10^8$ and thus not suitable for left-handed materials. In order to reduce permittivity value, Pendry suggested a continuous wire array design which can reduce the plasma frequency significantly and attain negative permittivity $\epsilon \approx -1$. Furthermore, the value of permittivity and the plasma frequency are fully controllable by geometrical parameters. The wire array design shown in Fig. 1.5(a) consists of periodically arranged long infinite wires of radius r and separated by a lattice constant a. The effective ϵ of the wire array is identical to the bulk metal permittivity despite the much lower plasma frequency. As illustrated in Fig. 1.5(b), below the plasma frequency ω_p, absolute part of permittivity is negative, this region can be used in left-handed materials.

There are two effects which contribute in reducing the plasma frequency of the continuous wire array design. First, the effective electron density, n_{eff} is reduced to a large extent by the factor of the volume employed by the thin metallic wire is very less as compared to vacuum space. The n_{eff} can be calculated by the factor of metal volume and vacuum volume, $n_{eff} = n\pi r^2/a^2$. Secondly, due to the self-inductance of metallic thin wires the electron motion is greatly slowed down [9]. The energy of magnetic field is proportional to $ln(a/r)$ which corresponds to its resultant self-inductance which increases the effective mass of electron greatly. Adding these two effects the plasma frequency, ω_p, of thin wire is manipulated to a much lower value as compared to bulk metal and it given as:

$$\omega_p^2 = \frac{2\pi c_0^2}{a^2 ln(a/r)} \tag{1.22}$$

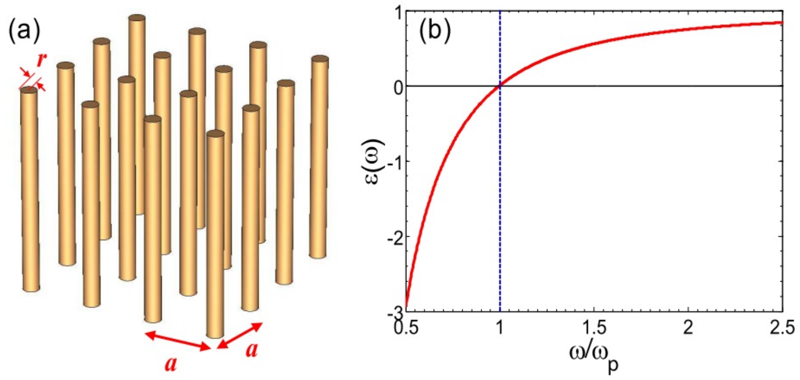

Figure 1.5: (a) The arrays of metallic wires of radius r and distance between wires a. (b) The real value of permittivity, $Re(\epsilon(\omega))$, is plotted as a function of the frequency, ω/ω_p. (*Source*: J. Zhou, Study of left-handed materials, Ph.D. Thesis, Iowa State University Ames, Iowa, 2008.)

From Eq. (1.22), one can easily see that the plasma frequency ω_p, only relies on radius of wire r, and the lattice constant a. By varying these physical parameters one can change the plasma frequency or the value of permittivity.

Though negative permittivity can be attained by metallic structures and other plasma media, one cannot realize a negative refractive index medium as evidenced by the fact that no material present in nature exhibits negative permeability. Pendry in year 1999, proposed a design of Split Ring Resonator (SRR) [8] which produces negative permeability for a narrow frequency spectrum on a particular polarization of incident EM wave. The SRR array is illustrated in Fig. 1.6(a). It consists of periodically organized arrays of two split ring structures built from copper which is a good conductor. A single unit cell as shown in Fig. 1.6(b) have lattice constant a, radius of inner ring, r, the ring width, w, the gap between inner and outer ring, d, and the gap on the inner and outer ring, g_1 and g_2. If incident EM wave is applied with the electric field, E, parallel to the plane of SRR it will induce circulating current in both the rings (inner and outer) and also accumulate charges between the gaps of inner and outer rings. Due to this, each SRR individual unit cell behaves as a series of LRC circuits with capacitance, C, across the gap between the rings and inductance, L, of the rings. The effective permeability, μ_{eff}, can be derived as [9]:

$$\mu = 1 - \frac{A\omega^2}{\omega^2 - \omega_m^2 + i\omega\Gamma_m}, \tag{1.23}$$

$$\omega_m = \frac{3ac_0^2}{\pi ln(2w/d)r^3)}, \tag{1.24}$$

$$\Gamma_m = \frac{2a\sigma}{r\mu_0}, \tag{1.25}$$

$$A = \frac{r^2\Pi}{a}, \tag{1.26}$$

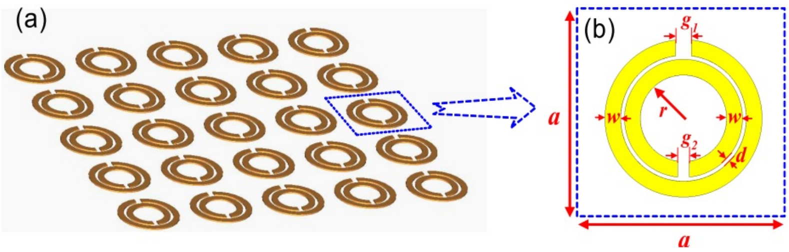

Figure 1.6: (a) The SRRs with recurrence distance, a. (b) Enlarged/Zoomed version of single unit cell. (*Source*: J. Zhou, Study of left-handed materials, Ph.D. Thesis, Iowa State University Ames, Iowa, 2008.)

Here ω_m and Γ_m are the resonance frequency and the damping factor respectively and μ_0 is the permeability in vacuum. Both ω_m and Γ_m are functions of conductivity (σ) of metal and are related to geometric parameters such as, a, w, d and r. The SRRs array effective permeability as a function of frequency is shown in Fig. 1.7. Above resonance frequency, ω_m, the negative value of permeability is attained for a narrow frequency spectrum.

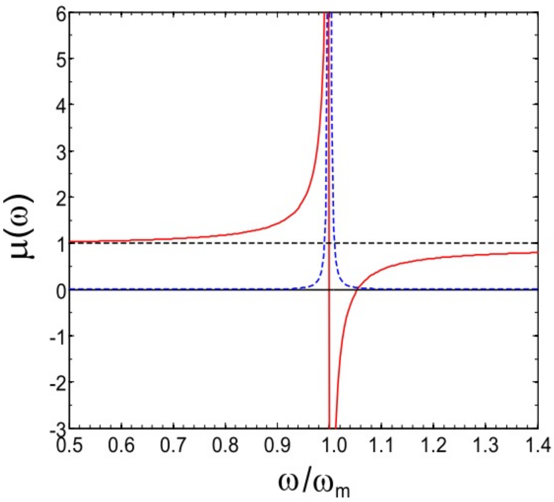

Figure 1.7: The real and the imaginary parts of the permeability, $\mu(\omega)$, are plotted as a functions of the frequency, ω/ω_m, here ω_m is the resonance frequency. The red solid line and blue dashed lines represent respectively the real and the imaginary part of the permeability. (*Source*: J. Zhou, Study of left-handed materials, Ph.D. Thesis, Iowa State University Ames, Iowa, 2008.)

1.1.4 Effective medium theory

The arrays of metallic wire and SRR are responsible for negative permittivity and permeability, respectively. Can we achieve a medium of negative permittivity and permeability through these designs? To investigate this we have to recall the idea of permittivity and permeability. The main objective in characterizing the macroscopic parameters such as permittivity, ϵ, and permeability, μ, of the medium is to exhibit a *homogeneous perspective* of the electromagnetic characteristics of a medium. For example, when EM wave interacts with glass in that scenario visible light wavelength is hundred times larger than the atomic size of which glass is composed. In practice, atomic details can be averaged, and can replace inhomogeneous medium details by homogeneous material characteristics such as permittivity and permeability. Both are macroscopic electromagnetic parameters. From this point of view, normal materials are also composite materials where atoms and molecules are individual constituents and the constituents size is much smaller than EM wave's wavelength [10].

So, a periodic structure having unit cells of dimension, a, can be considered as a homogeneous medium and the EM response of individual unit cell can be regarded as an effective response of the whole structure. Therefore, we can define the limitations for the geometry of the unit cell as,

$$a << \lambda \tag{1.27}$$

If above condition is full-filled, the externally applied EM wave will not see the smaller details of structure inside each unit cell and such periodic arrangement can be assumed as a homogeneous media. In such scenario, permittivity and permeability are legitimate concepts. In case, if this condition is not satisfied the internal structure of the unit cell will refract and diffract EM wave and that leads to material characteristics which are not observed in a homogeneous medium.

1.1.5 Experimental realization of left-handed materials

To realize a material having simultaneous values of negative permittivity and permeability, respectively, a design of the composite structure was proposed combining arrays of metallic rods and SRR, respectively [2]. Composite structure preserves its negative permittivity through metallic rods and negative permeability through SRR element. Presuming that both the structures will not intervene each other, this composite will conserve both the negative permittivity and permeability through long wires and SRR's, respectively. Consequently, the negative refractive index will be achieved. The practical realization of such double negative material was first presented by Smith et al. in 2000 through the design illustrated in Fig. 1.8(a). In this experiment, the transmission was measured through wire array and SRR array individually and merging both the arrays. As illustrated in Fig. 1.8(b) SRR structures having the negative permeability created a stop-band. However, addition of array of wires, converted this stop-band into a passband due to the effective negative values of permittivity and permeability. Later various left-handed material samples were proposed and fabricated which confirmed the existence of LHM's [11–13].

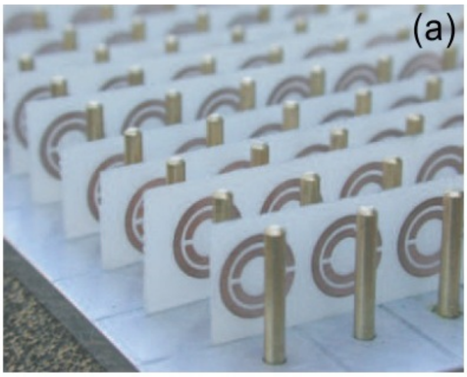

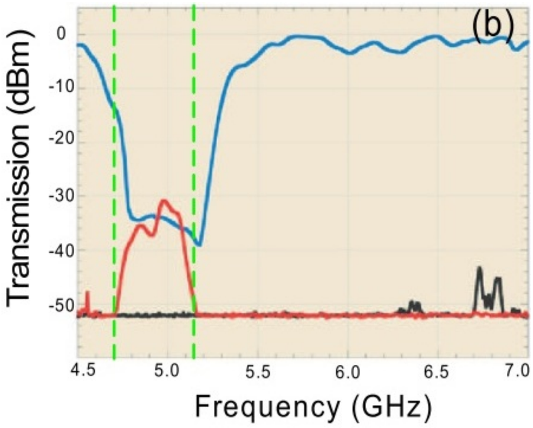

Figure 1.8: (a) Smith et al., used composite LHM which consists of metallic posts and SRRs realized by lithography on a circuit board. (b) The transmission through wires only, SRRs only, and both wires, and SRRs respectively shown by black, blue and red colours. (*Source*: J. Zhou, Study of left-handed materials, Ph.D. Thesis, Iowa State University Ames, Iowa, 2008.)

The negative refraction phenomena were demonstrated by a 2-D left-handed material having prism-like shape [2]. In this demonstration, a microwave beam was incident on the prism and on the other side of the prism transmission of refracted wave was measured. It was observed that refracted wave bent in a negative direction and calculated refractive angle followed the Snell's Law when refractive index, n, was considered to be negative. Other research groups also performed similar experiments on other composite structures which indeed exhibits negative refraction behavior [14, 15].

1.1.6 Chiral metamaterial

Chiral metamaterial is a new class of metamaterials which has been proposed recently to attain negative refractive index through alternative chiral route having additional capability to tailor the polarization state of the incident EM wave. This finds application in many areas including microwave communication, optical communication, contrast imaging microscopy, molecular biotechnology and optical mineralogy. The terminology "chiral structure" describes those structures which lack mirror symmetry in any plane. For a planar chiral structure if its mirror image cannot be superimposed. The size and thickness of unit cell in chiral metamaterial is much smaller than the wavelength of the incident EM wave. It has also been demonstrated that backward wave may propagate in chiral media [16]. The slab of chiral material can focus the beam of the incident wave and can be utilized as a perfect lens [16]. Twisted Swiss-role metal structures and canonical helix are 3D chiral metamaterials that have been proposed in the microwave range in order to realize chiral metamaterial with a feature of negative refraction [17]. However, fabrication of such 3D chiral metamaterial is usually difficult. Meanwhile, the planar chiral geometry was proposed and fabricated from microwave frequency to optical regime [18]. It showed very strong optical activity in the microwave, near-infrared and visible spectrum range. For example in terms of rotary power per wavelength the planar chiral structure has five orders of magnitude as compared to the gyrotropic crystal of quartz in microwave spectral region. It has been demonstrated that the strong optical activity is observed in the structure due to the presence of magnetic resonance which originate from the anti-parallel current in the metallic wires [17].

The electromagnetic characteristics of chiral metamaterial are described in terms of electric and magnetic field cross coupling coefficients. The propagation of electromagnetic wave from this media can be modelled as a reciprocal bi-isotropic media and it obey the following constitutive relations [17]:

$$\begin{pmatrix} D \\ B \end{pmatrix} = \begin{pmatrix} \epsilon_0\epsilon & -i\kappa/c_0 \\ i\kappa/c_0 & \mu_0\mu \end{pmatrix} \begin{pmatrix} E \\ H \end{pmatrix} \tag{1.28}$$

Here μ_0 and ϵ_0 are permeability, and permittivity of vacuum respectively. μ and ϵ are permeability and permittivity of chiral media. κ is chirality that measures the amount of cross-coupling between magnetic and electric field and c_0 is the speed of light in vacuum. The presence of κ will break the degeneracy of two circularly polarized waves. Due to that, in a chiral medium, refractive index of one circularly polarized wave is higher than the other. Assuming time dependence of the form $e^{-i\omega t}$, the left circular polarized (LCP,−) and right circular polarized (RCP,+) wave defined as $E\pm = \frac{1}{2}E_0(\hat{\mathbf{x}} \mp i\hat{\mathbf{y}})$. For LCP and RCP wave the refractive index is [18]:

$$n\pm = \sqrt{\epsilon_r\mu_r} \pm \kappa = n_0 \pm \kappa \tag{1.29}$$

Here (+) and (−) stands for RCP and LCP. The impedance is same for both LCP and RCP wave and is given by $z/z_0 = \sqrt{\mu/\epsilon}$, where z_0 is the vacuum impedance.

From Eq. (1.29) it can be observed that if chirality κ is strong enough for one circularly polarized wave, even if the values of ϵ_r and μ_r are positive, refractive index may become negative while for other circular polarized wave it may remain positive. The value of polarization azimuth rotation angle θ is proportional to chirality κ, where $\theta = \kappa k_0 d$. Here d and k_0 are the thickness of slab and wave vector in the vacuum.

Thus, the chiral material exhibits large rotary power such as bilayer chiral structures and this will raise the value of chirality, κ. Such a large value of κ will increase the possibility to possess negative refraction in a chiral material. In recent studies, the negative refraction has been confirmed experimentally on bilayer rosette structure [16].

1.1.7 Hyperbolic metamaterial

Hyperbolic Metamaterial (HMM) is another prominent category of the metamaterials. It is a uniaxial and non-magnetic material which merges the reflection properties of metals and transparent properties of dielectrics [19]. HMM can be considered as a polaritonic crystal where merged states of light and matter give rise to electromagnetic state density. Now a days HMM (also known as indefinite index media) provides metamaterial a viable platform in order to realize it in optical and high-frequency spectrum. Some hyperbolic composites having hyperbolic dispersion were realized experimentally from near-IR to far-IR and from UV to visible frequencies spectrum [20]. Sub-diffraction imaging, negative refraction, sub-wavelength modes, lifetime engineering and spontaneous engineering are some applications of HMM's [19]. The possible emerging applications of hyperbolic metamaterial in heat transport and acoustics makes this area of great interest among the research community [21].

The name Hyperbolic metamaterials evolves from the isofrequency surface topology. In free-space, the isotropic and linear dispersion behavior of EM wave signifies a spherical isofrequency surface. It can be described by the relation $k_x^2+k_y^2+k_z^2 = \omega^2/c^2$ and is shown in Fig. 1.9(a). Here $k = [k_x, k_y, k_z]$ is wavevector, ω is radiation frequency and c is the light velocity in free space. If the considered medium is a uniaxial and propagating wave is an extraordinary wave (TM wave) then, the isofrequency relation is modified to [19]:

$$\frac{k_x^2 + k_y^2}{\epsilon_{zz}} + \frac{k_z^2}{\epsilon_{xx}} = \frac{\omega^2}{c^2} \tag{1.30}$$

In an uniaxial media the tensor dielectric permittivity can be written as $\epsilon = [\epsilon_{xx}, \epsilon_{yy}, \epsilon_{zz}]$ here $\epsilon_{xx} = \epsilon_{yy} = \epsilon_{\|}$ are in-plane components and $\epsilon_{zz} = \epsilon_{\perp}$ is the out of plane component. The free-space spherical isofrequency surface modifies to an ellipsoid for the

HMM case.

If the medium is extremely anisotropic such that $\epsilon_{\parallel}.\epsilon_{\perp} < 0$, then the isofrequency surface becomes open hyperboloid as shown in Fig. 1.9(b, c). This requires that material should behave like a dielectric in one direction and metal in other direction. Such kind of material is not readily available in nature in the optical spectrum. However, it can be realized through nanostructured artificial media.

HMM can be classified in two categories: Type-I and II. In Type-I category, one element of dielectric tensor is negative ($\epsilon_{zz} < 0; \epsilon_{xx}; \epsilon_{yy} > 0$) shown in Fig. 1.9(b) but in case of Type-II HMMs two elements of dielectric tensor are negative ($\epsilon_{zz} > 0; \epsilon_{xx}; \epsilon_{yy} < 0$) shown in Fig. 1.9(c). If all elements of dielectric tensor are negative or positive in that case it behaves like metal or a dielectric respectively. The Type-I HMM is less reflective than Type-II because it is less metallic than its type-II counterpart.

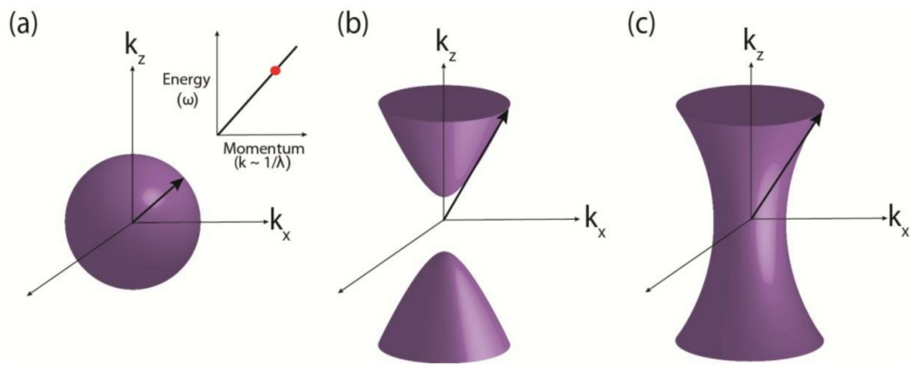

Figure 1.9: The topology of k-space. (a) For free-space spherical isofrequency surface. (b) For uniaxial extremely anisotropic media (HMM Type-I:$\epsilon_{zz} < 0; \epsilon_{xx}; \epsilon_{yy} >$ 0) hyperboloid isofrequency surface.(c) For uniaxial extremely anisotropic media (HMM Type-II:$\epsilon_{zz} > 0; \epsilon_{xx}; \epsilon_{yy} < 0$) hyperboloid isofrequency surface. (*Source*: P. Shekhar, J. Atkinson and Z. Jacob, Hyperbolic metamaterials: fundamentals and applications,Nano Convergence, 2014.)

1.1.7.1 Realization and materials

There are two realistic ways to attain hyperbolic dispersion. For the purpose of hyperbolicity, it requires metallic characteristics in one direction and dielectric characteristics in the other. Therefore a building block of HMM must contain both metal and insulator materials. Microscopically metal building block originate propagating high-k modes which are responsible for hyperbolic dispersion of the material. The metal building block has properties of polaritonic which permit light-matter coupling to create high-k waves. For hyperbolic metamaterial phonon-polaritonic or plasmon-polaritonic metal is necessary. The coupling of near-field surface plasmon polaritons (SPPs) at each interface of a metal-dielectric results in high-k modes. In dielectric-metal, superlattice produced high-k modes are called Bloch modes.

There are two ways to construct HMM either 1D HMM or 2D HMM [19]. The 1D HMM consists of multilayer alternative disks of metal and dielectric as shown in Fig. 1.10(a). For homogenization operating wavelength should be far greater than the layer thickness. For attaining hyperbolic behavior in distinct wavelength regimes a broad choice of high index dielectrics and plasmonic metals are available. Gold and silver with alumina is an excellent selection for the HMM in ultraviolet (UV) frequency spectrum. The plasma frequencies of those metals lie in UV range. Near to the plasma frequency reflectivity of those metals decreases and the super-lattice of metal-dielectric attains high transmission with Type I HMM. Near-infrared (IR), gold and silver exhibits highly reflective metallic behavior and are not suitable. Therefore, other plasmonic materials, engineered with lower plasma frequencies through doping are utilized.

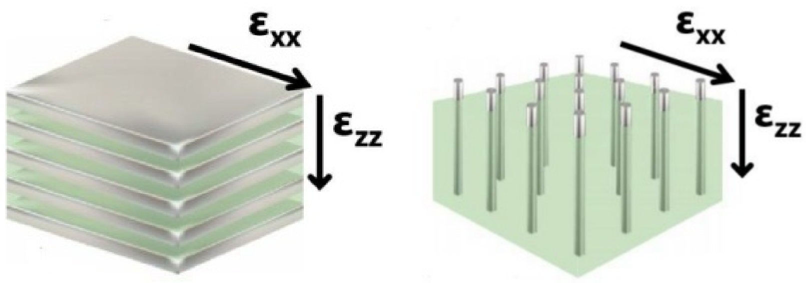

(a) (b)

Figure 1.10: (a) Alternate layers of metals and dielectrics. Creating a multilayer geometry which has superlattice of metal-dielectric. (b) Dielectric host embedded by metallic nanorods structure. (*Source*: P. Shekhar, J. Atkinson and Z. Jacob, Hyperbolic metamaterials: fundamentals and applications,Nano Convergence, 2014.)

The 2D HMM is an another way of attaining hyperbolic behaviour. It consists of dielectric host having metallic nanorods. Silver and gold metals are usually used for nanorods and alumina is used as dielectric host. High transmission, low losses and wide bandwidth are the key advantages of this design. Also the large reflectivity problem of 1D HMM does not exist in this design.

1.2 The Helix

The Helix is a well-known waveguide structure of Microwave engineering which was invented by R.Kompfner [5]. From earliest times it is utilized as a slow wave structure in traveling wave tubes. It is also used in backward-wave oscillators and all low and medium power traveling wave amplifiers [22]. Helix is also utilized in high-frequency delay lines and highly directive broadband antennas [5].

The helical structure is shown in Fig.1.11(a) and is made up of a metallic wire with a radius, a, and the periodicity or pitch of winding, p, the diameter of the wire is δ. In Fig. 1.11(b), the expanded view of the helix is shown. The pitch angle, ψ, is a ratio of the pitch, p, and circumference, $2\pi a$,

$$tan(\psi) = \frac{p}{2\pi a} \tag{1.31}$$

Initially it was believed that an EM wave propagates along the metallic wire of

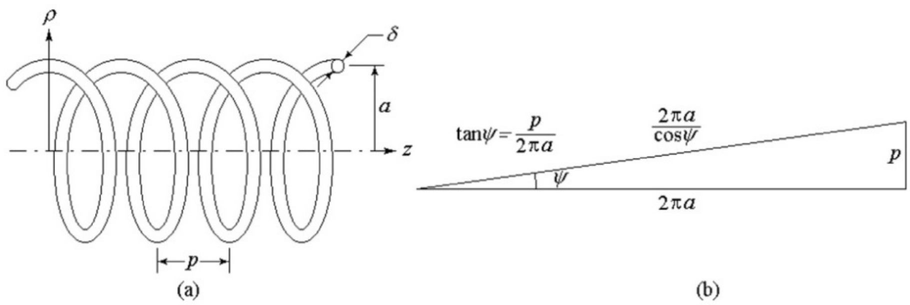

Figure 1.11: (a) the helix and (b) its expanded view

helix with the speed of light c and its velocity in z direction is the ratio of helix pitch (p) to $2\pi a/cos(\psi)$ times the speed of light (c) [5],

$$v_z = \frac{p}{2\pi a/cos(\psi)}c = sin(\psi) \tag{1.32}$$

This is the famous *Helical wave model* which is the simplest model of helix. As per this model the system is non-dispersive and v_z is not dependent on frequency. This approximation is correct in the regime of high frequencies. However in the regime of lower frequencies a practical helix becomes a dispersive system [5].

The boundary conditions of helix are skewed and complicated and difficult to deal with, in order to find the solutions of field. Therefore, different authors have proposed different physical models [5]. Among them most used and popular models are *sheath helix model* [22] and *tape helix model* [22].

1.2.1 The sheath helix

The sheath helix physical abstraction is proposed by J. R. Pierce and is derived from the solutions of Maxwell's equations which exhibits many of the characteristics close to an actual helix. The sheath helix is an infinitesimally thin cylindrical surface, which conducts only in helical direction, as shown in Fig. 1.12. The sheath is conducting perfectly with the plane perpendicular to the axis in a direction making an angle ψ, but it is not conducting in normal to the direction of conduction. A physical closeness of this model could be obtained by considering a flat tape of width p, wound in a cylindrical form of radius a and each winding being wound next to each other.

Further, it is assumed that the number of wires is infinitely large and spacing between wires is infinitesimal. In these limits, wires can be replaced by sheet or sheath which conducts only in the direction of wire and the structure can be considered as perfect sheath helix. This model is reported to be a good approximation to the actual helix when there are large number of turns per guided wavelength,

$$\frac{\lambda_z}{2} >> p, \quad i.e., \quad \beta p << \pi \tag{1.33}$$

These conditions are explicitly required when the validity of uniform system is assumed.

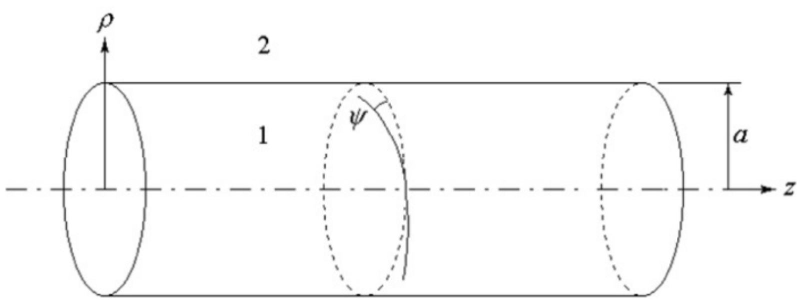

Figure 1.12: The sheath helix

1.2.1.1 Boundary conditions

On the surface of sheath helix three boundary conditions are applicable. A boundary representative view of helix is shown in Fig. 1.13(a), where || and $\perp$ denotes the components parallel and normal to the helical wire direction receptively. At $\rho = a$, the conditions are as follows. On the surface tangential component of the electric field must be zero because conductivity is assumed to be infinite in that direction. This is expressed as:

$$E_{||1}(a) = 0, \qquad E_{||2}(a) = 0 \tag{1.34}$$

and the normal component to the direction of conduction is continuous:

$$E_{\perp 1}(a) = E_{\perp 2}(a) \tag{1.35}$$

In the conduction direction magnetic field component must be continuous because there is no surface current normal to magnetic field

$$H_{||1}(a) = H_{||2}(a) \tag{1.36}$$

The axial and azimuthal components, z and ϕ are related by following relations and illustrated in Fig. 1.13(b).

$$\begin{aligned} E_{||} &= E_z sin\psi + E_\phi cos\psi, \qquad & E_\perp &= E_z cos\psi - E_\phi sin\psi, \\ H_{||} &= H_z sin\psi + H_\phi cos\psi, \qquad & H_\perp &= H_z cos\psi - H_\phi sin\psi, \end{aligned} \tag{1.37}$$

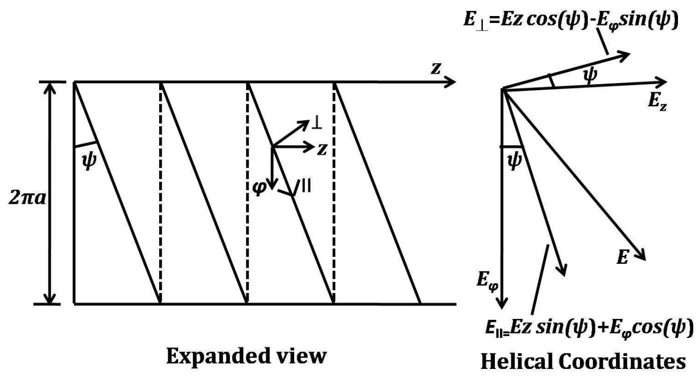

Figure 1.13: The developed view of sheath helix and the helical coordinate.

Then in terms of field components the boundary conditions (1.34) to (1.36) can be rewritten as:

$$E_{z1} sin\psi + E_{\phi 1} cos\psi = 0, \tag{1.38}$$

$$E_{z2} sin\psi + E_{\phi 2} cos\psi = 0, \tag{1.39}$$

$$E_{z1} cos\psi - E_{\phi 1} sin\psi = E_{z2} cos\psi - E_{\phi 2} sin\psi, \tag{1.40}$$

$$H_{z1} sin\psi + H_{\phi 1} cos\psi = H_{z2} sin\psi + H_{\phi 2} cos\psi, \tag{1.41}$$

1.2.2 The tape helix

In sheath helix model the biggest assumption is that helix is modeled as a cylinder and the air gap between the windings is not taken into account. Also, the sheath helix does not model the periodic behavior of the helix. In the tape helix these two assumptions have been taken into account and it was first investigated by Sensiper. It consists of thin metal ribbon wounded in the form of a helix. The width of the tape is, δ, as shown in Fig. 1.14. The thickness of the tape is zero and it considered to be infinitely conducting. The helix radius is, a, the helix pitch is p and pitch angle is:

$$tan(\psi) = \frac{p}{2\pi a} \tag{1.42}$$

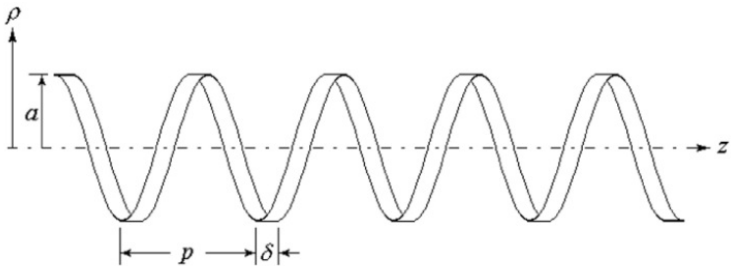

Figure 1.14: The tape helix

If a helix, as illustrated in Fig. 1.14, moves in z direction by a distance p then features of helix remain invariant. Also, if the helix is rotated by an angle θ (it can be considered to have moved by a radial distance of $p\theta/2\pi$) the helix features again remain invariant in this case. This periodic nature of helix puts some limitations on the nature of solutions. Cylindrical polar coordinate system is utilized in this context. If the solution of electric field is $E_1(r,\phi,z)\ e^{-i\beta(p\theta/2\pi)}$ then $E_1(r,\phi+\theta,z+p\theta/2\pi)$ is also a solution. It can be seen that due to periodic nature of helix the points (r,ϕ,z) and $(r,\phi+\theta,z+p\theta/2\pi)$ are indistinguishable from each other. The term $e^{-i\beta(p\theta/2\pi)}$ is the propagation vector of the wave. The solution of electric field $E_1(r,\phi,z)$ is periodic in the z direction with periodicity p (propagation vector $e^{-i\beta z}$ is not included) and it is also periodic in ϕ direction. Therefore, in terms of double Fourier series E_1 can be expressed as [5],

$$E_1(r,\phi,z) = \sum_{m=-\infty}^{\infty}\sum_{n=-\infty}^{\infty} E_{1,mn}(r)e^{-im\phi-i2n\pi z/p}e^{-i\beta z} \tag{1.43}$$

Here $E_{1,mn}(r)$ is a vector function of r. It is necessary that $E_{1,mn}(r)e^{-i\beta z}$ remains unchanged when ϕ and z are replaced by $\phi+\theta$ and $z+p\theta/2\pi$. Therefore

$$e^{-im\phi-i2n\pi z/p} = e^{-im(\phi+\theta)-i2n\pi(z+p\theta/2\pi)/p} \tag{1.44}$$

The above condition is satisfied if $m=n$. Then Fourier series is reduced to single summation,

$$E_1(r, \phi, z) = \sum_{n=-\infty}^{\infty} E_{1,n}(r) e^{in\phi} e^{-i\beta_n z} \tag{1.45}$$

where

$$\beta_n = \beta_0 + \frac{2\pi n}{p} \tag{1.46}$$

1.2.2.1 Boundary conditions

For an ideal conducting tape helix, the boundary conditions at $\rho = a$ are as follows.

1. For all ϕ and z, the tangential component of the electric field is continuous.
2. The interruption in a tangential component of magnetic field is equivalent to the density of surface current having its direction perpendicular to the magnetic field.
3. On the tape surface, tangential component of the electric field is zero.

For above conditions, mathematical expressions are written as follow [5].

$$E_{z1}(a) = E_{z2}(a), \tag{1.47}$$

$$E_{\phi 1}(a) = E_{\phi 2}(a), \tag{1.48}$$

$$H_{z2}(a) - H_{z1}(a) = -J_{s\phi}(a), \tag{1.49}$$

$$H_{\phi 2}(a) - H_{\phi 1}(a) = J_{sz}(a), \tag{1.50}$$

$$E_t(a) = 0, \quad for \quad \frac{p\phi}{2\pi} - \frac{\delta}{2} \; < \; z \; < \; \frac{p\phi}{2\pi} + \frac{\delta}{2} \tag{1.51}$$

Here 1 and 2, denotes region 1 ($\rho \leq a$) and region 2 ($\rho \geq a$), respectively. On the surface $\rho = a$ and $E_t(a)$ represents tangential component of electric field, $J_{s\phi}(a)$ and

$J_{sz}(a)$ are densities of surface current on the surface in the directions of ϕ and z, respectively.

1.3 Slow Wave Applications, Background and Motivation for Present Thesis Work

Slow Wave is an emerging area of research which promises many potential applications in the field of future Optical Communication Networks (OCN), Microwave Photonics (MWP), Communication Networks etc. A device that can slow or even stop the EM wave is very much in demand, nowadays, since they can dynamically control the flow of EM wave [34]. Such Slow Wave Devices (SWD's) are designated as Optical Buffers (OB's) or Variable delay optical lines [35]. These devices have emerged as key elements for future OCN's and information processing systems. In order to realize future OCN architecture, the Optical Data Packet Switching (ODPS) is highly desirable. For ODPS, it is necessary to synchronize incoming data packets and regulate data traffic at network nodes or to implement congestion and contention resolution in the core routers. Nowadays, electrical routers perform these operations through large banks of Static Random Access Memory (SRAM). In future this activity will be performed by optical buffers. As compared to electric buffer the main advantage of an optical buffer is its low cost. In ODPS the cost per bit transmission of data is less as compared to its electric counterpart which makes it more desirable. Therefore, the optical buffer should have low heat production, low power consumption and a small footprint. Hence extensive research is going on to realize equivalent optical data packet switching (ODPS). For the purpose of a flexible optical buffer, it is required that buffer should be transparent for packet length and provides the dynamic delay. It is also required that the buffer should have low dispersion and optical power loss [34].

As described, optical buffers and memories are the key components to realize ODPS. The mechanism of slow wave is vital for the development of such devices. The application of optical memories, optical buffers and delay lines ranges from optical storage, optical data processing, optical delay line, filters, phase shifter to microwave photonics (MWP) devices. MWP is another emerging area of research where photonics is involved in order to process microwave signals. The slow wave structures in MWP enables synchronizing the time delay or phase shift of microwave signal which modulates the optical carrier. Slow wave devices also cater to other potential applications such as [35]

- Noise reduction
- Advanced time-domain signal processing
- Clock resynchronization
- Pulse compression
- More sensitive interferometers
- Enhancing linear and nonlinear effects
- Particle acceleration

It is a well-known fact that the wave velocity or group velocity is dependent on the dispersion characteristics of the medium. For slow wave or reduced group velocity, a medium should have sharp spectral characteristics which cause large dispersion. There are two possible ways to introduce dispersion in a device either by introducing a material or from structural aspect. Therefore, various proposed slow wave schemes are broadly classified in two categories (1) material induced dispersion or (2) structure induced dispersion. The conventional methods such as electromagnetically induced transparency [23], quantum-dot semiconductor optical amplification [24], coherent population oscillation [25] and stimulated Brillouin scattering [26] come in the category of material induced dispersion. Usually, these methods are less preferred at room temperatures due to their strong temperature dependence and other inherent limitations [27]. For instance, quantum-dot semiconductor optical amplifiers produce very small delays, Electromagnetic induced transparency requires ultracold atomic gasses, stimulated Brillouin scattering and coherent population oscillations have very narrow bandwidths. Usually, at room temperatures, structure induced dispersion methods are preferred because these methods are independent of temperature and at the same time they are easier to implement. Photonic crystals (PC's) and surface plasmon polaritons (SPP's) based methods fall in the category of structure induced dispersion. However, PC's based methods have inherent issues of high multimode generation and strong impedance mismatch in the slow light regime. This makes it difficult to launch light energy in a single mode. On the other hand, SPP's are very sensitive to surface roughness and its excitation is also difficult [27].

Recently, some research groups have proposed Slow Wave Devices (SWD's) based on metamaterials. In the last few years, metamaterials have shown immense potential in many areas of science and technology. Their extraordinary features and applications have generated enormous research interest among various research groups around the world in exploiting such properties for different engineering as well as physical sciences applications. The feature of slow wave with Metamaterials was first investigated by Tsakmakidis et al. [27] where they established connection between two modern realms of sciences, slow wave and metamaterial by proposing an axially varying three-layer planar heterostructure composed of metamaterial (negative index or left-handed material) core and dielectric (positive index or right-handed material) cladding. They explained the phenomenon of slowing and trapping of the wave by negative Goos-Hanchen lateral displacement at the interfaces of different media where the different thickness of linearly tapered waveguide correspond to different propagating frequencies guided fields stop, which they named "trapped rainbow"effect. Later different research groups around the world have proposed various slow wave structures by utilizing metamaterial properties [28–33].

Suwailam et al. [28] studied the EM wave propagation characteristics of a metamaterial slab waveguide and they found that both TM- and TE- modes travel with speed less than the speed of light. A similar observation was also reported by Erfaninia et al. [29], where they found that group velocity is greatly reduced in multilayered metamaterial waveguide. Savo et. al. [30] reported, experimentally, slow-light in GHz regime through the mechanism of mode degeneracy in a planar metamaterial waveguide. The waveguide consists of a core of dielectric material and a cladding of single negative material realized by the periodic arrangement of split ring resonators. Gennaro et. al. [31] experimentally demonstrated the propagation of a remarkably slow wave in GHz regime from metamaterial waveguide. The waveguide was made of interleaved periodic arrays of split ring resonators and metallic wires. He et al. [32] studied dielectric slab waveguide having metamaterial substrate and reported propagation of slow wave inside the guide. Huang et al. [41] studied anisotropic metamaterial cylindrical guide and observed that EM wave can be slowed and even stopped inside the waveguide. Jiang et al. [33] investigated an air waveguide with anisotropic metamaterial cladding and reported slowing and stopping of the wave inside the waveguide.

From the above mentioned studies, it can be concluded firmly that the presence of metamaterial medium can be used to slowed down the EM wave. In microwave engineering helical waveguides also have the inherent characteristics of slow wave due to its skewed boundary conditions. For a long time it has been widely used as a slow wave device over a wide bandwidth in Travelling Wave Tubes [22], Backward Wave Oscillators [22] and Helical antennas [5].

In present thesis work, we have proposed different Helical Slow Wave Devices (SWD's). The first objective is to investigate the characteristic of a helical guide when its characteristics are superimposed with metamaterial properties. In literature, most of the studies are related to planar [27–29, 36–39] as well as cylindrical [40, 41] waveguides where complex mode behavior has been studied in the context of different applications. Very few investigations are found on helix structure and to the best of our knowledge no one has investigated the helical structure with metamaterial with prospective application in the field of optoelectronics and microwave photonics.

The second objective is to explore the effect on **Slow Wave** when helical guide slow wave behaviour is superimposed with metamaterial properties. As described above both the structures have slow wave characteristics. Additionally helical waveguide has a comparatively wider bandwidth.

1.4 Organization of Thesis

This research work includes analysis and design of novel helical slow wave devices embedded with metamaterial medium for optoelectronics as well as microwave photonics applications. For each proposed structure analytical characterization as well as their possible engineering feasible design is presented and discussed. The complete description of research work is organised as follows:

In **chapter-2**, the dispersion characteristics of a left-handed material (LHM) or Metamaterial Loaded Helical Guide (MLHG) are analytically solved and numerically computed for different metamaterial medium properties as well as helical guide parameters. The modal behaviour of this structure has been studied with an aim to achieve ultra slow wave over wide bandwidth which finds potential applications in optical switches and memories for optical processing. Significant amount of phase velocity reduction has been achieved in comparison to free space or loaded with normal dielectric column. Other modal properties such as presence of two fundamental modes - backward and forward wave and their lower cut-off frequencies (LCF) as well as bandwidth spectrum are also discussed thoroughly.

In **chapter-3**, we study propagation characteristics of dispersive Metamaterial Loaded Helical Guide (DMHG). As compared to MLHG structure, described in chapter-2, here the considered metamaterial medium is dispersive in nature. Non-dispersive metamaterial medium has not been successfully realized so far. The motivation behind this study is to analyze and present the actual design of DMLHG structure that has capability to slow or even trap the EM wave.

Considered metamaterial dispersive behaviour is described through Drude model [59]. Analytical-computational characterizations of DMLHG structure have been done to visualize various modal characteristics of the structure. It is observed that metamaterial insertion enhances helical guide slow wave behaviour and supports forward wave (FW), backward wave (BW) as well as mode degeneracy. Obtained mode degeneracy mechanism leads to trapping of EM wave. In order to realize proposed DMLHG structure, we present two possible designs. A novel FF-shaped metamaterial cell has been characterized and proposed in order to realize dispersive nature inside the helical guide. The S-parameters of the designed FF-shape structures are obtained from electromagnetic simulation and have been used to extract effective permittivity and permeability values. It is observed that the structure simultaneously exhibits negative permittivity and permeability values over a wide frequency range. An experiment has also been performed with an aim to verify the transmission parameters of the conceived FF-shaped metamaterial cell.

The simulation results verify the presence of characteristics observed in analytical study such as FW, BW and mode-degeneracy, but with slightly shifted frequency spectrum.

In **chapter-4**, we have investigated, Epsilon Negative (ENG) Cladded Metamaterial Loaded Helical Guide Structure (CMLHG). The motive behind this study is: (i) to design and realize a slow-wave delay line in the form of optical fibre/cable and (ii) to avoid external interference by introducing cladding in the structure. For ENG-CMLHG structure, analytical equation has been derived and computed numerically to analyze its dispersion characteristics in the THz frequency spectrum. Significant amount of phase velocity reduction is achieved in comparison to the helical guide when (i) it is in free space and not cladded (ii) it is cladded with doubly positive material and loaded with metamaterial. We have also reported that helical waveguide physical dimensions ((mainly radius and pitch angle) act as tuning tools to control the phase velocity. The Electric field intensity distribution over the cross section of the waveguide has also been studied which shows that as the frequency increases the electric field distribution is more confined to the core region of the waveguide.

In **chapter-5**, we report slow wave propagation characteristics of Extremely Anisotropic Metamaterial Loaded Helical Guide (EAMLHG). The motivation behind using Extremely Anisotropic Metamaterial is to overcome the fabrication limitations of DMLHG structure for high frequency spectrum (THz to visible).

An analytical expression has been theoretically derived and numerically computed to get exact solutions of all possible guided modes of propagation. Anisotropy is defined in terms of positive longitudinal permittivity and negatives transverse permittivity. The waveguide supports Hybrid (HE) mode propagation and possesses characteristics of Backward Wave (BW) mode, Forward Wave (FW) mode, zero-group velocity and mode-degeneracy. The large value of effective index of BW mode and mode-degeneracy mechanism leads to slowing and trapping of EM wave. Closed-form guided mode energy propagation expression has been also derived and computed which exhibits zero power for the mode degeneracy point. These types of waveguides can be used as filter, phase shifter and optical buffer in optoelectronics applications as well as in microwave circuits.

In **chapter-6**, we have summarized and concluded the thesis research work and the possible directions of future proposed works is also discussed.

Chapter 2

Metamaterial Loaded Helical Guide*

2.1 Introduction

Enormous research interest has been shown by different research groups [42–46] [28, 52, 53] around the world to exploit the exotic properties of metamaterial for different engineering as well as physical science applications [54–58]. One such application is to find out the electromagnetic complex mode behaviour and wave steering properties (also called dispersion engineering) of different electromagnetic structures when these structures are either embedded with metamaterial or the structure itself is made up of metamaterial. There are a number of such investigations reported in the literature. Cory et al. [42] studied surface wave propagation along metamaterial cylindrical guide for both real and imaginary transverse wave-numbers and found that transverse propagation coefficient of first TEz and TMz mode could be real or imaginary. Shu et al. [43] studied surface wave propagation in the grounded metamaterial slab in which they discussed about complex wave and evanescent surface

*This work has been published in *Progress In Electromagnetics Research M*, Vol. 35, 11-19, 2014.

wave mode. They observed that the value of normalized effective dielectric constant (ϵ_{eff}) for evanescent surface wave mode is high as compared to $\epsilon_{ri}\mu_{ri}$ (inside) and $\epsilon_{ro}\mu_{ro}$ (outside). Cory et al. [44] studied metamaterial slab guide and observed that it can be used as a filter due to the appearance of band-pass region. Bae et al. [45] studied the guided mode in metamaterial slab having a real and imaginary transverse wave number. They found that cut-off exists for all modes in real transverse wave number, and guided modes are also present in imaginary transverse wave number. Baccarelli et al. [46] studied metamaterial grounded slab and presented condition for suppression of proper surface wave (ordinary and evanescent surface wave) that made the considered structure a good candidate for planer antenna substrate. Ruppin [47] studied the surface polaritons modes of a semi-infinite left-handed medium and demonstrated how they can be observed using the attenuated total reflection (ATR) technique. Darmanyan et al [48] studied the properties of surface EM wave at the interface of left-handed and conventional medium, and they observed that both p- and s- surface wave modes do not coexist in the same frequency range. They also calculated surface modes Poynting vector, density of energy and velocity of energy transfer. Kats et al [49] also studied the EM surface wave at the interface of left-handed medium and demonstrated that 2D interfaces separating 3D metamaterial can exhibit properties of 2D left-handed media for surface waves. They found that the total energy flux and group velocity of these waves are anti-parallel to the phase velocity. Leskova et al [50] [51] studied scattering of an EM wave from, and its transmission through a slab of random surface of a left-handed medium. Engheta [52] presented an idea of phase compensator using metamaterial in thin sub wavelength cavity.

In this Chapter, Metamaterial Loaded Helical Guide (MLHG) is proposed and studied as Slow wave Device (SWD). As described in Chapter-1, Metamaterial and Helical guide both possess the characteristics of slow wave. The objective of the present investigation is to study the effect on slow wave characteristics when helical guide slow wave behaviour is superimposed with metamaterial properties.

2.2 Dispersion Relation

The structure used for analysis is a sheath helix of radius a and pitch angle ψ as shown in Fig. 2.1. The diameter of the wires is infinitesimally small and infinite number of wire in a tape is assumed. Spacing between adjacent wires is very small at the same time they are insulated with each other. It conducts only in a direction making an angle ψ with the plane tangential to the axis [22]. Region-I is metamaterial media, which is assumed to be non-dispersive, isotropic and homogeneous and region-II is free space.

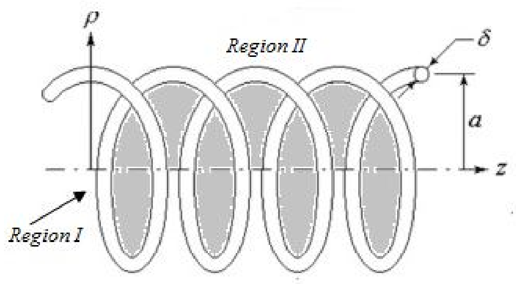

Figure 2.1: Helix of radius $'a'$, Region-I (inner region) is metamaterial medium and Region-II (outer-region) is free-space.

The Borgnis' potentials for metamaterial loaded helical guide of radius $\rho = a$ and for $e^{jn\phi}$ turn variations are written as [22]:

$$U_i = A_{n,i}C_{n,i}(k_i\rho)e^{jn\phi}e^{-j\beta z} \tag{2.1}$$

$$V_i = B_{n,i}C_{n,i}(k_i\rho)e^{jn\phi}e^{-j\beta z} \tag{2.2}$$

Here, $i = 1$ for region-I ($\rho < a$) and $i = 2$ for region-II ($\rho > a$). A_i and B_i are field coefficients, $C_{n,i}$ is needed Bessel function of order n, which describe modal behaviour of the wave.

The field equations in two regions are written as:

$$E_{z,i} = -k_i^2 A_i C_{n,i}(k_i\rho) e^{jn\phi} e^{-j\beta z} \tag{2.3}$$

$$E_{\rho,i} = [-j\beta \mathrm{k_i} A_i C'_{n,i}(k_i\rho) + \frac{\omega\mu_i \mathrm{n}}{\rho} B_i C_{n,i}(k_i\rho)] e^{jn\phi} e^{-j\beta z} \tag{2.4}$$

$$E_{\phi,i} = [\frac{n\beta}{\rho} A_i C_{n,i}(k_i\rho) + (j\omega\mu_i k_i) B_i C'_{n,i}(k_i\rho)] e^{jn\phi} e^{-j\beta z} \tag{2.5}$$

$$H_{\mathrm{z,i}} = -{k_i}^2 B_i C_{n,i}(k_i\rho) e^{jn\phi} e^{-j\beta z} \tag{2.6}$$

$$H_{\rho,i} = \left[\frac{-\omega\epsilon_i n}{\rho} A_i C_{n,i}(k_i\rho) - j\beta k_i B_i C'_{n,i}(k_i\rho)\right] e^{jn\phi} e^{-j\beta z} \tag{2.7}$$

$$H_{\phi,i} = \left[-j\omega\epsilon_i k_i A_i C'_{n,i}(k_i\rho) + \frac{n\beta}{\rho} B_i C_{n,i}(k_i\rho)\right] e^{jn\phi} e^{-j\beta z} \tag{2.8}$$

Here, $(')$ is derivative of Bessel function with respect to its argument. ϵ_1 and μ_1 are media parameters of region-I and are negative real numbers. ϵ_2 and μ_2 are positive real numbers. k_1 and k_2 are transverse wave numbers for region-I and region-II respectively, β is the longitudinal phase coefficient. Relation between k_i and β is given by the equation:

$$k_i = \sqrt{\beta^2 - {k_{\mathrm{oi}}}^2} \tag{2.9}$$

Here, k_{oi} $(= \omega\sqrt{\epsilon_i\mu_i})$ is the propagation vector. For guided mode propagation, field in region-II should decay exponentially in the transverse direction. Due to that $C_{n,2}(k_2\rho)$ is replaced by modified Bessel function of second kind $K_n(k_2\rho)$. Due to skewed boundaries, helical guide supports slow wave prorogation. Therefore, $C_{n,1}(k_1\rho)$ is replaced by modified Bessel function of first kind $I_n(k_1\rho)$.

At boundary $(\rho = a)$, electric field is continuous in the direction of propagation and magnetic field is continuous normal to the direction of propagation. In terms of ϕ

and z, boundary conditions for the helical guide at $\rho = a$, are written as [5]:

$$E_{z,1} = E_{z,2} \tag{2.10}$$

$$E_{\phi,1} = E_{\phi,2} \tag{2.11}$$

$$E_{z,1} = -E_{\phi,1} cot(\psi) \tag{2.12}$$

$$E_{z,2} = -E_{\phi,2} cot(\psi) \tag{2.13}$$

$$H_{z,1} + H_{\phi,1} cot(\psi) = H_{z,2} + H_{\phi,2} cot(\psi) \tag{2.14}$$

The field expressions from Eqs. (2.3) to (2.8) are substituted into the corresponding boundary conditions in Eqs. (2.10) to (2.14) and a set of four linear homogeneous equations with four unknown constants A_1, A_2, B_1 and B_2 are obtained. A non-trivial solution of the fields exists only if the 4×4 determinants formed by the coefficients of the unknown constants in the set of equations vanishes. The obtained determinant is:

$$\begin{vmatrix} m_1 & m_2 & 0 & 0 \\ 0 & 0 & m_3 & m_4 \\ m_5 & m_6 & m_7 & m_8 \\ m_9 & m_{10} & m_{11} & m_{12} \end{vmatrix}$$

where,

$m_1 = \left(-k_1^2 \sin(\psi) + \frac{n\beta}{a} \cos(\psi)\right) I_n \left(k_1 a\right)$

$m_2 = j\omega\mu_1 k_1 \cos(\psi) I_n' \left(k_1 a\right)$

$m_3 = \left(-k_2^2 \sin(\psi) + \frac{n\beta}{a} \cos\psi\right) K_n \left(k_2 a\right)$

$m_4 = j\omega\mu_2 k_2 cos(\psi) K_n'(k_2 a)$

$m_5 = (k_1^2 cos(\psi) + \frac{n\beta}{a}\ sin(\psi)) I_n(k_1 a)$

$m_6 = (j\omega\mu_1 k_1 \sin\psi) I_n' (k_1 a)$

$m_7 = -\left({k_2}^2 \cos\psi + \frac{n\beta}{a} \sin\psi\right) K_n (k_2 a)$

$m_8 = -j\omega\mu_2 k_2 \sin(\psi) K_n' (k_2 a)$

$m_9 = j\omega\epsilon_1 k_1 \cos(\psi) I_n' (k_1 a)$

$m_{10} = \left(k_1^2 \sin(\psi) - \frac{n\beta}{a} \cos(\psi)\right) I_n (k_1 a)$

$m_{11} = -j\omega\epsilon_2 k_2 \cos(\psi) K_n' (k_2 a)$

$m_{12} = -\left({k_2}^2 \sin(\psi) - \frac{n\beta}{a} \cos(\psi)\right) K_n (k_2 a)$

Equating determinant to zero resulting Eigen-value equation for β is:

$$\begin{aligned} k_o a^2 c\epsilon_1 k_1 \cot(\psi) \frac{I_n' (k_1 a)}{I_n (k_1 a)} - \frac{Y^2}{k_o a^2 c\mu_1 k_1 \cot(\psi)} \frac{I_n (k_1 a)}{I_n' (k_1 a)} - \\ k_o a^2 c\epsilon_2 k_2 \cot(\psi) \frac{K_n' (k_2 a)}{K_n (k_2 a)} r^2 + \frac{X^2 r^2}{k_o a^2 c\mu_2 k_2 \cot(\psi)} \frac{K_n (k_2 a)}{K_n' (k_2 a)} = 0 \end{aligned} \tag{2.15}$$

Here r=$k_1 a/k_2 a$, $X = (k_2 a)^2 - n\beta \mathrm{a} \cot(\psi)$, $Y = (k_1 a)^2 - n\beta \mathrm{a} \cot(\psi)$, k_o=$\omega\sqrt{\epsilon_o \mu_o}$, ϵ_o and μ_o are free space permittivity and permeability.

The dispersion relation Eq. (2.15) is further algebraically re-derived for various special cases:

1. For $n = 0$

$$\begin{aligned} k_o a^2 c\epsilon_1 k_1 \cot(\psi) \frac{I_0' (k_1 a)}{I_0 (k_1 a)} - \frac{k_1 a}{k_o a c\mu_1 \cot(\psi)} \frac{I_0 (k_1 a)}{I_0' (k_1 a)} - \\ k_o a^2 c\epsilon_2 k_2 \cot(\psi) \frac{K_0' (k_2 a)}{K_0 ((k_2 a)} r^2 + \frac{k_2 a r^2}{k_o a \mathrm{c}\mu_2 \cot(\psi)} \frac{K_0 (k_2 a)}{K_0' (k_2 a)} = 0 \end{aligned} \tag{2.16}$$

2. For ψ=0 and $n = 0$

$$\frac{\epsilon_1}{\epsilon_2} \frac{I_n'(k_1 a)}{I_n(k_1 a)} - r \frac{K_n'(k_2 a)}{K_n(k_2 a)} = 0 \tag{2.17}$$

3. For ψ=0 and $n \neq 0$

$$k_o ac\left[\epsilon_1 k_1 a\frac{I_n'(k_1a)}{I_n(k_1a)} - r^2\epsilon_2 k_2 a\frac{K_n'(k_2a)}{K_n(k_2a)}\right] - \frac{n^2\beta^2}{k_o ac}\left[\frac{1}{\mu_1 k_1 a}\frac{I_n(k_1a)}{I_n'(k_1a)} - \frac{1}{\mu_2 k_2 a}\frac{K_n}{K_n'}\right] = 0 \tag{2.18}$$

4. For ψ=90 and any n

$$r\frac{I_n'(k_1a)}{I_n(k_1a)} - \frac{\mu_1}{\mu_2}\frac{K_n'(k_2a)}{K_n(k_2a)} = 0 \tag{2.19}$$

Propagation vectors in Eq. (2.9) have been normalized with respect to the helix radius a, in both the region and rewritten as:

For region-I:

$$k_1 a = \sqrt{(\beta \mathrm{a})^2 - (k_{\mathrm{o}1}a)^2} \tag{2.20}$$

For region-II:

$$k_2 a = \sqrt{(\beta \mathrm{a})^2 - (k_{\mathrm{o}2}a)^2} \tag{2.21}$$

By solving Eqs. (2.20) and (2.21) one can find:

$$k_2 a = \sqrt{(k_1a)^2 + (k_{o1}a)^2 - (k_{o2}a)^2} \tag{2.22}$$

2.3 Results and Analysis

Dispersion equation (2.15) is a transcendental equation, which has been solved numerically as well as graphically to compute the longitudinal phase coefficient as a function of frequency $k_o a$. Mathematica 7.0 software package has been used for finding out the roots numerically. Obtained roots are verified by graphical procedure. For that, βa in Eq. (2.15) is replaced by $\sqrt{((k_{o1}ak_2a)^2 - (k_{o2}ak_1a)^2)/((k_1a)^2 - (k_2a)^2)}$ using Eqs. (2.20) and (2.21) and plotted between k_1a versus k_2a. Same variations are also plotted using Eq. (2.22). Superposition of these two graphs (not shown here) provides the value of βa.

For surface wave propagation $k_1 a$ and $k_2 a$ should be positive. Due to this, only those values of βa are considered as roots, which are higher as compared to $k_{o1}a$ and $k_{o2}a$.

2.3.1 Dominant mode ($n = 0$)

In Fig. 2.2, normalized longitudinal phase coefficient ($k_o a/\beta$a) has been plotted as a function of propagation vector ($k_o a$) for three cases when helix is: (i) in free space, (ii) loaded with DPS material and (iii) loaded with metamaterial. A comparative study has been made among three cases to understand complex mode propagation behaviour such as- Backward Wave (BW) mode, Forward Wave (FW) mode, phase velocity, and bandwidth spectrum.

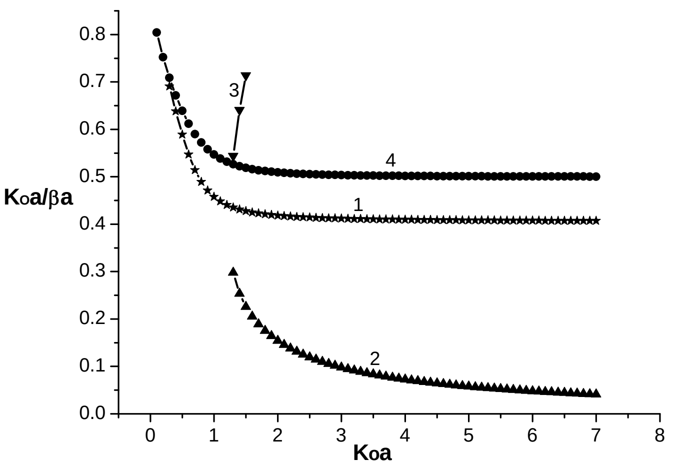

Figure 2.2: Variation of $k_o a/\beta$a vs $k_o a$ at $n = 0$ and $\psi = 30°$. free-space case ($\epsilon_{r1} = 1$, $\mu_{r1} = 1$) represented by •, DPS material ($\epsilon_{r1} = 2$, $\mu_{r1} = 1$) loading represented by $\star$, metamaterial ($\epsilon_{r1} = -2$, $\mu_{r1} = -1$) loading represented by ▲ and ▼.

In case of metamaterial loading at low frequencies two fundamental modes (2 and 3 in Fig. 2.2) propagate simultaneously having LCF at $k_oa = 1.3$. Mode 3 having a positive slope in dispersion graph and negative group velocity, which exhibits a BW property. At higher frequencies from $k_oa = 1.6$ onwards, only forward ultra slow mode 2 propagates which has positive group velocity. As we increase the frequency, normalized phase velocity (k_oa/βa $= v_p$/c) of mode 2 start to vary from 0.297, and it reduces to 0.040 at higher frequencies.

While in case of DPS medium, mode 1 (in Fig. 2.2) has LCF at $k_oa = 0.3$. The normalized phase velocity varies from 0.690 and is almost constant at 0.406 at higher frequencies ($k_oa = 7$) which is 1.23 times less as compared to free-space case (4 in Fig. 2.2).

Lowest achieved normalized phase velocity in metamaterial medium is 10 times less as compared to DPS medium. This implies that the presence of metamaterial medium enhances the slow-wave behaviour of the helical guide.

2.3.2 Higher order modes

Similar graphs are plotted for first ($n = 1$) higher-order mode in Fig. 2.3. In case of metamaterial loading at low frequencies two fundamental modes (3 and 4 in Fig. 2.3) coexist in the guide. Mode 4 is a BW mode having a positive slope in the dispersion plot and has negative group velocity. From $k_oa = 0.8$, onwards only forward ultra slow mode 3 exists in the guide. Normalized phase velocity of mode 3 starts varying from 0.05 and increases up to $k_oa = 0.8$, afterwards it reduces and almost becomes constant at 0.04 for higher frequencies. In case of DPS medium two fundamental modes, 1 (FW mode) and 2 (BW mode) are propagate (in Fig. 2.3) till $k_oa = 0.4$. After that only, forward wave mode propagates and its normalize phase velocity (k_oa/βa $= v_p$/c) varies from 0.05 to 0.36.

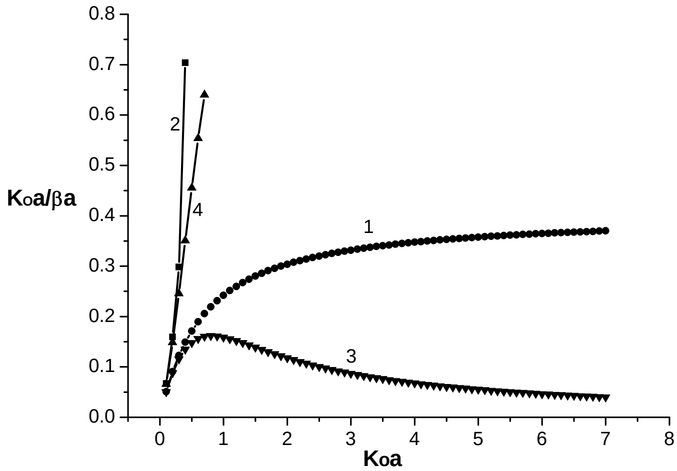

Figure 2.3: Variation of k_oa/βa vs k_oa at $n = 1$ and $\psi = 30\,°$. DPS material ($\epsilon_{r1} = 2$, $\mu_{r1} = 1$) loading represented by ● and ■, metamaterial ($\epsilon_{r1} = -2$, $\mu_{r1} = -1$) loading represented by ▼ and ▲.

In case of metamaterial loading, slowest achieved normalized phase velocity is 0.04, which is 9 times lower as compared to their DPS medium counter-part. This again signifies the presence of metamaterial medium further increases the slow behaviour of the helical guide.

2.3.3 Effect of physical design parameters

Helical guide contains two design parameters namely radius (a) and pitch angle (ψ). In the above results radius (a) is normalized with propagation vector k_oa. Therefore, its effect could be understood by making the frequency constant. Helix pitch angle (ψ) effects on the behaviour of slow wave propagation have been shown in Figs. 2.4 and 2.5.

At lower frequencies, two modes (BW and FW mode) propagate simultaneously. Modes described as 1, 3 and 5 (in Figs. 2.4 and 2.5) propagate as forward wave mode and modes 2, 4 and 6 (in Figs. 2.4 and 2.5) propagate as a BW mode for pitch angles 30, 20, and 10 degrees respectively.

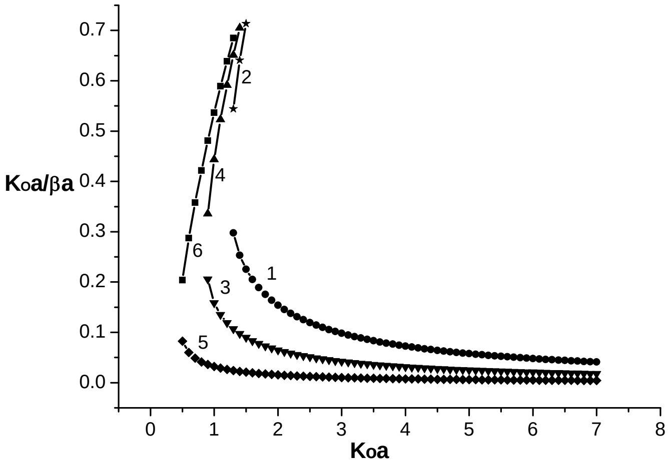

Figure 2.4: Variation of k_oa/βa *vs* k_oa at $n = 0$ in metamaterial ($\epsilon_{r1} = -2$, $\mu_{r1} = -1$) loading for $\psi = 30^\circ$ represented by $\star$ and $\bullet$, 20° represented by ▼ and ▲ and 10° represented by ⧫ and ■.

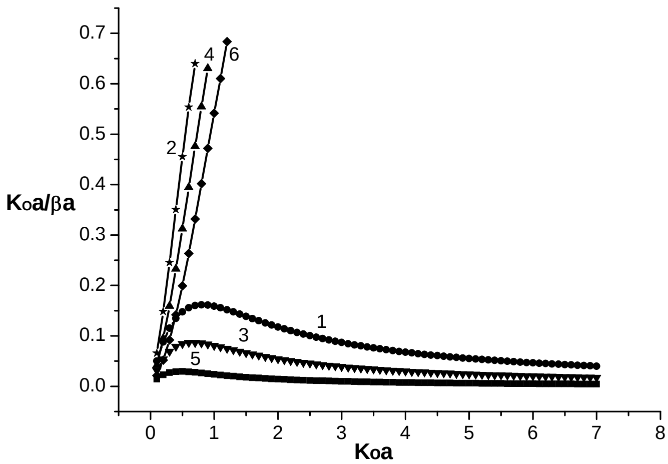

Figure 2.5: Variation of k_oa/βa *vs* k_oa at $n = 1$ in metamaterial ($\epsilon_{r1} = -2$, $\mu_{r1} = -1$) loading for $\psi = 30^\circ$ represented by $\star$ and $\bullet$, 20° represented by ▼ and ▲ and 10° represented by ⧫ and ■.

In dominant mode, bandwidth spectrum of BW mode increases with reduction in pitch angle (bandwidth in 30° is $k_oa = 1.3$ to 1.5, 20° is $k_oa = 0.9$ to 1.4 and 10° is $k_oa = 0.5$ to 1.3). Similar observations are seen in higher order ($n = 1$) mode (bandwidth in 30° is $k_oa = 0$ to 0.7, 20° is $k_oa = 0$ to 0.9 and 10° is $k_oa = 0$ to

1.2).

Normalized phase velocity of forward wave mode (1, 3 and 5 in Figs. 2.4 and 2.5) decreases with decrease in pitch angle (summarized in Table 2.1) that enhances the ultra slow wave behaviour of the helical guide.

Table 2.1: LCF of dominant mode ($n = 0$) and V_p/c of dominant and first higher order mode ($n = 1$) for different pitch angles.

ψ	LCF in $k_o a$	V_p/c ($n = 0$) at $k_o a = 7$	V_p/c ($n = 1$) at $k_o a = 7$
30°	1.3	0.0409	0.0400
20°	0.9	0.0177	0.0175
10°	0.5	0.0043	0.0043

2.3.4 Effect of metamaterial medium on guide dispersion behaviour

Metamaterial media properties (ϵ_1 and μ_1) play a very important role in reducing the phase velocity of the wave in order to achieve ultra slow wave. Three representative examples: (a) case I ($\epsilon_{r1} = -1.5, \mu_{r1} = -1$; $\epsilon_{r2} = 1, \mu_{r2} = 1$) (b) case II ($\epsilon_{r1} = -2, \mu_{r1} = -1$; $\epsilon_{r2} = 1, \mu_{r2} = 1$) and (c) case III ($\epsilon_{r1} = -5, \mu_{r1} = -1$; $\epsilon_{r2} = 1, \mu_{r2} = 1$) are considered for analysing these effects by varying ϵ_{r1} and keeping μ_{r1} constant.

In dominant mode, bandwidth spectrum of BW mode (2 and 4 in Fig. 2.6) reduces (bandwidth in case I is $k_o a = 2.1$ to 2.4 and in case II is $k_o a = 1.3$ to 1.5) with increase in $|\epsilon_{r1}|$ and it disappears in case III. Conversely bandwidth spectrum of forward wave mode (1, 3 and 5 in Fig. 2.6) increases due to reduction in lower cut-off value (summarized in Table-2.2). Observed normalised phase velocity of forward wave mode is almost 8 times slower in case III as compared to case I reported in Table-2, which attributes the role of metamaterial properties in order to achieve ultra slow wave.

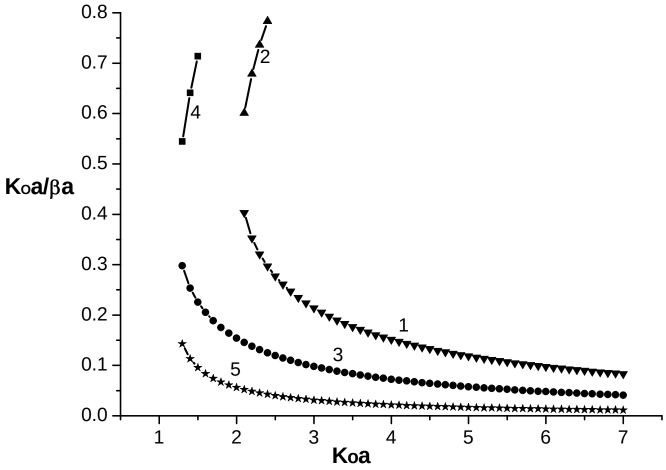

Figure 2.6: Variation of k_oa/βa vs k_oa at n=0 and $\psi = 30\,^{\circ}$, for case I ($\epsilon_{r1} = -1.5$, $\mu_{r1} = -1$; $\epsilon_{r2} = 1$, $\mu_{r2} = 1$) represented by ▼ and ▲, case II ($\epsilon_{r1} = -2$, $\mu_{r1} = -1$; $\epsilon_{r2} = 1$, $\mu_{r2} = 1$) represented by • and ■, and case III ($\epsilon_{r1} = -5$, $\mu_{r1} = -1$; $\epsilon_{r2} = 1$, $\mu_{r2} = 1$) represented by $\star$.

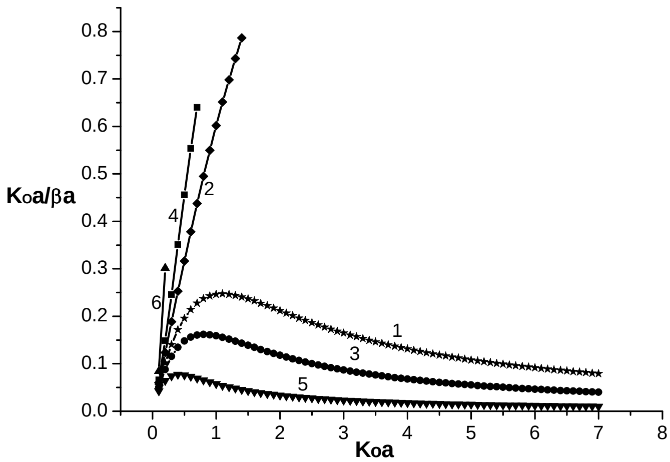

Figure 2.7: Variation of k_oa/βa vs k_oa at $n = 1$ and $\psi = 30\,^{\circ}$, for case I ($\epsilon_{r1} = -1.5$, $\mu_{r1} = -1$; $\epsilon_{r2} = 1$, $\mu_{r2} = 1$) represented by ♦ and $\star$, case II ($\epsilon_{r1} = -2$, $\mu_{r1} = -1$; $\epsilon_{r2} = 1$, $\mu_{r2} = 1$) represented by • and ■, and case III ($\epsilon_{r1} = -5$, $\mu_{r1} = -1$; $\epsilon_{r2} = 1$, $\mu_{r2} = 1$) represented by ▼ and ▲.

Similar observation is found in first higher order ($n = 1$) mode where bandwidth spectrum of BW mode (2, 4, and 5 in Fig. 2.7) reduces (bandwidth in case I is

$k_o a = 0$ to 1.4, case II is $k_o a = 0$ to 0.7 and case III is $k_o a = 0$ to 0.2) with increase in $|\epsilon_{r1}|$. The normalized phase velocity of forward wave mode is summarized in Table-2.2.

Table 2.2: LCF of dominant mode ($n = 0$) and V_p/c of dominant and higher order modes ($n = 1$) in different cases.

Case	LCF ($n = 0$) in $k_o a$	$V_p/c(n = 0)$ at $k_o a = 7$	$V_p/c(n = 1)$ at $k_o a = 7$
case I	2.1	0.0830	0.0792
case II	1.3	0.0409	0.0400
case III	0.6	0.0101	0.0101

2.4 Discussion

In the above analysis, it has been observed that due to higher value of longitudinal phase coefficient (β), phase velocity of wave is greatly reduced as compared to normal helical guide.

Modal behaviour study reveals that the two fundamental modes, BW and FW, propagate simultaneously. Bandwidth of the BW mode is very small and it dies off very fast. On the other hand, forward wave mode has wider bandwidth spectrum. It is observed that normalized phase velocity decreases with increase in $|\epsilon_{r1}|$. Similar variation is also observed when the guide pitch angle is reduced. Similar behaviour of dispersion characteristics is observed as the propagation frequency increases, however it has lower phase and group velocity.

The minimum phase velocity is observed in case III with pitch angle $\psi = 10\,°$. If assumed guide radius is $a = 1$ mm and $k_o a = 50$ ($freq = 2.38\ THz$), then wave propagates with speed of 45860.46 meter per second, which is 6541 times less as compared to the speed of light (in Fig. 2.8). This reduction can be further enhanced by optimizing the metamaterial properties as well as the helix dimensions.

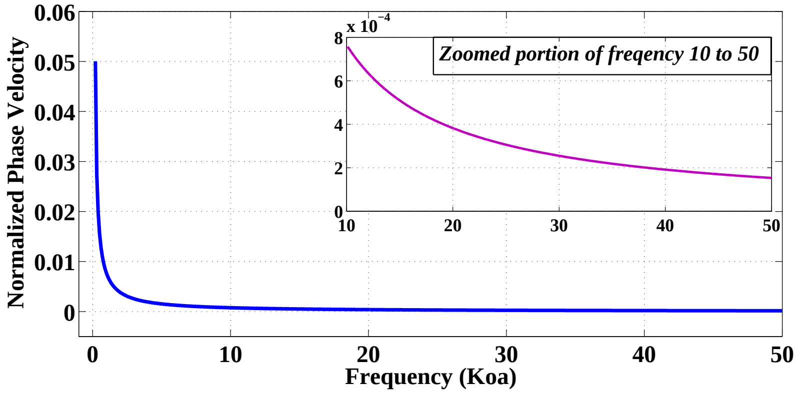

Figure 2.8: Variation of Normalized phase velocity (k_oa/βa) vs Frequency (k_oa) for a very large frequency range (up to THz) for the case III ($\epsilon_{r1} = -5$, $\mu_{r1} = -1$; $\epsilon_{r2} = 1$, $\mu_{r2} = 1$) at n=0 and $\psi = 10^\circ$

2.5 Summary

Here the dispersion characteristics ($\omega - \beta$ diagram) of a metamaterial loaded helical guide are analytically solved and numerically computed for different medium properties as well as helical guide parameters. The modal behaviour of this structure has been studied with an aim to achieve ultra slow EM wave over wide bandwidth. Significant amount of phase velocity reduction has been achieved in comparison to when the helix is in free space or loaded with normal dielectric medium. Other modal properties such as presence of two fundamental modes, BW and FW and their lower cut-off frequencies (LCF's) as well as the bandwidth spectrum is also revealed thoroughly.

Chapter 3

Dispersive Metamaterial Loaded Helical Guide*

3.1 Introduction

Chapter-2 described the Slow Wave Device (SWD) in case of a non-dispersive metamaterial. The present chapter deals with Dispersive Metamaterial Loaded Helical Guide (DMHG), wherein the metamaterial considered is dispersive in nature. Dispersive matamatreials are more realistic as compared to their non dispersive counter parts and can be realized practically. However, the non-dispersive metamaterials are yet to be explored and realized. The essence of this investigation is to present an actual design of SWD that has the capability to slow the EM (electromagnetic) wave or even trap it.

*This work has been published in *Optics Express*, Vol. 24, 2687-2700 (2016).

3.2 Helical Guide Design and Mode Analysis using Drude model

For the purpose of analysis, we consider a helical structure with radius a and pitch angle ψ, as shown in Fig. 3.1(a), on which guided EM wave is travelling along the z-direction. The current flow along the sheath is constrained to a direction which makes a constant angle $(90^o - \psi)$ with the axis of the helix. The tangential component of the electric field, $E_{||}$, (shown in Fig. 3.1(b)) is zero along the direction of current flow while its finite and continuous along the perpendicular direction of the current flow. Region-I is a dispersive metamaterial media and its dispersive behaviour is described by the Drude model [59]. Region-II is a free space medium.

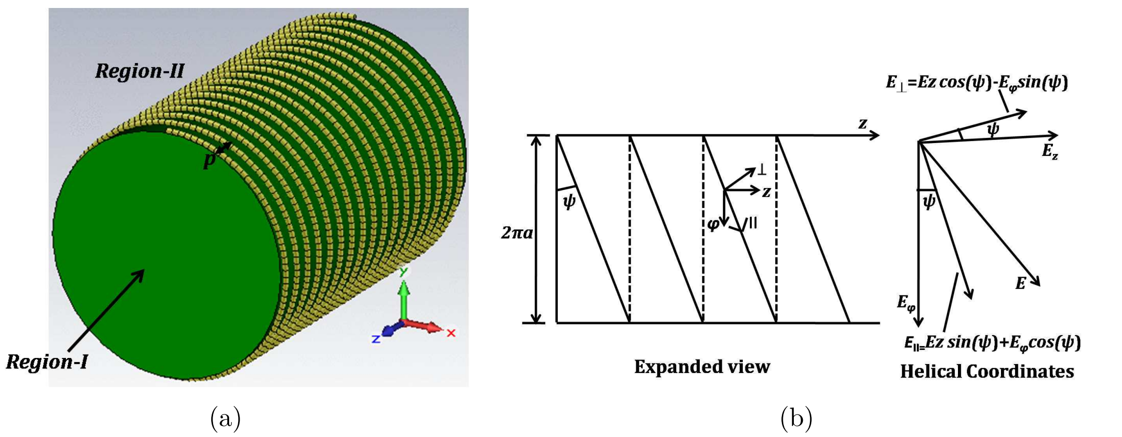

Figure 3.1: (a) Sheath helix of radius a, pitch p and pitch angle ($\psi = \tan^{-1} p/2\pi a$). Region I (inner region) is metamaterial medium and Region II (outer-region) is free-space. (b) Expanded view of sheath helix and its helical coordinates.)

Here we consider lossless Drude model which models cold plasma medium and its governing equations are written as:

$$\epsilon_{r1} = 1 - \frac{\omega_p^2}{\omega^2} \tag{3.1}$$

$$\mu_{r1} = 1 - \frac{F\omega^2}{\omega^2 - \omega_o^2} \tag{3.2}$$

Here F is filling factor, ω_o and ω_p are resonant and plasma frequency respectively. The values of $F = 0.56$, $\omega_o = 8\pi$ and $\omega_p = 20\pi$ are taken which are validated experimentally by Simth et al. [2]. Region II is free-space having permittivity and permeability values ϵ_{r2} and μ_{r2}, respectively.

The dispersion relation of the proposed DMLHG structure, which describes the modal behaviour of an EM wave, is analytically derived from dispersion relation of MLHG structure by defining ϵ_{r1} and μ_{r1} as a dispersive metamaterial parameters inside the helical guide (region 1) and written as:

$$\begin{aligned} k_o a^2 c\epsilon_1(\omega) k_1 cot(\psi) \frac{I_n'(k_1 a)}{I_n(k_1 a)} - \frac{Y^2}{k_o a^2 c\mu_1(\omega) k_1 cot(\psi)} \frac{I_n(k_1 a)}{I_n'(k_1 a)} - \\ k_o a^2 c\epsilon_2 k_2 cot(\psi) \frac{K_n'(k_2 a)}{K_n(k_2 a)} r^2 + \frac{X^2 r^2}{k_o a^2 c\mu_2 k_2 cot(\psi)} \frac{K_n(k_2 a)}{K_n'(k_2 a)} = 0 \end{aligned} \tag{3.3}$$

Here $r = k_1 a / k_2 a$, $X = k_2^2 - n\beta\cot(\psi)$, $Y = k_1^2 - n\beta\cot(\psi)$. $k_1 = (\beta^2 - k_{o1}^2)^{0.5}$ and $k_2 = (\beta^2 - k_{o2}^2)^{0.5}$, are transverse wave numbers. β is longitudinal phase coefficient. k_{o1} $(= \omega\sqrt{\epsilon_1\mu_1})$ and k_{o2} $(= \omega\sqrt{\epsilon_2\mu_2})$ are propagation vector of region 1 and 2. $(')$ is derivative of Bessel function. For guided mode propagation field should decay exponentially in region-II and the opposite is expected in region-I. Thus, modified Bessel function of second $(K_n(k_2 a))$ and first kind $(I_n(k_1 a))$ is used in region-II and I respectively, where n describes the modal behaviour of the wave.

For EM wave propagation in helical guide, the components of poynting vectors are [41]:

$$S_z = \frac{1}{4\Pi}(E_r H_\phi^* - E_\phi H_r^*) \tag{3.4}$$

$$S_r = \frac{1}{4\Pi}(E_z H_\phi^* - E_\phi H_z^*) \tag{3.5}$$

$$S_\phi = \frac{1}{4\Pi}(E_z H_r^* - E_r H_z^*) \tag{3.6}$$

Total power flow in different layers of waveguide is sum of power flow in each layer of guide [41]:

$$P_z = P_z^{in} + P_z^{out} \tag{3.7}$$

$$P_z^{in} = \int_0^a S_z r dr, \qquad P_z^{out} = \int_a^\infty S_z r dr \tag{3.8}$$

Obtained expression of P_z^{in} and P_z^{out} for proposed structure is:

$$\begin{aligned} P_z^{in} = & -\frac{A^2\beta\omega\epsilon_1 x^2 I_n^2(x) h_n'(x)}{4} - \frac{B^2\beta\omega\mu_1 x^2 I_n^2(x) h_n'(x)}{4} \\ & +iAB(\omega^2\epsilon_1\mu_1 k_1 - \beta^2) n \int_0^x I_n(x) I_n'(x) dx \end{aligned} \tag{3.9}$$

$$\begin{aligned} P_z^{out} = & -\frac{C^2\beta\omega\epsilon_2 y^2 K_n^2(y) g_n'(y)}{4} - \frac{D^2\beta\omega\mu_2 y^2 K_n^2(y) g_n'(y)}{4} \\ & +iAB(\omega^2\epsilon_2\mu_2 k_2 - \beta^2) n \int_y^\infty K_n(y) K_n'(y) dy \end{aligned} \tag{3.10}$$

Here $x = k_1 a$, $y = k_2 a$, $h_n'(x) = -x h_n^2(x) - 2/x h_n(x) + n^2/x^3 + 1/x$, $g_n'(x) = -x g_n^2(y) - 2/y g_n(y) + n^2/y^3 + 1/y$, $h_n(x) = I_n'(x)/(x I_n(x))$ and $g_n(y) = K_n'(y)/(y K_n(y))$. A, B, C and D are field coefficients and inter related to each other. Normalized power flow is [41]:

$$< P_z >= \frac{P_z^{in} + P_z^{out}}{|P_z^{in}| + |P_z^{out}|} \tag{3.11}$$

EM wave modal characteristics of DMLHG structure under study are described by solving dispersion Eq. (3.3) for its eigen-value solutions in terms of axial propagation constant, β. We have computed β as a function of k_o by using Findroot subroutine of MATHEMATICA 7.0 Package. For guided mode propagation, both k_1 and k_2 should be positive. Therefore only those roots are considered which are higher as compared to k_{o1} and k_{o2}.

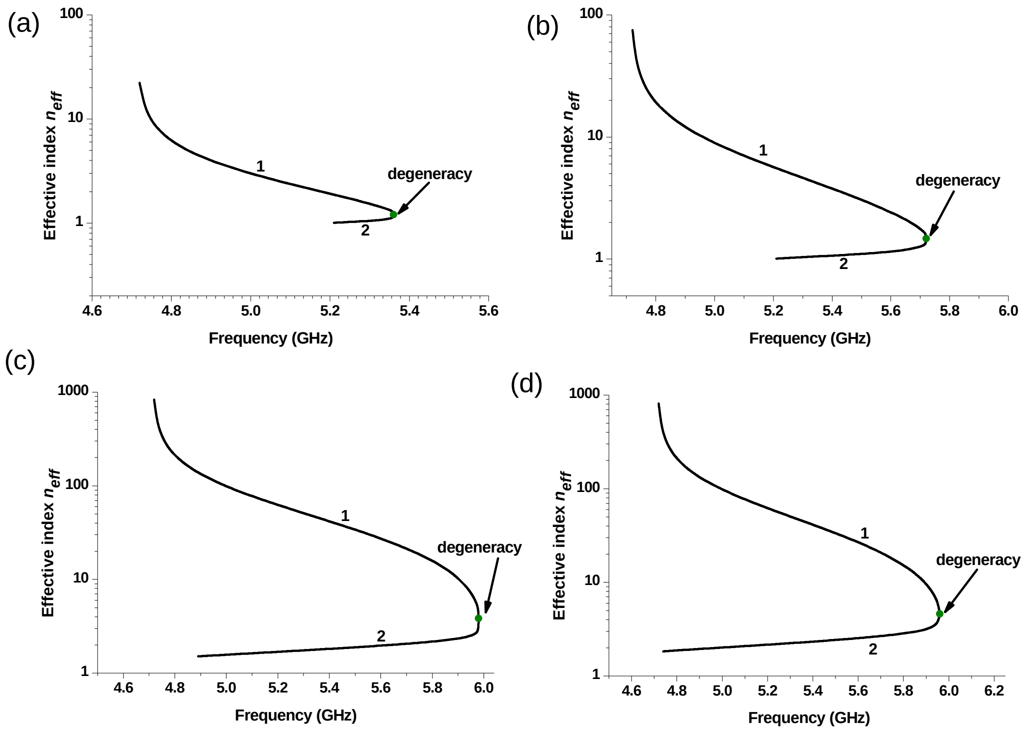

Figure 3.2: Variations of effective index, $n_{eff} = \beta/k_o$ as a function of frequency. Here Y-axis is plotted on log_{10} scale and X-axis is on linear scale. Two modes labelled as mode 1 (backward wave) and mode 2 (forward wave) are propagating simultaneously and meeting at green circle which represents degeneracy point. Figs. (a) and (b) are plotted for pitch angle 30^o and 10^o, respectively, while helical guide radius, a, is 100 mm for both the cases. Figs. (c) and (d) are plotted for helical guide radius 8 mm and 5 mm, respectively, while helical guide pitch angle is 0.9^o for both the cases.

Fig. 3.2 describes the EM-wave propagation characteristics of DMLHG structure for the dominant mode case ($n = 0$). Fig. 3.2(a), shows modal characteristics of DMLHG having pitch angle 30^o and radius 100 mm, respectively. Fundamental mode labelled as mode-1, has Lower Cut-off Frequency (LCF) at 4.72 GHz and exhibits a negative slope of $d(k_o)/d(\beta)$. This mode represents BW characteristics having anti-parallel group- and phase- velocities. First higher order mode (labelled as 2, in Fig. 3.2(a)) has LCF at 5.21 GHz and is considered as FW mode as it propagates with opposite features in comparison to mode-1. Mode-1 exhibits enhanced slow wave characteristics since its observed minimum normalized phase velocity ($v_p/c = k_o/\beta$) is 0.044 which is almost 22 times less than velocity of light.

Both modes propagate as Surface Plasmonic (SP) modes and meet at 5.36 GHz and this point is regarded as a mode-degeneracy point. Similar characteristics are also observed for other DMLHG parameters and are shown in Figs. 3.2(b), 3.2(c) and 3.2(d).

The helix parameters, namely, pitch angle (ψ) and its radius (a) provide a control of bandwidth spectrum for both BW- and FW- modes, effective index values as well as mode-degeneracy point. In Figs. 3.2(a) and 3.2(b) the effects of helix pitch angle variations (30^o and 10^o) are plotted by keeping helix radius ($a = 100$ mm) constant. From these two graphs it can be concluded that reduction in pitch angle increases the effective index and bandwidth spectrum of both modes. Also it can be seen that mode-degeneracy point is shifted at higher frequency. The effect of helix radius variations (8 mm and 5 mm) by keeping its pitch angle (0.9^o) constant are plotted in Figs. 3.2(c) and 3.2(d). Contrary to the earlier case, the reduction in guide radius reduces the effective index and bandwidth spectrum of both modes. At the same time mode-degeneracy point is also shifted to lower frequency. In Figs. 3.2(c) and 3.2(d), observed high value of effective index for the mode-1 resulted in minimum normalized phase velocity (v_p/c) 0.00120 and 0.00123, respectively. This substantial decrease in normalized phase velocity of mode-1 is attributed as ultra slow wave mode.

The characteristics of normalized group velocity (v_g/c) and normalized power flow (P_z) are plotted in Figs. 3.3(a) and 3.3(b) as a function of frequency. Both the graphs are derived from obtained values of axial propagation constant, β, from Eq. (3.3). For normalized group velocity ($v_g/c = dk_o/d\beta$) calculation β value was used in the expression $dk_o/d\beta$. In order to calculate normalized power flow, obtained values of β were put in Eqs. (3.9) and (3.10). From this power flow in different layers of waveguide are obtained which are P_{z1} and P_{z2}. Further the value of P_{z1} and P_{z2} were used in Eq. (3.11) to calculate $<P_z>$. From these graphs (shown in Figs. 3.3(a) and 3.3(b)), it can be seen that at mode degeneracy point group velocity reduces to zero and power flow vanishes. So, the point of mode-degeneracy corresponds to stopping of wave.

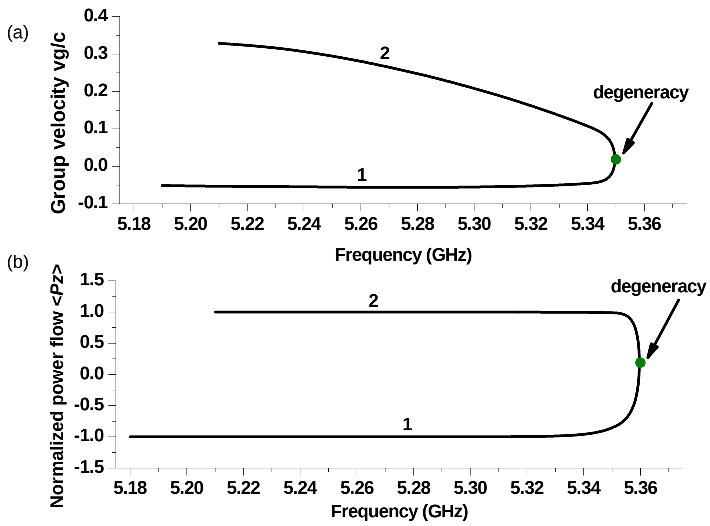

Figure 3.3: Variations of group velocity (v_g/c), Fig. 3(a), and normalized power flow (P_z), Fig. 3(b), as a function of frequency for helix pitch angle 30^o and radius 100 mm, respectively. Green circle representing the mode-degeneracy point above mode 2 and below that mode 1 are shown.

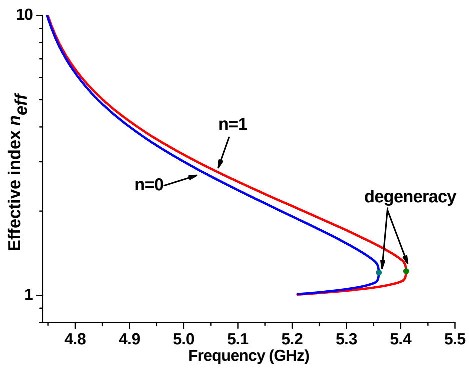

Figure 3.4: Variations of effective index, $n_{eff} = \beta/k_o$ as a function of frequency for dominant ($n = 0$) and higher ($n = 1$) mode case at pitch angle 30^o and radius 100 mm. Here Y-axis is plotted on log_{10} scale and X-axis is on linear scale.

When Eq. (3.3) is solved for higher order mode $n = 1$ case we obtain similar characteristics as that of $n = 0$ case. A comparative study between two modes ($n = 0$, $n = 1$) are shown in Fig. 3.4. It can be seen from the graph that effective index

n_{eff} is slightly increased for $n = 1$ mode in comparison to $n = 0$ mode. Thus due to increased value of effective index, slow wave behaviour of higher mode case is more enhanced as compared to dominant mode case. The higher cut off frequency (HCF) of BW and FW mode is also increased marginally (for example HCF of $n = 0$ and 1 respectively is 5.36 GHz and 5.41 GHz). This results in a slight increase in the bandwidth of the guide spectrum.

3.3 Design and simulation of DMLHG using CST Microwave Studio

In the above section, for analytical characterization of DMLHG structure, we used Drude model to include the dispersive nature of metamaterial. In order to realize such structure one needs to create metamaterial medium inside the helical guide. Here we are presenting two possible designs in order to realize DMLHG structure.

3.3.1 First DMLHG design

For first DMLHG design, we have chosen novel FF-shaped metamaterial cell as a unit cell for realizing metamaterial medium inside the helical guide. There are number of metamaterial cells already proposed in literature. However, we have proposed our own FF-shaped metamaterial cell. The description about its design, resonance, experimental results and phenomena of negative refraction have been discussed in subsequent subsections.

3.3.1.1 FF-Shaped Metamaterial Cell*

*The investigation regarding FF-Metamaterial cell has been submitted in *IEEE Microwave and Component Letter*.

In Fig. 3.5, FF-shaped unit cell on geometric scale is shown. It consists of two F-shaped copper strips, facing each other and printed on FR-4 substrate. The value of permittivity and loss tangent for the substrate is 4.3 and 0.025, respectively.

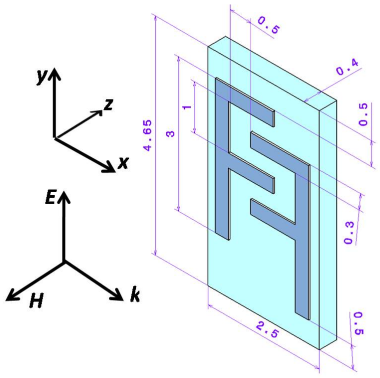

Figure 3.5: Single side FF-metamaterial unit cell. FF shape metallic inclusion is printed on FR-4 substrate

From the equivalent circuit model approach we can draw the circuit model of the structure as shown in Fig. 3.6 [60]. Here inductance L is produced by area covered by metallic strip and capacitance C_1 is produced by the gap between the strips.

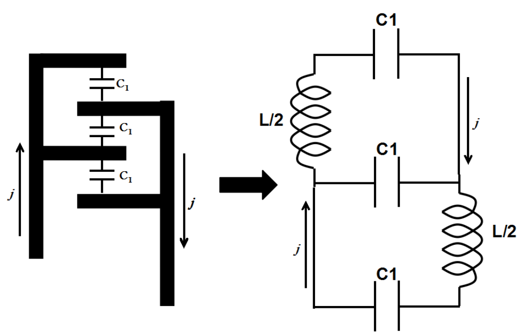

Figure 3.6: Equivalent circuit model of FF-unit cell.

In order to demonstrate the left-handed characteristics of the structure, we performed numerical simulation of the slab having one unit cell in x direction and ten unit cells in y direction [12] using commercially available tool, CST Microwave studio. For simulation, perfect magnetic conductor and perfect electric condutor boundaries are utilized in z- and y- directions, respectively. The EM wave is excited along x-direction on yz-plane. The polarisation of the incident EM wave is such that the electric field lies along the y-direction. The calculated S-parameters (S_{11} and S_{21}) in amplitude and phase are presented in Figs. 3.7 and 3.8 respectively.

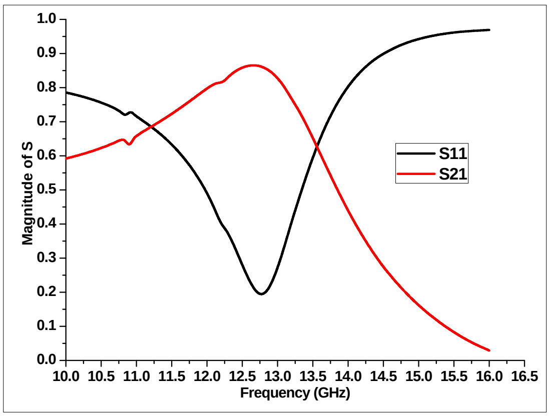

Figure 3.7: Magnitude of simulated transmission (S_{21}) and reflection (S_{11}) *vs* frequency.

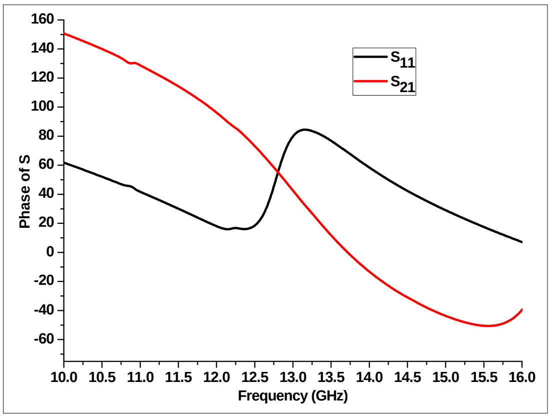

Figure 3.8: Phase of simulated transmission (S_{21}) and reflection (S_{11}) *vs* frequency.

These simulated scattering parameter results are further used in obtaining the values of wave impedance z, and refractive index n, through Eq. (3.12) and (3.13) by applying homogenization approach described in [61].

$$z = \pm\sqrt{\frac{(1+S_{11})^2 - S_{21}^2}{(1-S_{11})^2 - S_{21}^2}} \tag{3.12}$$

$$n = \frac{1}{k_o d}[(ln(e^{ink_od}))'' + 2\pi m - i(ln(e^{ink_od})'] \quad (3.13)$$

Here k_o is wave number, d is thickness of slab, (.)' and (.)" represent real and imaginary values of the operator.

From that corresponding values of ϵ and μ can be retrieved from, $\epsilon = n/z$ and $\mu = nz$, shown in Fig. 3.9. Results show an overlapping frequency range 10.659 to 13.186 GHz for which both permittivity- and permeability- values are negative. For this spectrum single sided structure behaves as a left handed material.

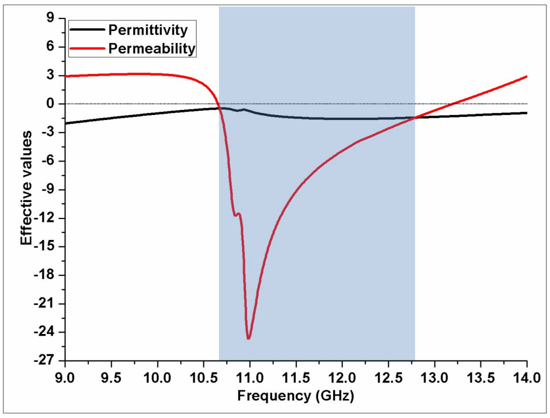

Figure 3.9: Extracted effective values of permittivity and permeability

Experimental Results

The FF-shaped metamaterial described and simulated above has been manufactured. For that FF shaped simulated circuit patterns are printed on a FR-4 substrate having a thickness of 0.4 mm. The sample slab under testing consists of 18 unit cells in z direction and 10 unit cells in y direction (shown in Fig. 3.10). The experimental set-up consists of two horn antennas and vector network analyzer (VNA) of Rohde & Schwarz, Model No. ZVA49.

The experiment has been carried out in the spectrum within the fabricated structure which exhibits pass band characteristics due to its left-handed property. The sample is placed in between the transmitting and receiving horn antennas connected at the 2-ports of a VNA. The measured transmission characteristics presented in Fig. 3.11,

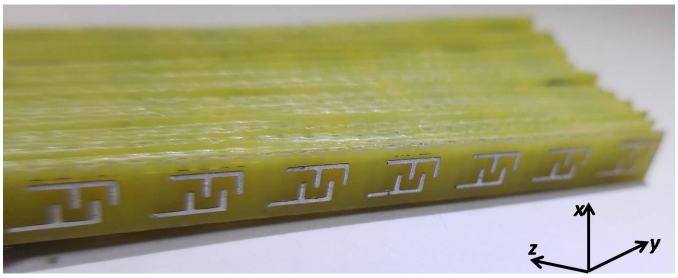

Figure 3.10: Fabricated FF-metamaterial structure.

exhibits a 3dB pass band of 10.87 to 13.9 GHz which matches closely to the simulated results. The slight discrepancy in the results could be attributed to the inherent defects in fabrication of the material or other free space losses that were not included in the simulations.

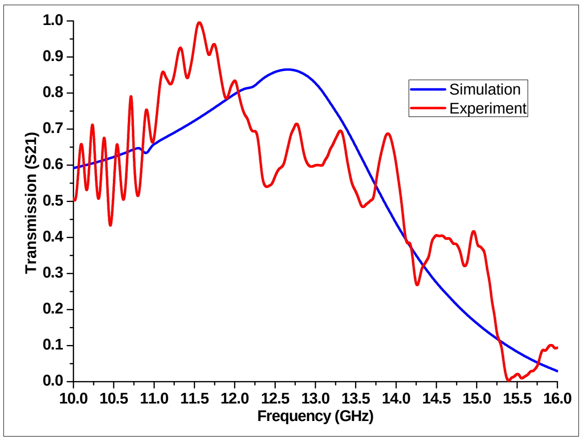

Figure 3.11: Measured Transmission coefficient (S_{21} vs frequency.)

Demonstration of Negative Refraction

To demonstrate negative refraction of FF-shaped metamaterial through Snell's law we simulated wedge shape slab made-up of FF-cells [11, 14, 15] in CST Microwave Studio. For that purpose we positioned wedge in between two magnetic conducting walls in xy-plane. This condition in simulator is achieved by setting perfect magnetic boundary conditions. In our wedge shaped model we increase the length in the x direction by two such unit cells while there is an increase of one unit cell in

y direction. This wedge contains 20 rows and 10 columns can be considered as effectively homogeneous media if wavelength is much larger than size of unit cell. A rectangular metallic channel is used to channelize the EM wave and incident normally on the first layer of wedge and then propagate inside the wedge.

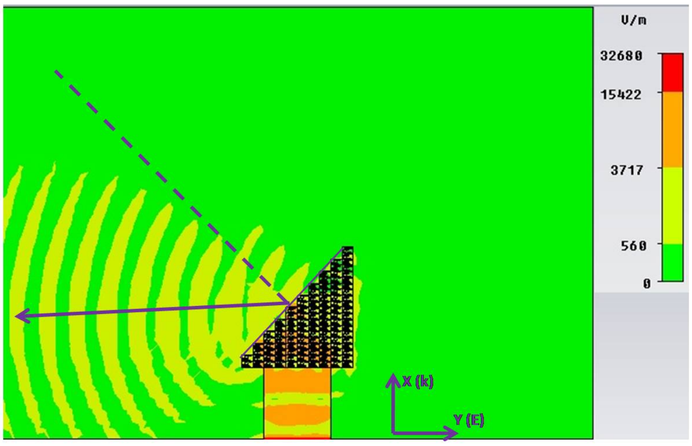

Figure 3.12: The Electric field distribution for the wedge shape structure made from FF-shaped metamaterial at frequency of 12 GHz.

This wedge model exhibits left-handed behaviour only if the EM wave is polarized with proper orientation with respect to FF-unit cells. Therefore, EM wave is incident in x direction through metallic rectangular channel with electric field along y direction and magnetic field along z direction. Figure 3.12 shows the electric field distribution for electromagnetic wave incident at 12 GHz. Here, dashed line shows the direction normal to the surface and solid line denotes the direction of refracted wave. It is seen that both the refracted and incident waves with respect to surface normal are on same side or wave is refracted in left direction. However, when such a wave incident upon simple wedge shaped structure without having FF-shaped inclusions the wave is refracted in right direction as shown in Fig. 3.13. This proves the phenomena of negative refraction for proposed structure.

3.3.1.2 DMLHG design

In order to design a DMLHG structure following procedures have been adopted:

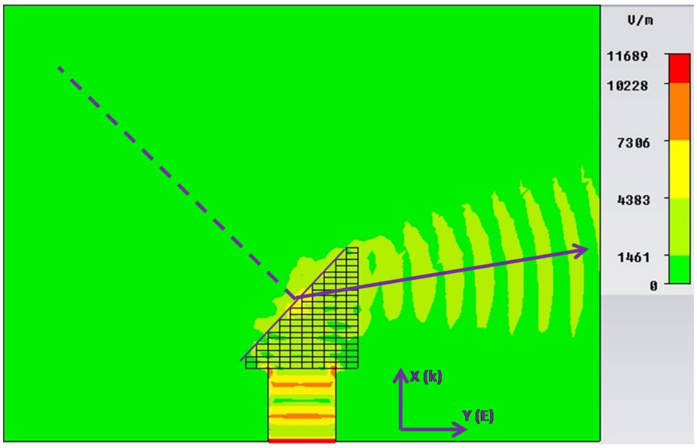

Figure 3.13: The Electric field distribution for the wedge shape structure made from FR-4 dielectric material at frequency of 12 GHz.

(a) First we created a hollow cylindrical structure of a flexible FR-4 material. Its radius, width and thickness are 5.18 mm, 2.5 mm and 0.5 mm, respectively. On its inner wall FF-shaped metallic inclusions were arranged with a periodicity of 1 mm in azimuthal direction. This way an azimuthally arranged FF-shaped unit cell in cylindrical geometry as shown in Fig. 3.14(a) is created.

(b) A helix having wire radius and pitch of 0.05 mm and 0.08 mm respectively was wounded over this cylindrical structure. This whole arrangement formed a DMLHG unit cell as shown in Fig. 3.14(b).

(c) An array of unit cells was now arranged axially to realize the DMLHG structure as shown in Fig. 3.15(a)

To examine the pass band characteristics or resonance characteristics of designed DMLHG structure (shown in Fig. 3.15(a)) a full wave time domain simulation of the structure is performed. For this purpose, we excited EM wave in the structure through a coaxial-feed arrangement. It works as a source for our structure and its schematic is shown in Fig. 3.16(a). The detailed parameters of coaxial-feed are dielectric core diameter $b = 2.4$ mm, dielectric permittivity $\epsilon_r = 2.1$, inner conductor diameter $a = 0.6$ mm and cut off frequency of 43.9 GHz. The position of

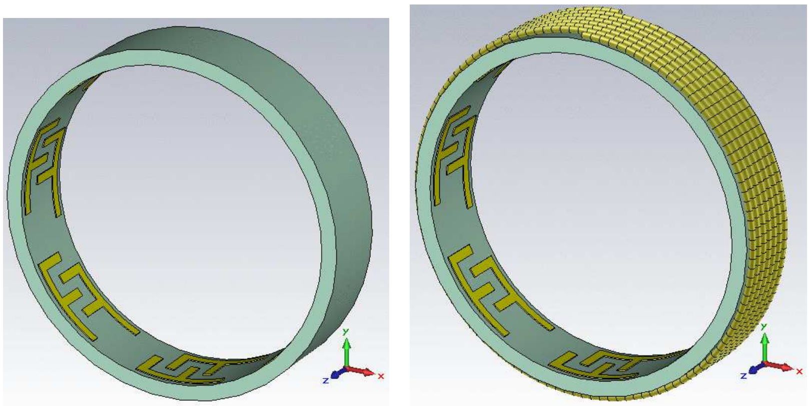

(a) (b)

Figure 3.14: (a) Azimuthally arranged FF-shaped unit cells. (b) The unit cell of DMLHG structure.

source during excitation of DMLHG structure is shown in Fig. 3.16(b). Obtained transmission- and reflection- coefficients results are shown in Fig. 3.15(b). Here, it can be seen that simulated DMLHG structure possesses a pass band/resonance bandwidth of 12.5 to 14.5 GHz. This spectrum matches with the pass-band spectrum of FF-shaped metamaterial cell.

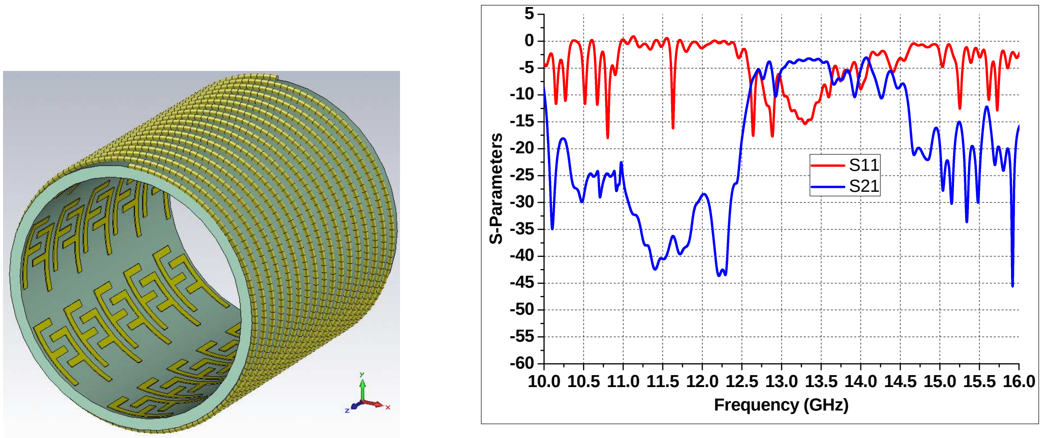

(a) (b)

Figure 3.15: (a) The Designed DMLHG structure. (b) The S-parameter transmission (S_{21}) and reflection (S_{11}) results of DMLHG.

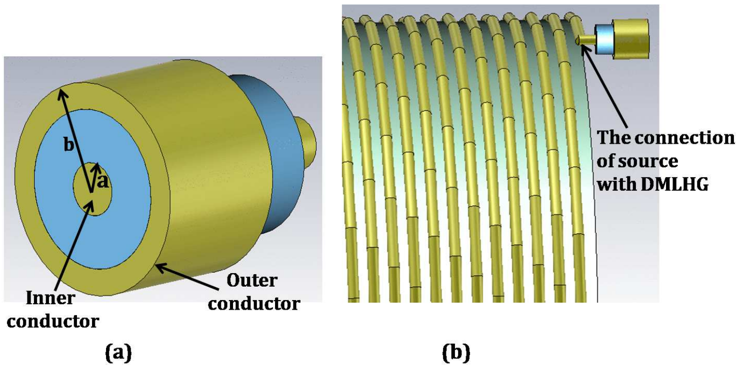

Figure 3.16: (a) Schematic of coaxial feed. (b) Connection arrangement of coaxial feed with DMLHG structure.

The pass band characteristics of DMLHG structure signify that within this spectrum DMLHG structure will exhibit the guided mode propagation characteristics, as well. In order to visualize and analyse the modal behaviour of this structure we have performed an Eigen-mode simulation of unit cell (shown in Fig. 3.14(b)) of the designed structure with periodic boundary conditions in $+z$ and $-z$ directions. The obtained Eigen-mode characteristics are plotted in Fig. 3.17(a). From the graph it can be seen that DMLHG structure supports both FW and BW mode. Both modes are propagating in the frequency-range of 13.7 to 14.5 GHz and they are degenerate at a critical frequency of 14.4 GHz. The existence of BW mode in the DMLHG structure signifies the essence of metamaterial loading inside the structure. In order to bring out the significance of metamaterial loading, an Eigen-mode simulation of unit cell of the helix has been performed when it is in free space. Obtained dispersion graph is shown in Fig. 3.17(b). It is observed that helix supports propagation of FW mode over a very wide bandwidth spectrum 15 to 55 GHz and there is no BW mode as well as degeneracy point.

The power flow and group velocity characteristics are plotted in Figs. 3.18(a) and 3.18(b), respectively. From these graphs it can be seen that at critical frequency or degeneracy point, power flow vanishes and group velocity also becomes zero. The high value of propagation coefficient and mechanism of degeneracy leads to slowing and eventually stopping of the EM wave.

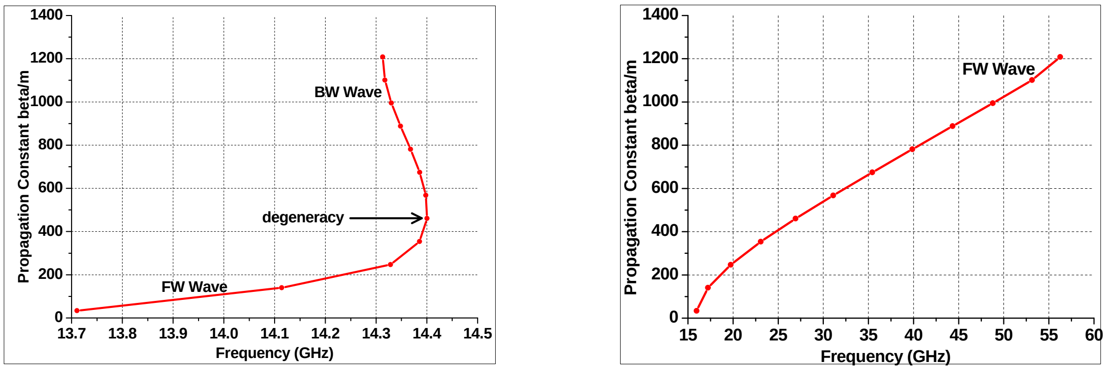

(a) (b)

Figure 3.17: The dispersion graph of the cases: when helical guide is in (a) Loaded with FF-unit cells or DMLHG structure. (b) free-space

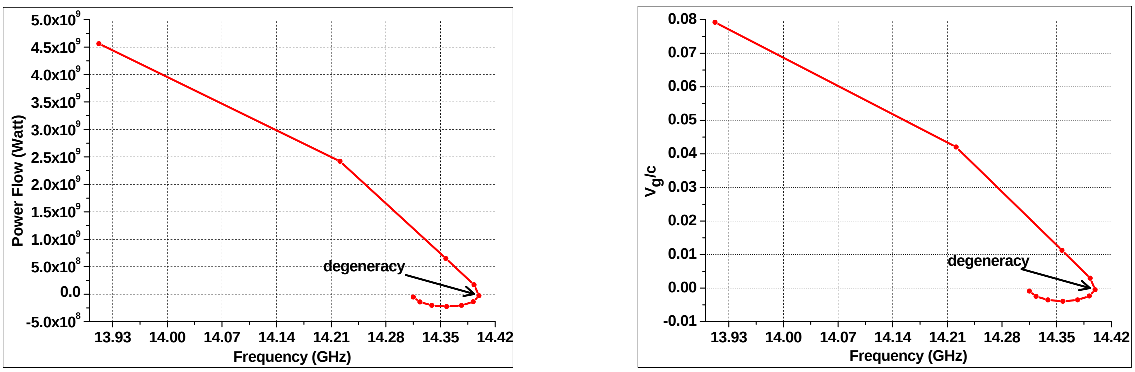

(a) (b)

Figure 3.18: The DMLHG structure plot of (a) Power flow *vs* frequency. (b) Group velocity *vs* frequency.

At critical frequency, absolute longitudinal magnetic field (H_z) distributions are plotted in Fig. 3.19 for different time intervals. The presence of slow wave effect in the structure can be easily seen as wave packet gets more and more compressed as phase advances with time. At the time of maximum wave packet compression shown in time interval-3, wave packets become stand still or trapped for a while. Thereafter a new wave packet train gets started and this process repeats itself. However, it is not possible to hold or trap a wave packet forever in the lossy medium.

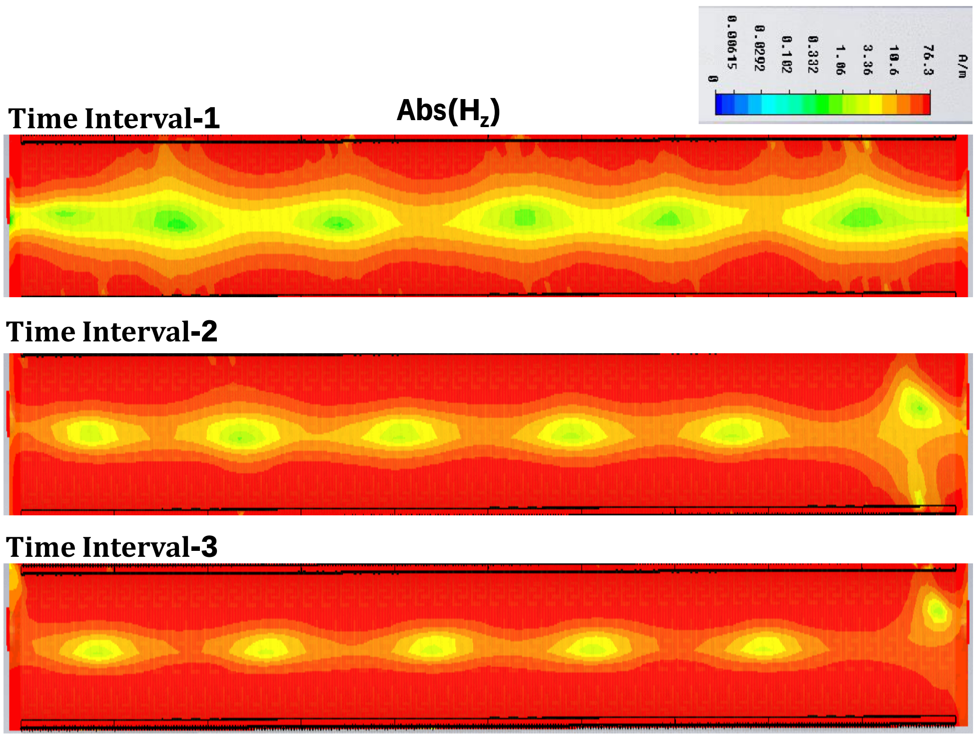

Figure 3.19: At critical frequency the amplitude of longitudinal magnetic field (H_z) is plotted along the length of FF-Shaped Metamaterial Loaded DMLHG structure.

3.3.2 Second DMLHG design

An alternative to FF-shaped metamaterial cell is the S-shaped metamaterial cell [62] that is also considered to realize the DMLHG structure. It has resonance spectrum between 8.72 to 9.28 GHz. The design procedure is the same as we have described in earlier case. The S-Shaped loaded DMLHG structure is shown in Fig. 3.20(a).

In order to figure out the pass band of this design we have performed a full wave time domain simulation of this structure (shown in Fig. 3.20(a)). For that purpose DMLHG structure is excited by coaxial feed at both ends. Obtained transmission-

(S_{21}) and reflection- (S_{11}) coefficients results are shown in Fig. 3.20(b). It is observed that this arrangement also possesses a pass-band or resonance band which almost overlaps the pass-band spectrum of S-shaped metamaterial cell.

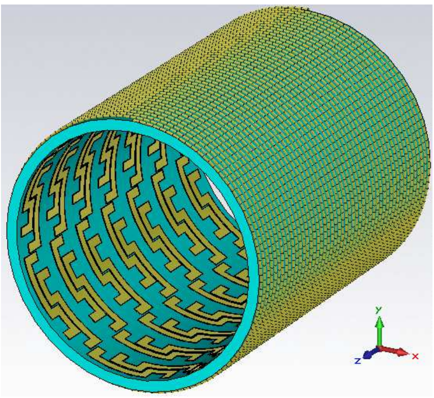

(a)

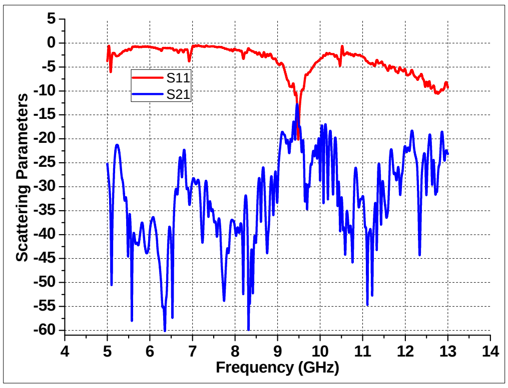

(b)

Figure 3.20: (a) The S-Shaped metamaterial cells loaded DMLHG structure (b) its transmission (S_{21}) and reflection (S_{11}) results.

The Eigen mode simulation of unit cell S-shaped DMLHG structure (shown in Fig. 3.21(a)), for its obtained pass band spectrum (shown in Fig. 3.21(b)), is performed as we did for the first case. The modal dispersion characteristics is shown in Fig. 3.21(b) where it can be seen that this design also exhibits BW mode, FW mode and mode-degeneracy behaviour.

The electromagnetic simulation of these two designs reveal similar characteristics as reported in analytical characterization. But resonance characteristics or pass band characteristics are observed in a slightly shifted frequency spectrum. The reason behind this could be Drude model which is used as a dispersive parameter in analytical study. While in simulations study actual field configurations modify the effective constitutive parameters.

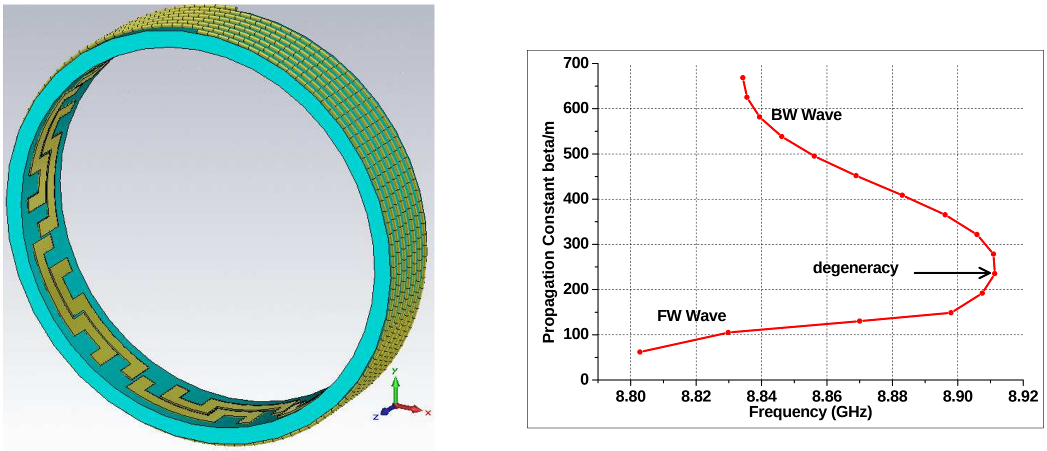

(a)

Figure 3.21: (a) The unit cell of DMLHG structure loaded with SS-shaped metamaterial cells. (b) Its dispersion characteristics.

3.4 Engineering and Manufacturing Feasibility at Different Spectrum

In order to manufacture the DMLHG structure, one needs to design curved Metasurfaces inside the helical guide, which is possible by using flexible substrate materials [63] like polyimide, plastic, transparent conductive polyester, polyester, FR-4 etc. These substrate materials are widely used in manufacturing of Flexible electronics which can be folded and bended without any functional deformation.

The size of metamaterial inclusions on Metasurface is decided by the spectrum where DMLHG structure needs to operate. In order to realize DMLHG structure at very high frequency spectrum, the size of metallic inclusions should be in the order of μm or nm. Using present day IC (integrated circuit) fabrication technologies such as electron beam lithography and photo lithography such miniaturized design is possible. For 1 THz [64], 6 THz [65], 70 THz [66] and 200 THz [67], Split Ring

Resonator (SRR) have already been fabricated and its magnetic response is observed experimentally.

In the present study, both analytical and simulation characteristics have been presented in GHz spectrum. As described, the frequency range where DMLHG structure exhibited the characteristics of slowing and trapping of EM wave belongs to the spectrum where loaded metamaterial cell have a pass-band. So, we can shift or tune this spectrum by scaling the size of metamaterial cells. In table-1, we have presented the dimensions of FF-DMLHG structure for attaining similar characteristics in THz frequency range (in between 12 to 14 THz).

Table 3.1: Design of FF-DMLHG in THz Regime (dimensions in μm)

Helix radius	Wire radius	Pitch	FF-cell height (h)	FF-cell width (w)
5.68	0.05	0.08	4.65	2.5

3.5 Summary

In this Chapter, we have investigated the modal characteristics of a Dispersive Metamaterial Loaded Helical Guide (DMLHG). Analytical characterizations reveal that both FW and BW modes propagate simultaneously and are degenerate at the same frequency. The mechanism of mode-degeneracy leads to the stopping of the EM wave. BW mode propagates as a fundamental mode which possesses enhanced slow wave characteristics. Analytical findings have been verified by electromagnetic simulations of two practically feasible designs.

In this study, for the first time, we have coupled the characteristics of conventional helical slow wave structure with metamaterial properties for possible applications in contemporary field of slow waves and optoelectronics. Various waveguide based metamaterial designs have already been proposed for such applications. Most of these designs are in cylindrical [40, 41] or planar [27–29, 36–39] in shape and support multi-modal characteristics. We believe that DMLHG structure has two distinguished advantages (i) it supports single mode operation, therefore, excitation of the desired mode would be easier and (ii) at the same time its reconfigurability for different spectra is much easier which in turn cuts down the re-engineering costs wherein helix pitch angle provides an additional knob to control the wave velocity.

Other slow wave methods which are based on surface plasmon polaritons having issues of sensitivity to surface roughness and are relatively difficult to excite [27]. At the same time photonics crystal based devices possess multimodal characteristics [27]. As compared to these methods our structure doesn't have any issue of mode excitation and multimodal behaviour.

Chapter 4

ENG Cladded Metamaterial Loaded Helical Waveguide*

4.1 Introduction

The Slow Wave Device (SWD) proposed in this chapter is Epsilon Negative (ENG) Cladded Metamaterial Loaded Helical Guide (CMLHG). The Metamaterial Loaded Helical Guide (MLHG) is described in Chapter-2, had metamaterial was loaded as a core, inside the helical guide. In addition it may be possible that the MLHG can be cladded by some material such as DPS material, ENG material etc. Such cladding may affect its modal characteristics. Followings are the motives behind this investigation:

(a) To analyse the effect of cladding over slow wave performance of MLHG.

(b) To design of more enhanced slow wave device as compared to MLHG.

(c) To design a slow-wave delay line in the form of optical fiber/cable.

*This work has been published in *Journal of Electromagnetic Waves and Applications* (*TaylorFrancis*), Vol. 29, 2501-2511 (2015).

(d) To avoid external interference by introducing cladding in the structure.

4.2 Analytical Theory Formulation

The geometry of waveguide of interest is illustrated in Fig. 4.1. It consists of a sheath helix of radius, a, filled with metamaterial in region-I ($\rho < a$) having dielectric permittivity and permeability ϵ_1 and μ_1 respectively, and is cladded by epsilon negative (ENG) material in region-II ($a < \rho < b$) and having dielectric permittivity and permeability ϵ_2 and μ_2, respectively. The thickness of cladding layer is $b - a$ and it is surrounded by region III ($\rho > b$) which is a free-space medium having dielectric permittivity and permeability as ϵ_3 and μ_3 respectively. All media considered here are homogeneous, isotropic and non-dispersive.

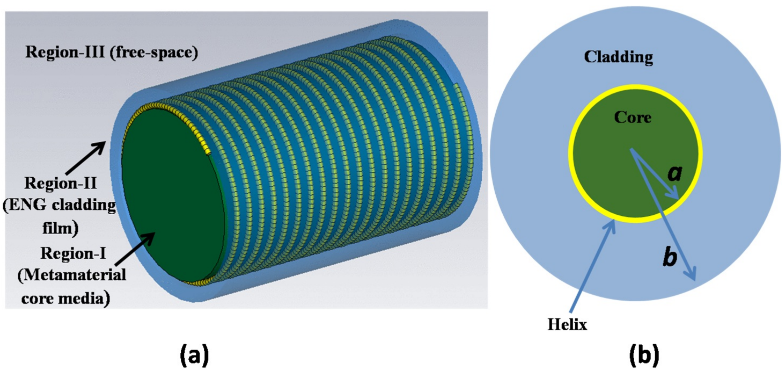

Figure 4.1: (a) Longitudinal view of ENG Cladded Metamaterial Loaded Helical Guide (CMLHG). Here region-I is metamaterial which is loaded inside helical guide. Region-II is ENG cladding layer. (b) Represents the cross sectional view of the structure.

The electric and magnetic field components in different regions are written as [5]:

$$E_{zi} = -k_i^2\Big(A_i I_n(k_i\rho) + B_i K_n(k_i\rho)\Big)e^{jn\phi}e^{-j\beta z} \tag{4.1}$$

$$H_{zi} = -k_i^2\Big(C_iI_n(k_i\rho) + D_iK_n(k_i\rho)\Big)e^{jn\phi}e^{-j\beta z} \tag{4.2}$$

$$E_{\phi i} = \Big(\frac{n\beta}{\rho}\Big(A_iI_n(k_i\rho) + B_iK_n(k_i\rho)\Big) + j\omega\mu_ik_i\Big(C_iI_n'(k_i\rho) + D_iK_n'(k_i\rho)\Big)\Big)e^{jn\phi}e^{-j\beta z} \tag{4.3}$$

$$H_{\phi i} = \Big(\frac{n\beta}{\rho}\Big(C_iI_n(k_i\rho) + D_iK_n(k_i\rho)\Big) - j\omega\epsilon_ik_i\Big(A_iI_n'(k_i\rho) + B_iK_n'(k_i\rho)\Big)\Big)e^{jn\phi}e^{-j\beta z} \tag{4.4}$$

$$E_{\rho i} = \Big(-j\beta k_i\Big(A_iI_n'(k_i\rho) + B_iK_n'(k_i\rho)\Big) + \frac{\omega\mu_in}{\rho}\Big(C_iI_n(k_i\rho) + D_iK_n(k_i\rho)\Big)\Big)e^{jn\phi}e^{-j\beta z} \tag{4.5}$$

$$H_{\rho i} = \Big(-j\beta k_i\Big(C_iI_n'(k_i\rho) + D_iK_n'(k_i\rho)\Big) - \frac{\omega\epsilon_in}{\rho}\Big(A_iI_n(k_i\rho) + B_iK_n(k_i\rho)\Big)\Big)e^{jn\phi}e^{-j\beta z} \tag{4.6}$$

Here A_i, B_i, C_i and D_i are field coefficients. The subscripts $i = 1, 2$ and 3 refer to region I, II and III, respectively, as shown in Fig. 4.1. $I_n(k_i\rho)$ and $K_n(k_i\rho)$ are modified Bessel functions of first and second kind respectively. Here n describes the modal behaviour of the waves. ($'$) represents the derivative of Bessel function with respect to its argument. Beta (β) is longitudinal phase coefficient. The transverse propagation constant, k_i, in guiding region and cladding regions are written as: $k_1 = \sqrt{\beta^2 - \epsilon_{r1}\mu_{r1}k_o^2}$ and $k_2 = \sqrt{\beta^2 + \epsilon_{r2}\mu_{r2}k_o^2}$, respectively, where $k_o = \omega\sqrt{\epsilon_o\mu_o}$.

4.2.1 Boundary conditions

(1) The finite field on the axis and its vanishing at the infinity this suggests that [5]:

$$B_1 = D_1 = A_3 = C_3 = 0 \tag{4.7}$$

(2) At helix boundary ($r = a$, between region I and II) the tangential components of electric and magnetic field are written as [5]:

$$E_{z1} = E_{z2}, E_{\phi 1} = E_{\phi 2}, E_{z1,2} = E_{\phi 1,2}cot(\phi), H_{z1} + H_{\phi 1}cot(\psi) = H_{z2} + H_{\phi 2}cot(\psi) \tag{4.8}$$

(3) At dielectric boundary ($r = b$, between region II and III) the electric and magnetic fields components for all $\phi-$ and $z-$ components are continuous [5]:

$$E_{z2} = E_{z3}, E_{\phi1} = E_{\phi2}, H_{z2} = H_{z3}, H_{\phi2} = H_{\phi3} \tag{4.9}$$

4.2.2 Dispersion relation

The system of eight linear homogenous equations are obtained after substituting field Eqs. (4.1) to (4.6) into corresponding boundary conditions Eqs. (4.7) to (4.9) at interface of regions I, II and regions II, III. The obtained eight equations are reduced to four equations after some algebraic and mathematical manipulations and having four variables, which are written as in the from of a determinant as shown below:

$$\begin{vmatrix} VI_n(k_2a) & VK_n(k_2a) & J_cI_n(k_2a) & Y_cK_n(k_2a) \\ WI_n(k_2a) & IK_n(k_2a) & VI_n(k_2a) & VK_n(k_2a) \\ PI_n(k_2b) & PK_n(k_2b) & RI_n(k_2b) & QK_n(k_2b) \\ -SI_n(k_2b) & -TK_n(k_2b) & PI_n(k_2b) & PK_n(k_2b) \end{vmatrix}$$

For EM wave propagation axial phase constant β should have finite value and it should satisfy the system of all eight homogenous equations. Eigen value solution of β requires the determinant of variable coefficient matrix to be zero. Obtained dispersion relation for hybrid mode after solving above determinant can be written as:

$$V\alpha\gamma P(R-Q)(I-W)+V^2P^2(\alpha-\gamma)^2+V^2(\alpha T-\gamma S)(\gamma R-Q\alpha)+P^2(\gamma Y_c-\alpha J_c)$$
$$(\gamma I-\alpha W)+(\gamma Y_cR-QJ_c\alpha)(T\gamma W-S\gamma I)+VP\alpha\gamma(Y_c-J_c)(T_S)=0 \tag{4.10}$$

Here, constants used in dispersion relation are given as:

$$V = k_2^2 - \frac{n\beta}{a}cot(\varphi), M = \frac{(k_1^2 a - n\beta cot(\varphi))^2}{\omega\mu_1 k_1 acot(\varphi)}\frac{I_n'(k_2a)}{I_n(k_2a)}, N = \frac{k_2^2\omega\epsilon_1 k_1 cot(\varphi)}{k_1^2}\frac{I_n(k_2a)}{I_n'(k_2a)}$$
$$J_c = -\omega\mu_2 k_2 cot(\varphi)\frac{I_n'(k_2a)}{I_n(k_2a)}, \alpha = I_n(k_2a)K_n(k_2b), Y_c = -\omega\mu_2 k_2 cot(\varphi)\frac{K_n(k_2a)}{K_n'(k_2a)}$$
$$W = M + N + y_1 cot(\varphi)\frac{I_n'(k_2a)}{I_n(k_2a)}, P = \frac{n\beta}{b}(1 - r_2^2), I = M + N + y_1 cot(\varphi)\frac{K_n'(k_2a)}{K_n(k_2a)}$$
$$R = \omega\Big(\mu_2 k_2\frac{I_n'(k_2b)}{I_n(k_2b)} - \mu_3 k_3\frac{k_2^2 K_n'(k_2b)}{k_3^2 K_n(k_2b)}\Big), Q = \omega\Big(\mu_2 k_2\frac{K_n'(k_2b)}{K_n(k_2b)} - \mu_3 k_3\frac{k_2^2 K_n'(k_3b)}{k_3^2 K_n(k_3b)}\Big),$$
$$S = \omega\epsilon_2\Big(k_2\frac{I_n'(k_2b)}{I_n(k_2b)} - k_3\frac{k_2^2 K_n'(k_3b)}{k_3^2 K_n(k_3b)}\Big), T = \omega\epsilon_2\Big(k_2\frac{K_n'(k_2b)}{K_n(k_2b)} - k_3\frac{k_2^2 K_n'(k_2b)}{k_3^2 K_n(k_2b)}\Big),$$
$$\alpha = I_n(k_2a)k_n(k_2b) and \gamma = I_n(k_2b)k_n(k_2a). \quad (4.11)$$

4.3 Results and Analysis

The dispersion behaviour of the structure is obtained by computing axial propagation coefficient (β) from dispersion relation (4.10). It is related with transverse wave vector in guiding media by $k_1 = \sqrt{\beta^2 - \epsilon_{r1}\mu_{r1}k_o^2}$, and in cladding film by $k_2 = \sqrt{\beta^2 + \epsilon_{r2}k_o^2}$ for ENG cladding and $k_2 = \sqrt{\beta^2 - \epsilon_{r2}k_o^2}$ for DPS cladding. For guided surface mode propagation, the values of phase constant β should be greater than $k_{o1}\sqrt{\epsilon_{r1}\mu_{r1}}$ for ENG cladding and for DPS cladding β should be greater than $k_{o1}\sqrt{\epsilon_{r1}\mu_{r1}}$ and $k_{o1}\sqrt{\epsilon_{r2}}$.

4.3.1 Metamaterial loading and ENG cladding effects on dispersion characteristics

Fig. 4.2, explains the normalised phase velocity ($k_o/\beta = v_p/c$) characteristics as a function of frequency for dominant mode case ($n = 0$). Phase velocity has been plotted in three situations - (i) when helix is loaded with metamaterial and cladded with ENG material, (ii) when helix is loaded with metamaterial and cladded with

DPS material, and (iii) when helix is in free space, to bring out the ENG cladding effects on phase velocity. From the graph it can be seen that in the case of both DPS and ENG cladding, normalised phase velocity decreases significantly in comparison to helix in free space. However decrease is more in ENG cladding. For example, at 200 THz, observed minimum normalized phase velocities (v_p/c) in three different scenario are 0.025, 0.034, 0.11, respectively. The reduction in normalised phase velocity in case (i) is 4.36 times more in comparison to case (iii), while this reduction in case (ii) is 3.29 times more in comparison to case (iii). However reduction in case (i) is almost 1.4 times more in comparison to case (ii).

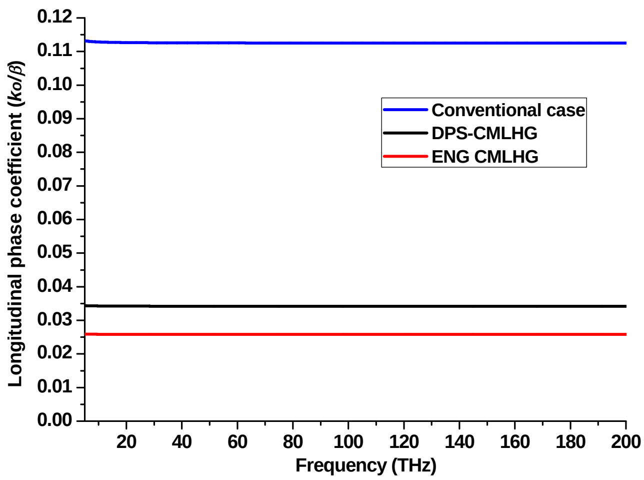

Figure 4.2: Dispersion characteristic (k_o/β vs frequency) for helical waveguide for different cases (a) Conventional case when helical guide is in free-space ($\epsilon_{r1} = 1$ and $\mu = 1$) only and no cladding (b) Helical guide loaded with metamaterial ($\epsilon_{r1} = -4$ and $\mu = -0.9$) with DPS material cladding ($\epsilon_{r1} = 1.1$ and $\mu = 1$), and (c) Helical guide loaded with metamaterial ($\epsilon_{r1} = -4$ and $\mu = -0.9$) with ENG material cladding ($\epsilon_{r1} = -1.1$ and $\mu = 1$). The values of outer radius is 50 μm, inner radius is 30 μm and pitch angle (ψ) is 10^o.

In Fig. 4.3, normalised phase velocity and effective index are plotted as a function of frequency for both dominant ($n = 0$) and higher order mode ($n = 1$) case. For lower frequency spectrum, higher order modes has lower phase velocity as compared to the dominant mode case, as shown in Fig. 4.3(a). This is due to large value of effective index which is plotted in Fig. 4.3(b). As the frequency increases, in both cases, both phase velocity and effective index values become almost constant. A very large value of propagation coefficient (β) is observed in both the cases having positive slope and positive group velocity that corresponds to forward ultra-slow wave mode. This fundamental mode propagates as a surface wave mode. Higher order modes are not observed over a wide band width.

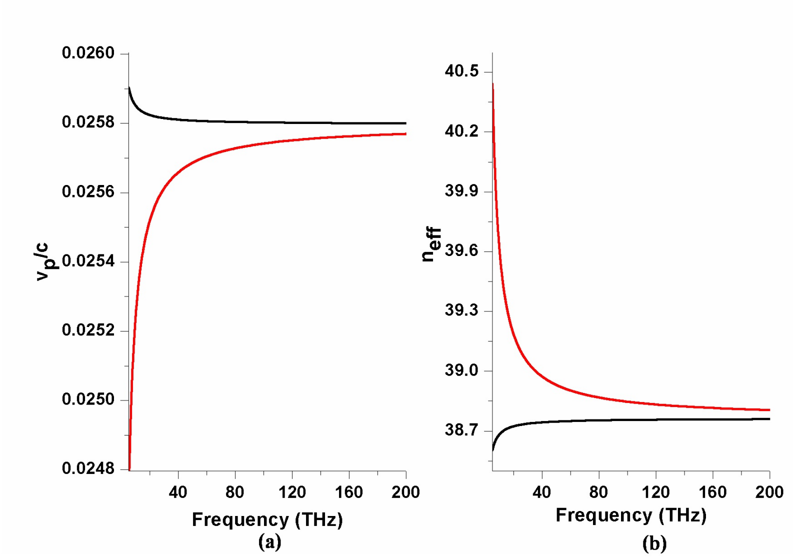

Figure 4.3: (a) The normalized phase velocity (v_p/c) and (b) Effective index ($n_{eff} = \beta/k_o$) of ENG CMLHG structure for both dominant mode ($n = 0$) and first higher order mode ($n = 1$) as a function of frequency at inner helix radius 30 μm, outer radius 50 μm and pitch angle 10^o.

The Electric field intensity distribution over the cross section of the ENG CMLHG is plotted in Fig. 4.4, for different frequencies. From the distribution it is observed that at lower frequency (5 THz), the electric field is confined in and around the core region (shown in Fig. 4.4(a)). As the frequency increases to 14 THz and 50 THz, electric field is more confined/concentrated in core region as shown in Fig. 4.4(b) and (c) and becomes very close to the centre of the core region. Such confinement is observed in the structure due to the presence of large values of longitudinal phase coefficients. This will produce higher values of effective index for the entire spectrum and that will lead to a strong confinement of EM wave.

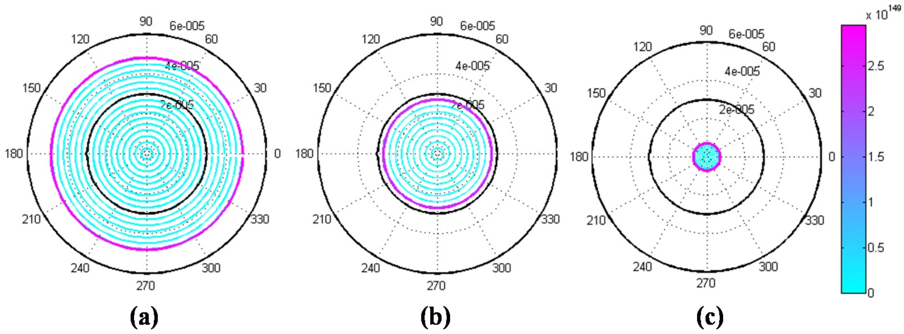

Figure 4.4: Contour plots of Electric field intensity distribution (n = 0 mode) over the cross section of ENG CMLHG structure for different frequencies such as 5 THz, 14 THz, and 54 THz which are represented by Figs4. (a), (b), and (c), respectively. The black inner circle represents the core region and outer circle is for cladding.

4.3.2 Helical guide geometrical effects on dispersion characteristics

Helical guide radius, a, cladding film radius, b, and helix pitch angle, ψ, are the three physical parameters that affect dispersion characteristics of the guide. Effect of helix radius or guiding medium radius is shown in Fig. 4.5. From the graph it is observed that increase in radius enhances slow wave characteristics of the guide at lower frequencies and it becomes almost constant at higher frequencies. As compared to the helix radius, cladding film radius b, exhibits almost negligible effects on dispersion characteristics which is not shown. The effects of pitch angle variations are shown in Fig. 4.6. The slow wave behaviour of guide is highly enhanced with decrease in pitch angle, for example at 5 THz normalised phase velocity, v_p/c, for 30^o is 0.08, for 20^o is 0.05, and for 10^o is 0.03. From the graph it can be seen that wave velocity has strong dependence on the helix pitch angle. The values of v_p/c reaches to 0.001 at pitch angle of 0.5^o, which could be further enhanced by varying the pitch angle.

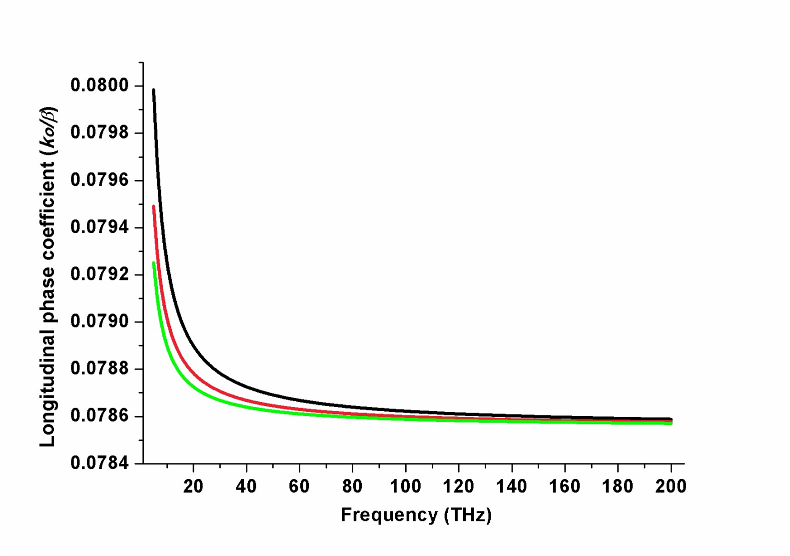

Figure 4.5: Dispersion characteristic (k_o/β vs frequency) of ENG CMLHG structure is plotted as a function of frequency for different inner helix radii, a, values: 10 μm, 20 μm and 30 μm and which are represented by black, pink and green colors, respectively. The value of outer radius is 50 μm and pitch angle, ψ, is 10^o.

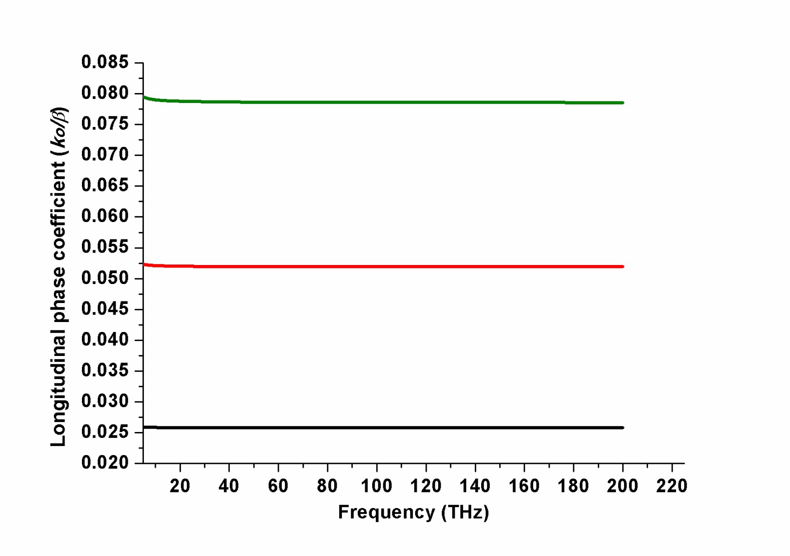

Figure 4.6: Dispersion characteristic (k_o/β vs frequency) of ENG CMLHG structure is plotted as a function of frequency for different pitch angle values:10^o, 20^o and 30^o and which are represented by black, red and green colors, respectively. The value of outer radius is 50 μm and inner radius is 30 μm .

4.3.3 Core and cladding medium properties effects on dispersion characteristics

Medium properties of guiding media and cladding film also affect dispersion characteristics of the guide. Fig. 4.7(a), shows the effect of ϵ_{r1}- values variation on phase velocity reduction as a function of frequency by keeping μ_{r1}- value constant. From the graph it can be seen that wave becomes more slower with increase in dielectric constant. For example at 30 THz, normalised phase velocity, v_p/c, for $\epsilon_{r1} = -10$ and $\mu_{r1} = -0.9$ is 0.04, for $\epsilon_{r1} = -4$ and $\mu_{r1} = -0.9$ is 0.07 and for $\epsilon_{r1} = -2$ and $\mu_{r1} = -0.9$ is 0.10. In Fig. 4.7(b), the effect of guiding media permeability is shown where slow wave characteristic is also enhance as increase in permeability values, for example at 30 THz, normalised phase velocity, v_p/c, for and $\epsilon_{r1} = -4$ and $\mu_{r1} = -0.9$ is 0.07, for $\epsilon_{r1} = -4$ and $\mu_{r1} = -0.5$ is 0.11 and for $\epsilon_{r1} = -4$ and $\mu_{r1} = -0.3$ is 0.15.

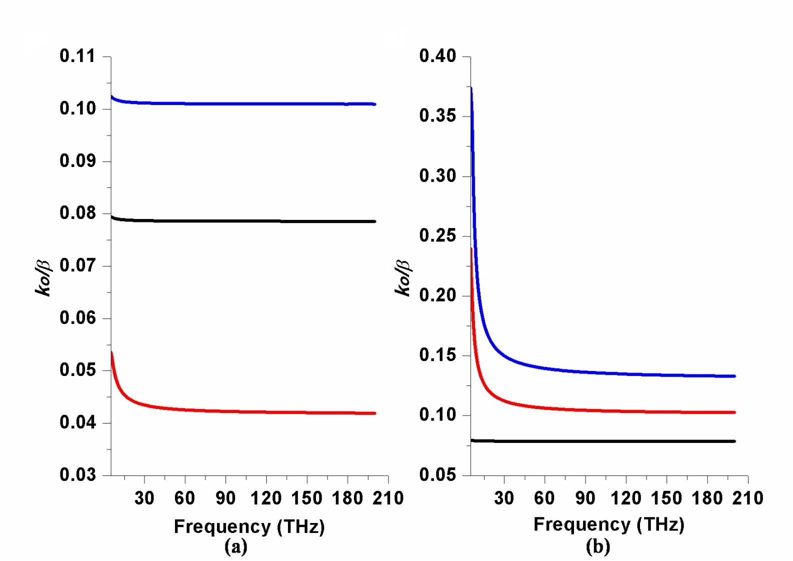

Figure 4.7: Dispersion characteristic (k_o/β *vs* frequency) of ENG CMLHG structure is plotted as a function of frequency for different metamaterial properties in the core region. (a) Represents the effect of change in permittivity values. Considered media values are: (i) $\epsilon_{r1} = -10$ and $\mu = -0.9$, (ii) $\epsilon_{r1} = -4$ and $\mu = -0.9$, and (iii) $\epsilon_{r1} = -2$ and $\mu = -0.9$, respectively which are represented by red, black and blue colors. (b) Represents the effect in change of permeability values. Considered values are: (i) $\epsilon_{r1} = -4$ and $\mu = -0.9$, (ii) $\epsilon_{r1} = -4$ and $\mu = -0.5$ and (iii) $\epsilon_{r1} = -4$ and $\mu = -0.3$, respectively which are represented by black, red and blue colors.

The effect of cladding film medium properties on slow wave characteristics is shown in Fig. 4.8, which is a non-magnetic medium. It is observed that increase in dielectric constant makes phase velocity slower. For example at 30 THz, v_p/c for $\epsilon_{r2} = -3.1$ is 0.068, for $\epsilon_{r2} = -2.1$ is 0.073, and for $\epsilon_{r2} = -1.1$ is 0.08, respectively.

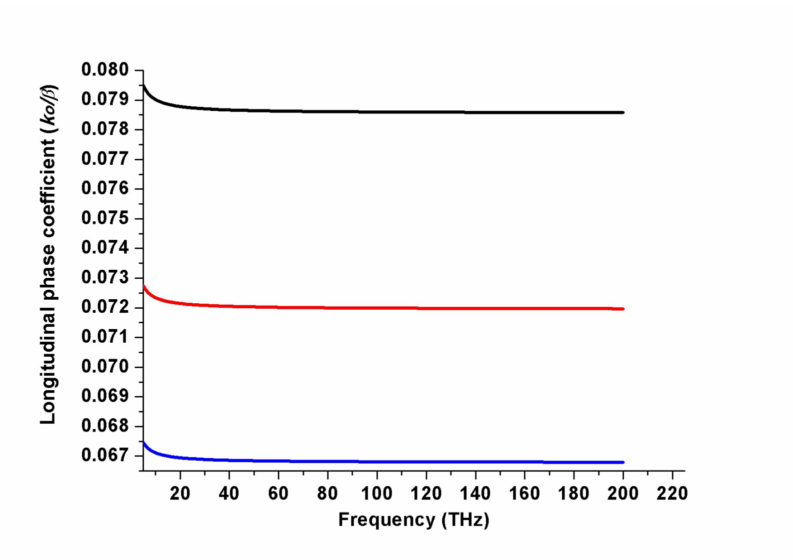

Figure 4.8: Dispersion characteristic (k_o/β *vs* frequency) of ENG CMLHG structure is plotted as a function of frequency for different ENG cladding medium properties (a) $\epsilon_{r2} = -1.1$ and $\mu = 1$ (b) $\epsilon_{r2} = -2.1$ and $\mu = 1$ and (c) $\epsilon_{r2} = -3.1$ and $\mu = 1$ which are represented by black, red and blue colors, respectively.

4.4 Designing Feasibility of ENG Cladded Metamaterial Loaded Helical Guide at THz to Optical Frequencies

For fabricating proposed structure one needs to create metamaterial region inside helical guide. In the above analysis, the effect of fixed negative values of ϵ_r and μ_r are described over the frequency range. However, in realistic metamaterial cases both ϵ_r and μ_r are dispersive [5]. Hence, metamaterial cells are designed in such a way that the negative values of ϵ_r and μ_r lie in the desired frequency spectrum. In literature, several metamaterial geometries are proposed in microwave regime. For achieving similar characteristics in THz regime the size of metamaterial cell should be in the order of nm. Through present day fabrication technologies such as electron beam lithography, photo lithography etc. these sizes can be realized. For 1 THz [64], 6 THz [65], 70 THz [66] and 200 THz [67], SRR (split ring resonators) is already fabricated and its magnetic response achieved experimentally. Other possible ways to realize such metamaterial medium inside helical guide is by filling it by anisotropic metamaterial. Many anisotropic metamaterials are proposed and demonstrated in literature [68, 69] for THz and optical frequency range.

For cladding film, metal can be used. It exhibits negative dielectric constant at frequencies of interest. The value of metal dielectric constant at any frequency (ω) is decided by plasma frequency of metal, ω_p, which depends on free-electron density in that crystal which is an intrinsic property of the metal. The plasma frequency could be tailored by some other ways such as proper design of diameter of metallic photonic crystal or by semiconductor doping. Also by proper design of metal-dielectric lattice plasma frequency can be altered. Thus, the value of dielectric constant can be engineered for desired limit.

4.5 Summary

In this Chapter, we have analyzed and characterized an ENG Clad metamaterial loaded helical waveguide as a slow wave device to control wave velocity from THz to optical frequency range. It supports fundamental mode with large reduction in wave velocity over a wide bandwidth. The wave velocity could be engineered by setting material parameters. The helical waveguide radius and the pitch angle provide extra knobs to control the wave velocity. The contour plots of the electric field distribution show that this structure supports a highly confined optical wave which can find applications in imaging, sensing and optical signals processing. This structure has distinct advantages such as large reduction in group velocity and almost constant phase velocity over a wide bandwidth.

Chapter 5

Extremely Anisotropic Metamaterial loaded Helical Guide*

5.1 Introduction

In this Chapter we present, Extremely Anisotropic Metamaterial loaded Helical Guide (EAMLHG) as a Slow Wave Device (SWD). The extremely Anisotropic Metamaterial is a uniaxial medium having tensor permittivity $(\epsilon_{xx}; \epsilon_{yy}; \epsilon_{zz})$ also known as Hyperbolic Metamaterial (HMM). In optical spectrum, metamaterial medium can also be realized through Hyperbolic Metamaterial (HMM). As compared to the left-handed metamaterial (*Sec.* 3.3.1), the realization of metamaterial medium through HMM is comparatively easier.

Many such Extremely Anisotropic Metamaterial (EAM) have been fabricated and tested experimentally [68, 69]. Such realizations opened the door for their varied applicability and ease the fabrication of metamaterials at optical frequency range.

*This work has been submitted in *IEEE Journal of Light Wave Technology*.

Recently, some groups have superimposed anisotropic metamaterial characteristics with waveguide structures to achieve slow wave. Huang et al. [37] have investigated anisotropic nano wires and found that electromagnetic wave can be slowed or even trapped inside a waveguide. Similar observations have also been reported by Jiang et al. [36] where they have studied an anisotropic metamaterial cladded air waveguide and found that different thickness of waveguide correspond to different frequencies that are being stopped.

The motive behind this work is to avoid fabrication limitations faced in Dispersive Metamaterial Loaded Helical Guide (DMLHG) and introduce an alternative SWD that has similar capabilities as observed in DMLHG such as slowing and trapping of EM wave. However, it is quite possible that the future technological advances may rule out the fabrication limitations of DMLHG.

5.2 EM Wave Propagation and Power Flow on Extremely Anisotropic Waveguide

The geometry of the structure under study is shown in Fig. 5.1, where helical guide is loaded with Extremely Anisotropic Metamaterial (EAM). For EAM, the value of permittivity in the transverse direction is negative while it is positive in longitudinal direction. The tensor values of permittivity in x, y, z directions are ϵ_x, ϵ_y and ϵ_z respectively and related by Eq. (5.1). Region I (inner region) is filled with extremely anisotropic metamaterial media and Region II (outer-region) is free-space.

$$\epsilon_x = \epsilon_y = \epsilon_t, \quad \epsilon_z \neq \epsilon_t \tag{5.1}$$

where ϵ_t is transverse permittivity.

We consider the EM wave propagation in the helical guide of radius a along z

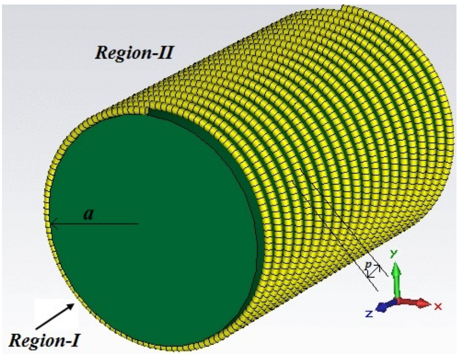

Figure 5.1: An extremely anisotropic metamaterial loaded helical waveguide of radius a and pitch p. The waveguide is aligned along the z direction.

direction with $e^{jn\phi}$ turn variations. The core *i.e.* region-I ($\rho < a$) is filled with extremely anisotropic metamaterial and region-II ($\rho > a$) outside helix is free-space. Here ρ is dimension from the center of the guide in xy plane. The field components for different regions are written and described in terms of various Bessel functions. For region-I, the field components are:

$$E_{z1} = AI_n(k_1\rho)e^{jn\phi}e^{j\beta z} \tag{5.2}$$

$$H_{z1} = BI_n(k_2\rho)e^{jn\phi}e^{j\beta z} \tag{5.3}$$

$$E_{\phi 1} = \frac{-1}{k_2^2}\Big(\frac{\beta n}{\rho}AI_n(k_1\rho) + i\omega\mu_1 k_2 BI_n'(k_2\rho)\Big)e^{jn\phi}e^{j\beta z} \tag{5.4}$$

$$H_{\phi 1} = \frac{-1}{k_2^2}\Big(i\omega\epsilon_t k_1 AI_n'(k_1\rho) - \frac{\beta n}{\rho}BI_n'(k_2\rho)\Big)e^{jn\phi}e^{j\beta z} \tag{5.5}$$

For Region-II:

$$E_{z2} = CK_n(k_3\rho)e^{jn\phi}e^{j\beta z} \tag{5.6}$$

$$H_{z2} = DK_n(k_3\rho)e^{jn\phi}e^{j\beta z} \tag{5.7}$$

$$E_{\phi 2} = \frac{-1}{k_3^2}\Big(\frac{\beta n}{\rho}CK_n(k_3\rho) + i\omega\mu_2 k_3 DK_n'(k_3\rho)\Big)e^{jn\phi}e^{j\beta z} \tag{5.8}$$

$$H_{\phi 2} = \frac{-1}{k_3^2}\Big(i\omega\epsilon_2 k_3 CK_n'(k_3\rho) - \frac{\beta n}{\rho}DK_n'(k_3\rho)\Big)e^{jn\phi}e^{j\beta z} \tag{5.9}$$

Here A, B, C and D are field coefficients and are determined by matching boundary conditions at the interface of different regions. The ($'$) on Bessel function represents its derivative. The medium parameters of region-I and II are ϵ_1, μ_1 and ϵ_2, μ_2 respectively. In region-I, transverse component of permittivity (ϵ_t) is negative and longitudinal component of permittivity (ϵ_z) is positive.

$$\epsilon_t < 0, \quad \epsilon_z > 0, \tag{5.10}$$

Beta (β) is the longitudinal propagation coefficient along the guide. It is related with transverse wave vectors (k_1, k_2 and k_3) and free-space propagation vector (k_o) by:

$$k_1 = \sqrt{\epsilon_z}\sqrt{\beta^2/\epsilon_t - k_o^2} \tag{5.11}$$

$$k_2 = \sqrt{\beta^2 - k_o^2\epsilon_t} \tag{5.12}$$

$$k_3 = \sqrt{\beta^2 - k_o^2} \tag{5.13}$$

At region-I and II boundary ($\rho = a$), helical waveguide boundary conditions [5] in term of ϕ and z are:

$$E_{z,1} = E_{z,2} \tag{5.14}$$

$$E_{\phi,1} = E_{\phi,2} \tag{5.15}$$

$$E_{z,1} = -E_{\phi,1}cot(\psi) \tag{5.16}$$

$$E_{z,2} = -E_{\phi,2}cot(\psi) \tag{5.17}$$

$$H_{z,1} + H_{\phi,1}cot(\psi) = H_{z,2} + H_{\phi,2}cot(\psi) \tag{5.18}$$

For deriving the dispersion equation of the structure, the field expressions (5.2) to (5.9) are substituted in corresponding boundary conditions (5.14) to (5.18) which produces a system of four linear homogeneous equations having four unknown constants A, B, C and D. A non-trivial solution of the fields exists only if 4×4 determinants formed by the coefficients of the unknown constants in the set of equations vanish. After some mathematical manipulation, obtained dispersion equation for Hybrid modes is shown below. Due to skewed boundary conditions helical guide only supports propagation of Hybrid (HE) modes.

$$k_o a^2 c\epsilon_t k_1 cot(\psi)\frac{I_n'(k_1a)}{I_n(k_1a)} - \frac{X^2}{k_o a^2 c\mu_1 k_2 cot(\psi)}\frac{I_n(k_2a)}{I_n'(k_2a)} - k_o a^2 c\epsilon_2 k_3 cot(\psi)R^2\frac{K'n(k_3a)}{K_n(k_3a)} + \frac{Y^2R^2}{k_o a^2 c\mu_2 k_3 cot(\psi)}\frac{K_n(k_3a)}{K_n'(k_3a)} = 0 \quad (5.19)$$

Here $X = (k_2a)^2 - n\beta a cot(\psi)$, $Y = (k_3a)^2 - n\beta a cot(\psi)$ and $R = k_2/k_3$.

The components of Poynting vectors for a propagating wave inside the helical guide are:

$$S_z = \frac{1}{4\pi}(E_rH_\phi^* - E_\phi H_r^*) \quad (5.20)$$

$$S_r = \frac{1}{4\pi}(E_zH_\phi^* - E_\phi H_z^*) \quad (5.21)$$

$$S_\phi = \frac{1}{4\pi}(E_zH_r^* - E_rH_z^*) \quad (5.22)$$

The total flow of power in the waveguide is summation of power flow in different layers of waveguide

$$P_z = P_z^{in} + P_z^{out} \quad (5.23)$$

with $P_z^{in} = 2\pi\int_0^a S_z r\,\mathrm{d}r$ and $P_z^{out} = 2\pi\int_a^\infty S_z r\,\mathrm{d}r$.

Obtained expressions for power flow inside and outside the waveguide are:

$$P_z^{in} = \frac{1}{4tau_2^2}\Big(- 2\beta\omega\epsilon_t tau_1^3 I_n^2(tau_1)PA^2 - 2\beta\omega\mu_1 tau_2^3 I_n^2(tau_2)PB^2 + i(\omega^2\mu_1 n\epsilon_t - \beta^2 n)AB \Big(\int_0^{tau_1}(I_{n-1}(x)I_n(vx) + I_{n+1}(x)I_n(vx))\,\mathrm{d}x \int_0^{tau_2}(I_{n-1}(x)I_n(zx) + I_{n+1}(x)I_n(zx))\,\mathrm{d}x\Big)\Big) \quad (5.24)$$

$$P_z^{out} = \frac{1}{4tau_3^2}\Big(- 2\beta\omega\epsilon_2 tau_3^3 K_n^2(tau_3)QC^2 - 2\beta\omega\mu_2 tau_3^3$$
$$K_n^2(tau_3)QD^2 + i(\beta^2 n - \omega^2\mu_1 n\epsilon_t)CD$$
$$\Big(\int_{tau_3}^{\infty} (K_{n-1}(x)K_n(x) + K_{n+1}(x)K_n(x))\,\mathrm{d}x\Big)\Big) \quad (5.25)$$

Here $tau_1 = k_1a$, $tau_2 = k_2a$, $tau_3 = k_3a$, $v = \sqrt{\epsilon_t/\epsilon_z}$, $z = \sqrt{\epsilon_z/\epsilon_t}$, $R = I_n'(x)/xI_n(x)$, $S = -K_n'(x)/xK_n(x)$, $P = -xR^2 - 2/xR + n^2/x^3 + 1/x$, $Q = xS^2 - 2/xS - n^2/x^3 - 1/x$.

The total normalized power flow is:

$$\Big\langle P_z \Big\rangle = \frac{P_z^{in} + P_z^{out}}{|P_z^{in}| + |P_z^{out}|} \quad (5.26)$$

5.3 Mode Analysis

The dispersion relation (5.19) is solved numerically, using Findroot subroutines of Mathematica Software package, for modal characteristics of the proposed structure. Usually we compute axial propagation constant (β) for respective values of free space propagation constant (k_o). However, in the present study, it is more convenient to compute k_o as a function of k_2. The value of longitudinal phase coefficient (β) is calculated through the relation $\beta = \sqrt{k_2^2 + \epsilon_t k_o^2}$. For guided mode propagation, the values of k_1, k_2 and k_3 should be positive. Thus the limit of k_o that allows guided mode propagation in the structure is $k_o^2 < \frac{k_2^2}{1-\epsilon_t}$. The considered extremely anisotropic metamaterial is non-dispersive in nature. For present analysis, we have considered the values of $\epsilon_t = -3$ and $\epsilon_z = 2$.

5.3.1 For dominate mode ($n = 0$)

A plot of $k_o a$ vs $k_2 a$ is plotted (in Fig. 5.2) for the dominant mode ($n = 0$). It is seen from the figure that a band of frequencies results in different modes and hence we refer to Fig. 5.2 as band spectrum of EAMLHG.

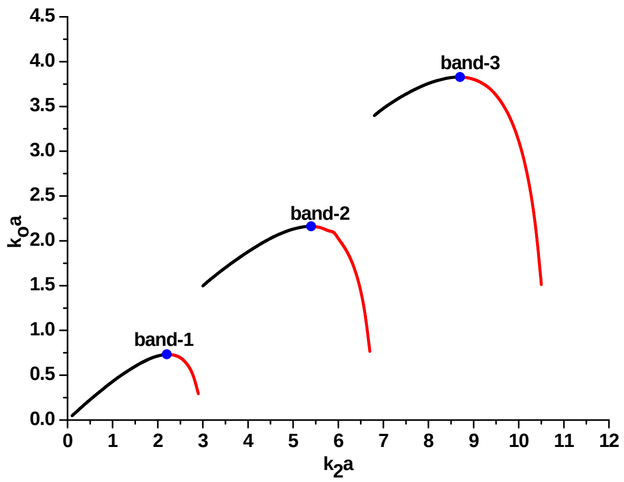

Figure 5.2: Guided HE mode characteristics of band spectrum of EAMLHG structure as a function of normalized propagation vectors. Here propagation vectors are normalised with waveguide radius a and have pitch angle $\psi = 30^o$, $\epsilon_t = -3$ and $\epsilon_z = 2$. The degeneracy point of forward and backward wave modes is shown by solid blue circle for every band spectrum.

We observe that for the first band spectrum mode (band-1), which occupies a spectrum of $k_o a = 0.047$ to 0.73, two guided modes are propagating simultaneously. The mode with $k_2 >> k_o$, having $d(k_2 a)/d(k_o a) < 0$, is designated/known as backward wave (BW) mode (shown in red colour) while the other is designated as forward wave (FW) mode (shown in black colour). Both the guided modes merge at a particular point which is called as mode-degeneracy point and is shown by a solid blue circle in Fig. 5.2. This point $d(k_2 a)/d(k_o a) = 0$ signifies the meeting of both the modes. Beyond this mode there is a forbidden region and thereafter second band mode spectrum having different frequency spectrum propagates. The computed values of effective index ($n_{eff} = \beta/k_o$) of these modes are shown in Fig. 5.3. From the graph it can be seen that BW wave modes have very high value of effective index in comparison to FW wave mode. For example, BW mode which propagates in the spectrum $k_oa = 0.76$ to 2.16 has effective index (n_{eff}) of 8.57 at $k_oa = 0.76$. The higher values of effective index result into lowering of the EM wave velocity.

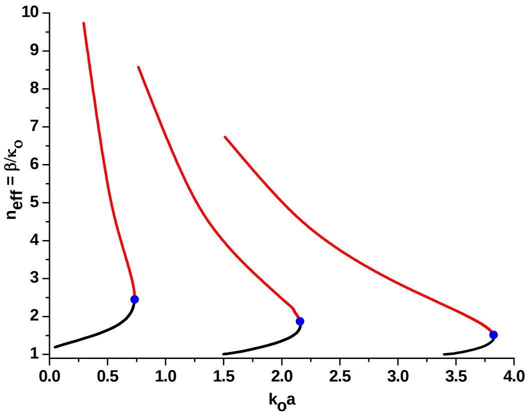

Figure 5.3: The Effective index (n_{eff}) characteristics of first three band spectra of EAMLHG structure as a function of normalized propagation vectors. Here propagation vectors are normalised with waveguide radius a and have pitch angle $\psi = 30^o$, $\epsilon_t = -3$ and $\epsilon_z = 2$. The degeneracy point of forward and backward wave modes of these band spectra is shown by solid blue circle.

We have considered axial propagation constant β positive throughout the Chapter to identify BW and FW mode propagation behaviour. Another way to define BW and FW mode would be in term of normalized power flow ($\langle P_z \rangle$). For $\langle P_z \rangle > 0$, the phase propagation and energy flow are in the same direction and the mode is a FW mode while for $\langle P_z \rangle < 0$, the energy flow and phase propagation are anti-parallel and the mode is BW mode. Mathematically this can be defined as:

$$P_z^{in} + P_z^{out} \leq 0 \quad if \quad d(k_oa)/d(k_1a) \leq 0 \tag{5.27}$$

$$P_z^{in} + P_z^{out} \geq 0 \quad if \quad d(k_oa)/d(k_1a) \geq 0 \tag{5.28}$$

The normalized power flow ($\langle P_z \rangle$) of the respective modes of Fig. 5.2 are computed using Eq. (5.26) and are plotted in Fig. 5.4. Here it can be seen that at degeneracy point, the value of normalized energy flow ($\langle P_z \rangle$) vanishes. The mode-degeneracy mechanism leads to slowing and eventual stopping of EM wave.

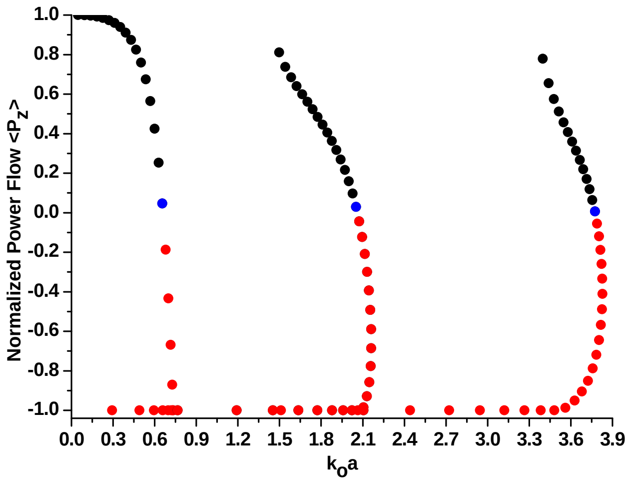

Figure 5.4: Normalized energy flow ($< P_z >$) characteristics of first three band spectra of EAMLHG structure as a function of normalized propagation vectors. Here propagation vectors are normalised with waveguide radius a and have pitch angle $\psi = 30^o$, $\epsilon_t = -3$ and $\epsilon_z = 2$. The degeneracy point of forward and backward wave mode is shown by solid blue circle.

5.3.2 For higher order mode ($n = 1$)

For the first higher order mode ($n = 1$) the band spectrum of the guide is shown in Fig. 5.5. The modal behaviour has similar characteristics as the fundamental mode ($n = 0$) with both BW and FW mode coexisting within same spectrum and meeting at mode-degeneracy point. The major noticeable observation is that bandwidth spectrum of BW mode propagation has increased while the bandwidth spectrum of FW mode has reduced significantly. Also, it can be seen that higher band spectrum supports larger BW mode bandwidth in comparison to FW mode.

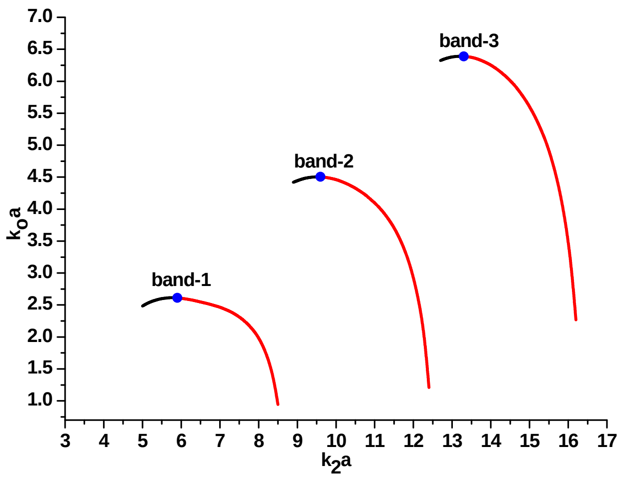

Figure 5.5: Mode band spectrum characteristics of EAMLHG for higher order ($n = 1$) HE mode as a function of normalized propagation vectors. Here propagation vectors are normalised with waveguide radius a and have pitch angle $\psi = 30^o$, $\epsilon_t = -3$ and $\epsilon_z = 2$. The degeneracy point for forward and backward wave mode is shown by blue solid circle.

In Fig. 5.6, the effective index characteristics of corresponding modes of Fig. 5.5, are computed and plotted. Here, it is observed that BW mode possesses higher value of effective index as compared to dominant mode. For example in BW mode (shown in Fig. 5.6) obtained value of effective index is $n_{eff} = 6.2$ at $k_oa = 1.9$ which is higher compared to $n_{eff} = 2.58$ obtained in dominant mode case at same frequency point.

The normalised power flow characteristics of higher order mode is also computed and plotted in Fig. 5.7. Similar to dominant mode here power flow also stops at mode-degeneracy point.

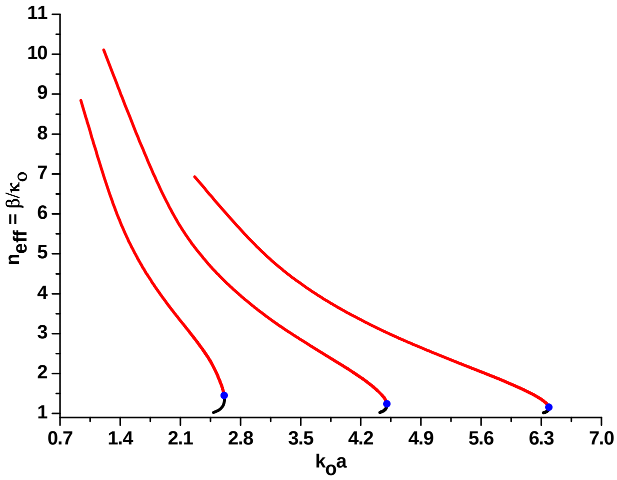

Figure 5.6: The Effective index (n_{eff}) characteristics of first three band spectra for higher order ($n = 1$) HE mode as a function of normalized propagation vectors. Here propagation vectors are normalised with waveguide radius a and have pitch angle $\psi = 30^o$, $\epsilon_t = -3$ and $\epsilon_z = 2$. The degeneracy point for forward and backward wave mode is shown by blue solid circle.

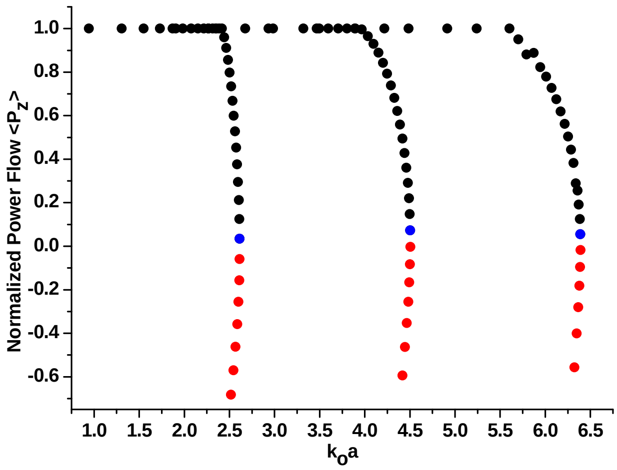

Figure 5.7: Normalized energy flow ($< P_z >$) characteristics of first three band spectra for higher order ($n = 1$) HE mode as a function of normalized propagation vectors. Here propagation vectors are normalised with waveguide radius a and have pitch angle $\psi = 30^o$, $\epsilon_t = -3$ and $\epsilon_z = 2$. The degeneracy point for forward and backward wave mode is shown by blue solid circle.

5.3.3 Effect of media parameters on modal behaviour

The anisotropic metamaterial media parameters such as tangential permittivity (ϵ_t) and longitudinal permittivity (ϵ_z) also affect dispersion characteristics of the guide. In order to understand the effect of these parameters we first analyse the effect of tangential permittivity at dominant mode case. We considered three representative cases: (a) $\epsilon_t = -1$, $\epsilon_z = 2$ (b) $\epsilon_t = -3$, $\epsilon_z = 2$ and (c) $\epsilon_t = -5$, $\epsilon_z = 2$. We have considered $\epsilon_z = 2$ (a fixed value) for all the three cases. In Fig. 5.8, dispersion graph is plotted for different tangential permittivity variations, it shows that with increase in the value of ϵ_t, the bandwidth spectrum of both FW and BW modes spectrum increases for example in case-(c) both modes propagate for a large spectrum in the guide. At the same time guide slow wave behaviour is more enhanced with increased ϵ_t values.

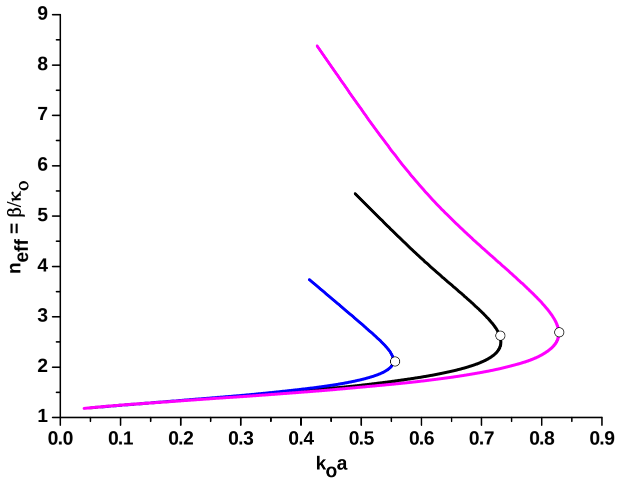

Figure 5.8: Effect of tangential permittivity (ϵ_t) variation on guided mode characteristics of EAMLHG at $n = 0$ and $\psi = 30$. Three different scenario cases: (a) $\epsilon_t = -1$, $\epsilon_z = 2$, (b) $\epsilon_t = -3$, $\epsilon_z = 2$ and (c) $\epsilon_t = -5$, $\epsilon_z = 2$ are shown by blue, black and magenta colours, respectively.

Similar to previous case in order to study the effect of longitudinal permittivity ϵ_z on the dispersion behaviour, we considered again three representative cases: (a)

$\epsilon_t = -3$, $\epsilon_z = 2$ (b) $\epsilon_t = -3$, $\epsilon_z = 4$ and (c) $\epsilon_t = -3$, $\epsilon_z = 6$. We have considered $\epsilon_t = -3$ (a fixed value) for all three cases. In Fig. 5.9 dispersion graph is plotted for different longitudinal permittivity variation cases which shows that with decrease in ϵ_z the bandwidth spectrum of both BW and FW modes increases and slow wave behaviour of guide is also more enhanced.

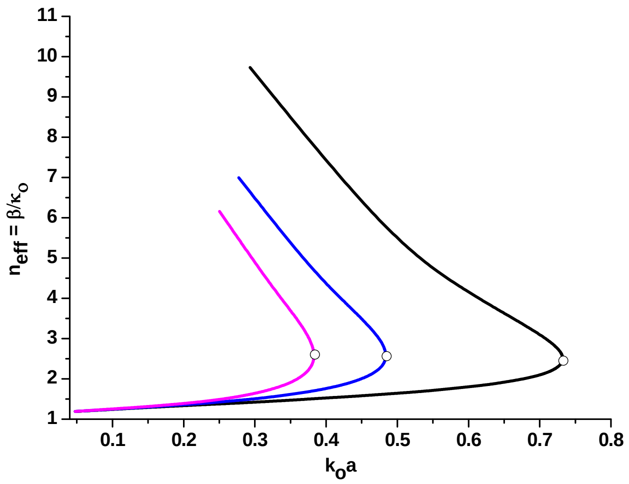

Figure 5.9: Effect of longitudinal permittivity (ϵ_z) variation on guided mode characteristics of EAMLHG at $n = 0$ and $\psi = 30$. Three different scenario: (a) $\epsilon_t = -3$, $\epsilon_z = 2$, (b) $\epsilon_t = -3$, $\epsilon_z = 4$ and (b) $\epsilon_t = -3$, $\epsilon_z = 6$ represented by black, blue and magenta colours, respectively.

5.3.4 Effect of physical parameters of the helical guide on modal behaviour

In the present model, in addition to metamaterial properties (ϵ_t and ϵ_z). Helix radius (a) and pitch angle (ψ) are the two physical dimensions of the waveguide which can affect the modal characteristics. In results described above, radius (a) is normalized with propagation vector by k_o. Therefore, the effect of radius can be understood by taking a constant frequency.

Thus the pitch angle is only remaining parameter whose effects need to be studied.

The effects of pitch angle variation on modal behaviour are plotted in Fig. 5.10. It is observed that reduction in pitch angle increases the effective index (n_{eff}) of the guide, for example maximum value of effective index (n_{eff}) at pitch angle, 30^o, 20^o and 10^o, are 9.7, 15.5 and 32.1, respectively. This increased value of effective index enhances slow wave behaviour of the guide. The change in pitch angle changes both electric and magnetic field configurations which modifies the dispersion properties in the waveguide and results in a much slower wave.

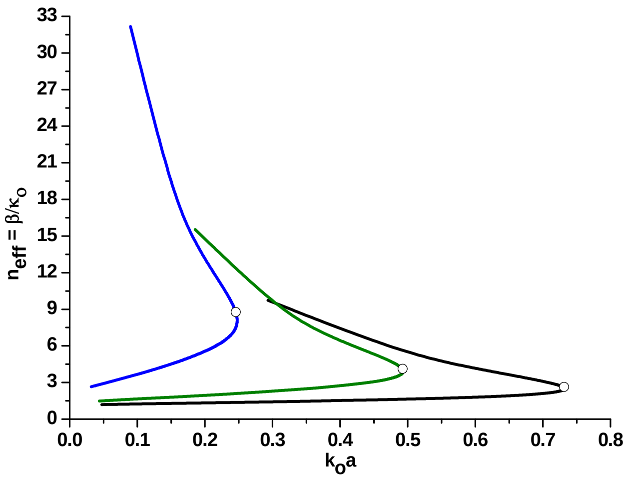

Figure 5.10: Effect of pitch angle variation on guided mode characteristics of EAMLHG. The black, green and blue colours represent pitch angles 30^o, 20^o and 10^o, respectively.

Also, the reduction in pitch angle reduces the bandwidth spectrum of both FW and BW modes. For example, the bandwidth of both the modes at pitch angle, 30^o, 20^o and 10^o are 0.68, 0.44 and 0.21 (is in term of $k_o a$), respectively. It can also be seen from the graph that change in pitch angle shifts the mode-degeneracy point. Therefore, position or frequency of stopping of wave can be tailored by adjusting pitch angle value. Thus helix pitch angle provides an extra knob to control its slow wave behaviour.

5.3.5 Comparison of extremely anisotropic metamaterial loaded helical guide with extremely anisotropic metamaterial cylindrical guide

In order to figure out the advantages of present investigation on EAMLHG over Extremely Anisotropic Metamaterial Cylindrical Guide (EAMCG) [37], we have compared modal characteristics of these two waveguides structure as shown in Fig. 5.11, when there is a helical winding over the EAMCG (present study) and when there is no helical winding over EAMCG [37]. From the graph, it is observed that due to helix winding over waveguide, a large value of effective index, n_{eff}, is achieved as compared to the EAMCG. This is due to inherent properties of helix which already possesses slow wave characteristics. Also it can be seen that cut off frequencies for both FW and BW modes are shifted to almost zero. Another major advantage of present study of EAMLHG structure is the helix pitch angle, ψ, which provides an extra knob to control the slow wave behaviour.

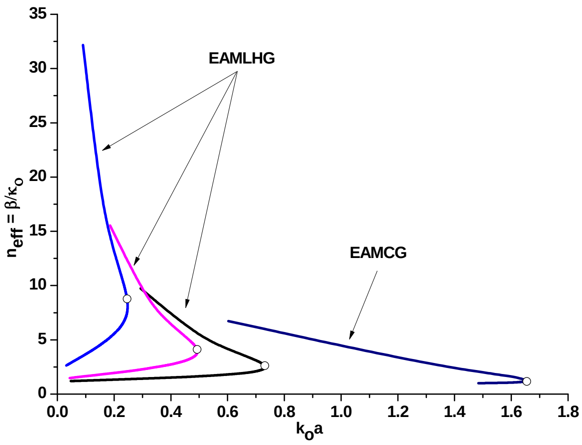

Figure 5.11: A comparison graph is plotted in between EAMLHG and Extremely Anisotropic Metamaterial Cylindrical Guide (EAMCG) for first guided HE mode. The black, pink and blue colours represent guided mode of EAMLHG for pitch angle 30^o, 20^o and 10^o, respectively. The blue colour represents guided mode of Extremely anisotropic cylindrical guide.

5.4 Design and Engineering Feasibility of Proposed Waveguide

For practical realization of the proposed waveguide structure one needs to create extremely anisotropic metamaterial media inside the helical guide. We have adopted the following procedure to realize such waveguide structure:

(a) First we arranged equally thick alternative disks (radius 60 nm and thickness 10 nm) of silver and glass. Considering the multi-layered structure of silver and glass having respective permittivity ϵ_m and ϵ_a the effective permittivity of such a multi-layered structure can be deduced as:

$$\epsilon_t = f\epsilon_m + (1-f)\epsilon_a \tag{5.29}$$

$$\epsilon_z = \frac{\epsilon_a \epsilon_m}{f\epsilon_a + (1-f)\epsilon_m} \tag{5.30}$$

Here f is the volume fraction. Silver behaves as a plasmonic material at optical frequencies which exhibits negative permittivity ($\epsilon_m < 0$) as a function of frequency [71]. For an example, at 450 THz, silver permittivity (ϵ_m) is -17.89 and glass permittivity is 2.25. For 50 % filling of each silver and glass discs and using above Eqs. (5.29) and (5.30), the calculated effective permittivity values of ϵ_t and ϵ_z, are -13.97 and 0.82, respectively. This arrangement will effectively look like a solid cylindrical waveguide possessing extremely anisotropic metamaterial properties from THz to optical frequency ranges.

(b) Once the solid cylinder is formed then one can wind thin wire of radius 3 nm in a form of helix having pitch angle 17^o over this cylinder. This complete arrangement is an EAMLHG structure, as shown in Fig. 5.12.

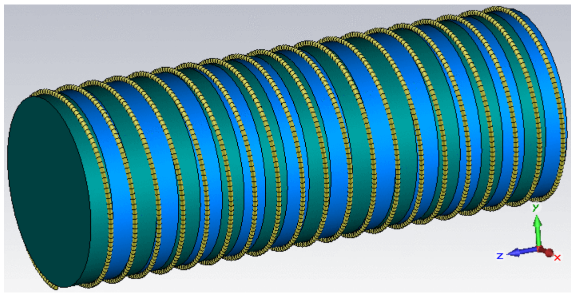

Figure 5.12: A sketch of the realization of an EAMLHG structure made of alternative disks of silver and glass.

To visualize the modal behaviour of this structure or to obtain effective index (n_{eff}) of this structure (shown in Fig. 5.12), we performed an analytical analysis of the structure by computing the value of transverse propagation coefficient (k_2) as a function of k_o. The dispersion graph of the structure is plotted in Fig. 5.13. We find that the highest value of effective index is $n_{eff} = 28$ at $k_o a = 0.251$ or $\lambda = 1.5$ μm, in BW mode. Both the waves FW and BW are degenerated at $k_o a = 0.374$ or $\lambda = 1$ μm and this point corresponds to the point of wave stopping.

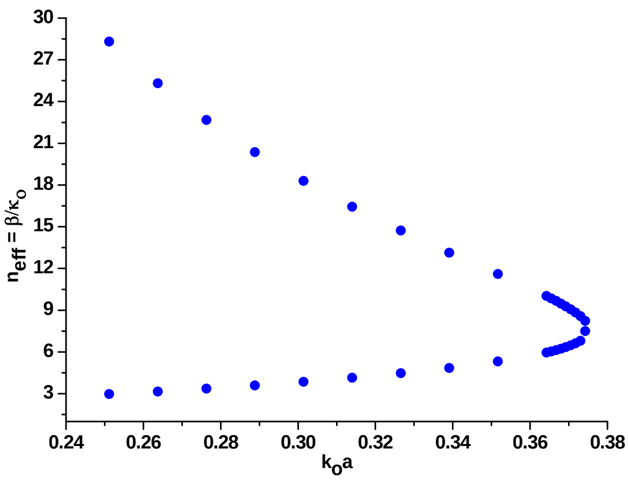

Figure 5.13: The analytical characteristics of effective index n_{eff} for fundamental HE mode of EAMLHG having radius (a) 60 nm and pitch angle (ψ) 17^o.

5.5 Summary

In summary, we proposed and studied, an extremely anisotropic metamaterial loaded helical waveguide which exhibits FW, BW and mode degeneracy characteristics. The Eigen-mode equation of the structure is derived analytically and computed to visualize modal behaviour. The expression of energy flow is also derived and analysed. It is observed that guide supports propagation of HE modes having very high value of effective index which can be engineered through helix pitch angle, ψ, unlike the other waveguide structures [37, 38, 41, 72].

The possible engineering realization of proposed waveguide is also discussed. The two distinguishing characteristics of the structure made up of extremely anisotropic metamaterial have been presented. The first one is that the BW mode that supports very high value of effective index (n_{eff}) and results in lowering the wave velocity. These structures can be utilized as filters and phase shifters in telecommunication and optics. The second feature of proposed waveguide is that both FW and BW modes coexist and are degenerate at critical frequency and at that point net power flow is zero or in other words wave has zero wave velocity. This attribute can be utilized to design compact optical buffer for integrated optical circuits.

Chapter 6

Summary and Future Scope

6.1 Summary

This dissertation work has been devoted to the analysis and design of novel Slow Wave Devices (SWD's). Through these devices we have addressed the possibilities of realization of optoelectronic devices such as optical buffers and optical memory, which are the key elements of future optical communication network architecture. Helical Waveguide, for a long time, is used as a structure induced slow wave device for various microwave to millimetre wave applications. On the otherhand, metamaterial medium, also, possesses slow wave characteristics which is classified as material induced slow wave as reported by different research groups. In order to achieve enhanced slow waves we have superimposed the properties of metamaterial with helical waveguide characteristics by proposing Metamaterial Loaded Helical Guide (MLHG) structure as a SWD in Chapter-2. The metamaterial medium considered here is non-dispersive in nature which is an ideal case of metamaterial. The Eigen value equation or the dispersion relation of the structure has been derived analytically. From analytical simulation we have demonstrated that this type of waveguide supports propagation of both FW and BW modes. The BW mode dies out rapidly in the guide but FW mode propagates as a ultra slow wave mode due to the presence of very large value of longitudinal propagation coefficient (β) in the waveguide. We have also analysed the effect of LHM properties and physical parameters of helical guide over slow wave characteristics. We have concluded that insertion of metamaterial in helical guide enhances slow wave behaviour of the guide drastically.

In Chapter-3, we have studied this structure (MLHG) by considering metamaterial as dispersive in nature, which is a more realistic case of metamaterial since non-dispersive metamaterials are not realized experimentally, yet. The dispersion relation of Dispersive Metamaterial Loaded Helical Guide (DMLHG) has been derived analytically. For analytical study, dispersive behaviour of metamaterial is modelled through Drude model and from simulations we have observed that it supports propagation of both FW and BW mode. The Lower Cutoff Frequency (LCF) of BW mode is lower than the FW mode and it propagates as ultra slow wave mode due to the presence of large value of longitudinal phase coefficients. Both modes propagate simultaneously and meet at common Higher Cutoff Frequency (HCF) and this point is regarded as mode-degeneracy point. The normalized power flow ($<P_z>$) is also zero at this point. Therefore, we have concluded that the mechanism of degeneracy leads to trapping or stopping of EM wave.

In order to design DMLHG structure, we have designed, fabricated and tested experimentally a novel FF-shaped metamaterial cell. This cells has been further arranged periodically both in axial- and radial- directions inside the helical guide in order to realize DMLHG structure. The designed structure is simulated numerically and it exhibits similar characteristics as we have reported in analytical study such as presence of FW and BW mode and phenomena of mode-degeneracy. At the point of mode-degeneracy power flow also becomes zero. So, the mechanism of degeneracy and high value of propagation coefficient leads to trapping and slowing of EM wave. In numerical simulation the phenomena of slowing and trapping of EM wave occurs in the spectrum of 12 to 14 GHz. In analytical simulation similar characteristics occur in the spectrum of 4 to 6 GHz. The reason behind this shift is Drude model which is used as a dispersive parameter in analytical study. While in simulations study actual field configurations modify the effective constitutive parameters of Drude model.

In Chapter-4, we have discussed the effect of cladding over slow wave characteristics of MLHG structure. Different cladding materials such as double positive material (DPS) and Epsilon Negative (ENG) Material effects are investigated. We have demonstrated analytically that the cladding enhances the slow wave characteristics of MLHG. However, in case of ENG Cladded MLHG (ENG-CMLHG) slow wave characteristics are enhanced greatly and improve by 4.36 and 1.4 times as compared to MLHG and DPS Cladded MLHG (DPS-CMLHG) cases, respectively. The electric field intensity distribution over the cross section of the waveguide has also been studied which attributes that as frequency increases electric field distribution is more confined to the core region of the waveguide which can find application in THz imagining.

In Chapter-5, we have presented Extremely Anisotropic Metamaterial Loaded Helical Guide (EAMLHG) as a SWD. The extremely Anisotropic Metamaterial is a uniaxial medium having tensor permittivity ($\epsilon_{xx}; \epsilon_{yy}; \epsilon_{zz}$) also known as Hyperbolic Metamaterial (HMM). As compared to left-handed metamaterial utilized in design of DMLHG, the realization of HMM is easier in high frequency regime, particular at optical frequency. Therefore, we proposed EAMLHG structure. The Eigen value relation or dispersion relation of the structure has been derived analytically. In analytical simulation we have observed similar characteristics as we observed in DMLHG case such as propagation of FW and BW modes, mechanism of mode-degeneracy and slowing and trapping of EM wave.

To design EAMLHG we have suggested an arrangement of stacked alternative disks of silver and glass inside the helical guide. Silver behaves as plasmonic material at optical frequency and exhibits negative permittivity. This multilayer geometry of silver and glass appears as a solid cylinder and having effectively Extremely Anisotropic Metamaterial (EAM) properties in THz to optical frequency spectrum. The designed structure has been investigated analytically and numerically and exhibits similar characteristics of slowing and trapping of EM wave.

Thus, in the present thesis work we have analysed, simulated and characterized novel slow wave devices, namely, MLHG, DMLHG, ENG-CMLHG, EAMLHG which are the combination of helical waveguide geometry and metamaterial properties.

In literature various cylindrical and planer based metamaterial waveguide have already been proposed for slow wave applications but all show multimodal behaviour. In comparison, DMLHG design exhibits single mode operation and does not have any issues related to multimodal propagation. However EAMLHG does show multimodal behaviour but it supports a very high value of effective index which in turn produces much slower wave as compared to the cylindrical and planar ones. The other added advantage of proposed helix based design is that it has "helix pitch angle" as an additional design parameter which provides an extra knob to control slow wave performance of the device. Our structures are also insensitive to surface roughness and are easier to excite as compared to other slow wave methods which are based on surface plasmon polaritons [27].

6.2 Future works

In this thesis work we thoroughly explored, for the first time, applications of metamaterial with helical guide in the contemporary field of slow wave and optoelectronics. Since, this is a primitive study in this area a wide range of research issues are still open. Following are the possible studies that can be explored further on the basis of present research work:

(a) In the present work only guided mode characteristics of the structures have been investigated. The leaky mode and radiation characteristics of these structures also can be investigated.

(b) Slow wave structure is major component of a Travelling Wave Tube (TWT) device. The applications of proposed SWD's can also be investigated for TWT's and other high power microwave devices.

(c) The fabrication and experimental study of proposed structures can be done for the validation of reported results and designs.

(d) Possible design of ENG-CMLHG can also be explored.

(e) In EAMLHG we considered only Type-II Hyperbolic Metamaterial (HMM) where tensor permittivity is negative in x and y directions ($\epsilon_x < 0, \epsilon_y < 0$) and positive in z direction ($\epsilon_{zz} > 0$). However Type-I HMM is also possible where tensor permittivity is positive in x and y directions ($\epsilon_x > 0$ and $\epsilon_y > 0$) and negative in z direction ($\epsilon_{zz} < 0$). The design and numerical simulation of EAMLHG structure can also be done with Type-I HMM.

(f) As discussed, DMLHG and EAMLHG structure exhibits trapping of EM wave as a function of both frequency and radius of the helix waveguide, which is normalized as $k_o a$. The simulation study can be further extended by designing the tapered helix geometry both in increasing or decreasing the helix radius. This study will throw more understanding of EM wave trapping characteristics as done by other groups for different geometries [27, 33, 41].

Bibliography

[1] Veselago, V. G., "The Electrodynamics of substances with simultaneous negative values of ϵ and μ," *Soviet Phys. Uspekhi*, Vol. 1, No. 4, 509–514, 1968.

[2] Shelby, R. A., D.R. Smith and S. Schultz, "Experimental verification of a negative index of refraction," *Science*, Vol. 29, 77–79, 2001.

[3] Vendik, I. B. and O. G. Vendik, "Metamaterials and their application in microwaves: A review," *Technical Physics*, Vol. 58, 1–24, 2013.

[4] Abbott. D, "Metamaterials in the Terahertz Regime," *IEEE Photonics Journal*, Vol. 1, 2009.

[5] Zhang, K and D. Li, *Electromagnetic Theory for Microwaves and Optoelectronic* , Springer, New York, 2008.

[6] Landau, L. D. and E. M. Lifshitz, and L. P. Pitaevskii, *Electrodynamics of Continuous Media*, Linacre House, Jordan Hill, Oxford, UK: Butterworth Heinemann, 1984.

[7] J. D. Jackson, *Classical Electrodynamics*, John Wiley, third ed., 1998.

[8] J. Pendry, A. Holden, D. Robbins, and W. Stewart, "Magnetism from conductors and enhanced nonlinear phenomena," *IEEE Trans. Microwave Theroy Tech.* Vol. 47, p. 2075, Nov 1999.

[9] Zhou, J., Study of left-handed materials, Ph.D. Thesis, Iowa State University Ames, Iowa, 2008.

[10] Eleftheriades and K. G. Balmain , *Negative-Refraction Metamaterials: Fundamental Principles and Applications*, Wiley-IEEE Press, 2005.

[11] J. H. Lvl, X. WeiHu1, M. Liu, B. R. Yan and L. H. Kong, "Negative refraction of a double L-shaped metamaterial," *J. Opt. A: Pure Appl. Opt.* vol. 11, pp. 01–05, 2009.

[12] D. Wang, L. Ran, H. Chen, M. Mu, J. A. Kong and B. Wu, "Experimental validation of negative refraction of metamaterial composed of single side paired S-ring resonators," *Appl. Phy. Lett.* vol. 90, 2007.

[13] F. Urbani, "Experimental analysis of novel single-sided left-Handed metamaterial," *IEEE Antennas and Wireless Propag. Lett.* vol. 09, pp. 720–723, 2010.

[14] P. Kolinko and D. R. Smith, "Numerical study of electromagnetic waves interacting with negative index materials," *Opt. Express* vol. 11.7, pp. 640–648, 2003.

[15] Z. Dong , S. Zhu, H. Liu , J. Zhu and W. Cao, "Numerical simulations of negative-index refraction in wedge-shaped metamaterials" *Phys. Rev. E* vol. 72, pp. 016607, 2005.

[16] Maradudin, A. A., *Structured Surfaces as Optical Metamaterials* , Cambridge University Press, 2011.

[17] Oh, S. S and O. Hess, "Chiral metamaterials: enhancement and control of optical activity and circular dichroism," *Nano Convergence*, 2015.

[18] Hannam, K, David A. Powell, Ilya V. Shadrivov, and Yuri S. Kivshar, "Broadband chiral metamaterials with large optical activity," *Physical Review B*, Vol. 89, 2014.

[19] Shekhar, P, J. Atkinson and Z. Jacob, and Y. S. Kivshar, "Hyperbolic metamaterials: fundamentals and applications," *Nano Convergence* , Vol. 89, 2014.

[20] Ferraria, L, Chihhui Wub,c, Dominic Lepaged, Xiang Zhangb,c, Zhaowei Liua , "Hyperbolic metamaterials and their applications," *Progress in Quantum Electronics*, Vol. 40, 2015.

[21] Drachev. V. P., V. A. Podolskiy, and A. V. Kildishev , "Hyperbolic metamaterials: new physics behind a classical problem ," *Optics Express*, Vol. 21, 2013.

[22] Basu, B. N., *Electromagnetic Theory and Application in Beam-Wave Electronics* , World Scientific, Singapore, 1996.

[23] M. D. Lukin and A. Imamoglu, "Controlling photons using electromagnetically induced transparency," *Nature* Vol. 413, 273–276 (2001).

[24] E. Gehrig, M. van der Poel, J. Mork, and O. Hess, "Dynamic Spatiotemporal Speed Control of Ultrashort Pulses in Quantum-Dot SOAs," *IEEE J. Quant. Electron.* Vol. 42, 1047–1054 (2006).

[25] M. S. Bigelow, N. N. Lepeshkin, and R. W. Boyd, "Superluminal and Slow Light Propagation in a Room-Temperature Solid," *Science* Vol. 301, 200–202 (2003).

[26] Y. Okawachi, M. S. Bigelow, J. E. Sharping, Z. Zhu, A. Schweinsberg, D. J. Gauthier, R. W. Boyd, and A. L. Gaeta, "Tunable All-Optical Delays via Brillouin Slow Light in an Optical Fiber," *Phys. Rev. Lett.* Vol.94, 153902 (2005).

[27] K. L. Tsakmakidis, A. D. Boardman, and O. Hess, "Trapped rainbow' storage of light in metamaterials," *Nature* Vol. 450, 397–401 (2007).

[28] Bait, M. M, Suwailam and Zhizhang Chen "Surface-Wave Along Double-Negative (DNG) Slab Waveguide," *Microwave and Optical Technology Letters*, Vol. 44, No. 06, 494–498, 2003.

[29] Erfaninia, H and A. Rostami "Group Velocity Reduction in Multilayer Metamaterial Waveguide," *Optik*, Vol. 124, 1230-1233, 2013.

[30] Salvatore, S, B. D. F. Casse, W. Lu and S. Sridhar "Observation of slow-light in a metamaterials waveguide at microwave frequencies ," *Applied Physics Letters*, Vol. 98, 171907, 2011.

[31] Gennaro, E. Di, P. V. Parimi, W. T. Lu, and S. Sridhar "Slow microwaves in left-handed materials ," *Phy. Rev. B*, Vol. 72, 033110, 2005.

[32] Bait, M. M, Suwailam and Zhizhang Chen "Slow Propagation of Electromagnetic Waves in a Dielectric Slab Waveguide With a Left-Handed Material Substrate ," *IEEE Microwave and Components Letters*, Vol. 16, No. 02, 2005.

[33] Jiang, T, Junming Zhao and Yijun Feng "Stopping light by an air waveguide with anisotropic metamaterial cladding ," *Optics Express*, Vol. 17, 102529, 2008.

[34] E.F. Burmeister, D.J. Blumenthal, J.E. Bowers "A comparison of optical buffering technologies," *Optical Switching and Networking* , 2007.

[35] Rodney S. Tucker, Pei-Cheng Ku, and Constance J. Chang-Hasnain "Slow-Light Optical Buffers: Capabilities and Fundamental Limitations," *Journal of Light Wave Technology*, Vol. 23, 2012.

[36] T. Jiang, J. Zhao, and Y. Feng, "Stopping light by an air waveguide with anisotropic metamaterial cladding," *Opt. Express* Vol. 17, 170–177 (2008).

[37] W. T. Lu, Y. J. Huang, B. D. F. Casse, R. K. Banyal, and S. Sridhar, "Storing light in active optical waveguides with single-negative materials," *Appl. Phys. Lett.* Vol. 96, 211112 (2010).

[38] Y. J. Huang, W. T. Lu, and S. Sridhar, "Slow microwave waveguide made of negative permiablity metamaterials," *Phys. Rev. A* Vol. 77, 063836 (2008).

[39] L. V. Alekseyev and E. Narimanov, "Slow light and 3D imaging with non-magnetic negative index systems," *Opt. Express* Vol. 14, 11184 (2006).

[40] Q. Zhang, T. Jiang1 and Y. Feng, "Slow-light propagation in a cylindrical dielectric waveguide with metamaterial cladding," *J. Phys. D: Appl. Phys.* Vol. 44, 475103 (2011).

[41] Y. J. Huang, W. T. Lu, and S. Sridhar, "Nanowire waveguide made from extremely anisotropic metamaterials," *Phys. Rev. A* Vol. 77, 063836 (2008).

[42] Cory, T and T. Blum, "Surface-wave propagation Along A Metamaterial Cylindrical Guide," *Microwave and Optical Technology Letters*, Vol. 44, No. 1, 31–35, 2005.

[43] Shu, W and J. M. Song, "Complete mode spectrum of a grounded dielectric slab with double negative metamaterials," *Progress In Electromagnetics Research*, Vol. 65, 103–123, 2006.

[44] Cory, T and T. Barger, "Surface-wave propagation along a metamaterial slab," *Microwave and Optical Technology Letters*, Vol. 38, No. 5, 392–395, 2003.

[45] Wu, B. I, Tomasz M. Grzegorczyk, Yan Zhang, and Jin Au Kong, "Guided modes with imaginary transverse wave number in a slab waveguide with negative permittivity and permeability," *Journal of Applied Physics*, Vol. 93, No. 11, 9386–9388, 2003.

[46] Baccarelli, P, Paolo Burghignoli, Fabrizio Frezza, Alessandro Galli, Paolo Lampariello, Giampiero Lovat and Simone Paulotto "Fundamental Modal Properties of Surface Waves on Metamaterial Grounded Slabs," *IEEE Transactions on Microwave Theory and Techniques,*, Vol. 53, No. 04, 1431–1442, 2005.

[47] Ruppin, R., "Surface polaritons of a left-handed medium," *Physics Letters A*, 277, 61–64, 2000.

[48] Darmanyan, S. A, M. Neviere b, A.A. Zakhidov, "Surface modes at the interface of conventional and left-handed media," *Opt. Commun.* , 225, 233–240, 2003.

[49] Kats, A. V, Sergey SavelâĂŹev, V. A. YampolâĂŹskii and Franco Nori1,4 , "Left-Handed Interfaces for Electromagnetic Surface Waves," *Physical Review Letters*, PRL 98, 073901-1–073901-4, 2007.

[50] Leskova, T. A, A. A. Maradudin, and I. Simonsen, "Scattering of electromagnetic waves from the random surface of a left-handed medium," *Proc. SPIE* , Vol. 4447, 6–16, 2001.

[51] Leskova, T. A, A. A. Maradudin, and I. Simonsen, "Coherent scattering of an electromagnetic wave from, and its transmission through, a slab of a left-handed medium with a randomly rough illuminated surface," *Proc. SPIE*, Vol. 5189, 22-35, 2003.

[52] Engheta, N, "An Idea for Thin Subwavelength Cavity Resonators Using Metamaterials With Negative Permittivity and Permeability," *IEEE Antennas and Wireless Propagation Letters*, Vol. 01, 10–13, 2002.

[53] Shadrivov, I. V, Andrey A. Sukhorukov, and Yuri S. Kivshar "Guided modes in negative-refractive-index waveguides ," *Physical Review*, E 67, 057602, 2003.

[54] Shelby, R. A, ,D. R. Smith, S. C. Nemat-Nasser, and S. Schultz "Microwave transmission through a two-dimensional, isotropic, left-handed metamaterial," *Applied Physics Letters*, Vol. 78, No. 4, 489–491, 2001.

[55] Itoh, T., "Prospects for metamaterials," *Applied Physics Letters* Vol. 40, No. 16, 972–973, 2004.

[56] Itoh, T., "Cloaking a receiving antenna or a sensor with plasmonic metamaterials," *ELSEVIER* Vol. 4, 153–159, 2010.

[57] Gil, M, J. Bonache and F. Martin "Metamaterial filters: A review," *ELSEVIER* Vol. 2, 186–197, 2008.

[58] Pendry, J. B., "Negative refraction makes a perfect lens," *Physical Review Letters*, Vol. 85, No. 18, 3966–3969, 200.

[59] N. W. Ashcroft and N. Mermin, *Solid State Physics* (Harcourt College Publisher, 1976).

[60] H. Chen, L. Ran, J. Huangfu, T. M. Grzegorczyk, and J. A. Kong, "Equivalent circuit model for left-handed metamaterials," *Journal of Appl. Phys.* Vol. 100, pp. 01–06, 2006.

[61] X. Chen, T. M. Grzegorczyk, B. Wu. Joe Pacheco, and J. Au Kong , "Robust method to retrieve the constitutive effective parameters of metamaterials," *Phys. Rev. E* Vol. 70, 2004.

[62] D. Wang, L. Ran, H. Chen, M. Mu, J. A. Kong, and B. Wu, "Experimental validation of negative refraction of metamaterial composed of single side paired S-ring resonators," *Appl. Phys. Lett.* Vol. 90, 254103 (2007).

[63] B. InterLingua, *Printing Technology for Flexible Substrates* (InterLingua, 2006).

[64] T.J. Yen, W.J. Padilla, N. Fang, D.C. Vier, D.R. Smith, J.B.Pendry, D.N. Basov, and X. Zhang, "Terahertz magnetic response from artificial materials," *Science* Vol. 303, 1494–1496 (2004).

[65] N. Katsarakis, G. Konstantinidis, A. Kostopoulos, R.S. Penciu,T.F. Gundogdu, M. Kafesaki, E.N. Economou, T. Koschny, and C.M. Soukoulis, "Magnetic

response of split-ring resonators in the far-infrared frequency regime," *Opt. Lett.* Vol. 30, 1348–1350 (2005).

[66] S. Zhang, W. Fan, B.K. Minhas, A. Frauenglass, K.J. Malloy, and S.R.J. Brueck, "Enhanced infrared transmission through subwavelength coaxial metallic arrays," *Phys. Rev. Lett.* Vol. 94, 033902 (2005).

[67] C. Enkrich, M. Wegener, S. Linden, S. Burger, L. Zschiedrich, F.Schmidt, J.F. Zhou, T. Koschny, and C.M. Soukoulis, "Magnetic metamaterials at telecommunication and visible frequencies," *Phys. Rev. Lett.* Vol. 95, 203901 (2005).

[68] G. Dolling, M. Wegener, C. M. Soukoulis, and S. Linden, "Negative-index metamaterial at 780 nm wavelength," *Opt. Lett.* Vol. 32, pp. 53-55, 2007.

[69] J. Yao, Z. Liu, Y. Liu, Y. Wang, C. Sun, G. Bartal, A. M. Stacy, and X. Zhang, "Optical Negative Refraction in Bulk Metamaterials of Nanowires," *Science* Vol. 321, pp. 930, 2008.

[70] A. Sihvola, *Electromagnetic Mixing Formulas and Applications*, Institute of Electrical Engineers, London, 1999.

[71] E. D. Palik, *Handbook of Optical Constants of Solids*, Institute of Electrical Engineers, Academic, New York, 1981.

[72] Y. A. Vlasov, M. O'Boyle, H. F. Hamann, and S. J. McNab, "Active control of slow light on a chip with photonic crystal waveguides," *Nature* Vol. 438, pp. 65-69, 2005.